AD-A166 462 SIMULATION DEVELOPMENT FOR SILO TEST PROGRAM (STP) 1/2
VOLUME 2 DETONATION CH..(U) SRI INTERNATIONAL MENLO
PARK CA J T ROSENBERG ET AL. 31 MAR 84
UNCLASSIFIED DNA-TR-84-219-V2 DNA001-82-C-0103 F/G 19/1 NL

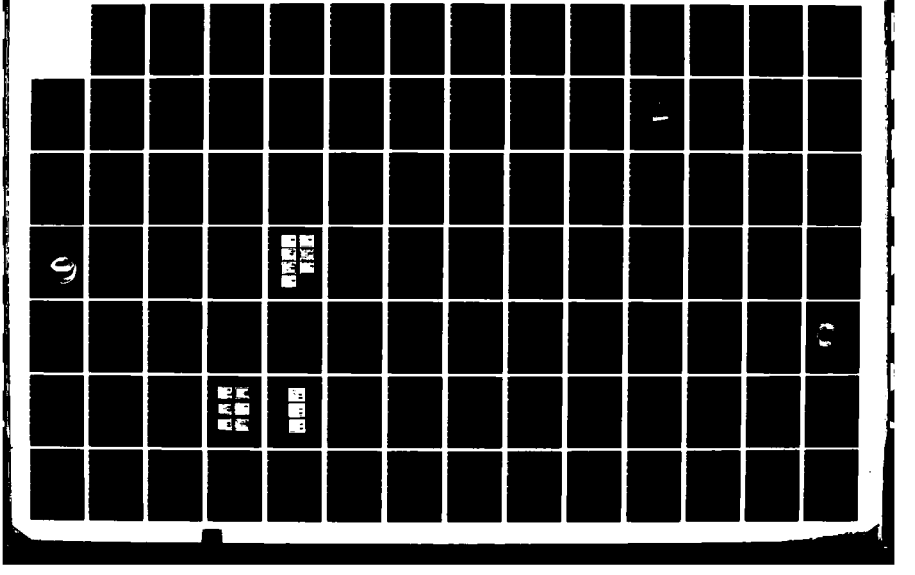

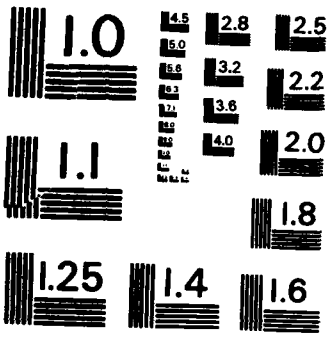

AD-A166 462

DNA-TR-84-219-V2

SIMULATION DEVELOPMENT FOR SILO TEST PROGRAM (STP)

Volume II—Detonation Characterization of NA/NP (Aqueous Nitric Acid/ Nitropropane) and NPN (Nitropropane Nitrate)

J.T. Rosenberg
D.C. Erlich, Contributor
D.D. Keough, Project Supervisor
SRI International
333 Ravenswood Avenue
Menlo Park, CA 94025-3434

31 March 1984

Technical Report

CONTRACT No. DNA 001-82-C-0103

THIS WORK WAS SPONSORED BY THE DEFENSE NUCLEAR AGENCY
UNDER RDT&E RMSS CODE B344083466 Y99QAXSD00046 H2590D.

Prepared for
Director
DEFENSE NUCLEAR AGENCY
Washington, DC 20305-1000

UNCLASSIFIED
SECURITY CLASSIFICATION OF THIS PAGE

AD-A166462

REPORT DOCUMENTATION PAGE

Form Approved
OMB No. 0704-0188
Exp. Date: Jun 30, 1986

1a. REPORT SECURITY CLASSIFICATION UNCLASSIFIED	1b. RESTRICTIVE MARKINGS
2a. SECURITY CLASSIFICATION AUTHORITY	3. DISTRIBUTION/AVAILABILITY OF REPORT Approved for public release; distribution is unlimited.
2b. DECLASSIFICATION/DOWNGRADING SCHEDULE N/A since UNCLASSIFIED	
4. PERFORMING ORGANIZATION REPORT NUMBER(S)	5. MONITORING ORGANIZATION REPORT NUMBER(S) DNA-TR-84-219-V2
6a. NAME OF PERFORMING ORGANIZATION SRI International 6b. OFFICE SYMBOL (If applicable)	7a. NAME OF MONITORING ORGANIZATION Director Defense Nuclear Agency
6c. ADDRESS (City, State, and ZIP Code) 333 Ravenswood Avenue Menlo Park, CA 94025-3434	7b. ADDRESS (City, State, and ZIP Code) Washington, DC 20305-1000
8a. NAME OF FUNDING/SPONSORING ORGANIZATION 8b. OFFICE SYMBOL (If applicable)	9. PROCUREMENT INSTRUMENT IDENTIFICATION NUMBER DNA 001-82-C-0103
8c. ADDRESS (City, State, and ZIP Code)	10. SOURCE OF FUNDING NUMBERS

PROGRAM ELEMENT NO.	PROJECT NO	TASK NO.	WORK UNIT ACCESSION NO.
62715H	Y99QAXS	D	DH006596

11. TITLE (Include Security Classification)
SIMULATION DEVELOPMENT FOR SILO TEST PROGRAM (STP) Volume II—Detonation Characterization of NA/NP (Aqueous Nitric Acid/Nitropropane) and NPN (Nitropropane Nitrate)

12. PERSONAL AUTHOR(S)
J.T. Rosenberg; Contributor: D.C. Erlich; and Project Supervisor: D.D. Keough

13a. TYPE OF REPORT	13b. TIME COVERED	14. DATE OF REPORT (Year, Month, Day)	15. PAGE COUNT
Technical	FROM 820111 TO 840331	1984, March 31	124

16. SUPPLEMENTARY NOTATION
This work was sponsored by the Defense Nuclear Agency under RDT&E RMSS Code B344083466 Y99QAXSD00046 H2590D.

17 COSATI CODES			18 SUBJECT TERMS (Continue on reverse if necessary and identify by block number)		
FIELD	GROUP	SUB-GROUP	High Explosive (HE)	Ammonium Nitrate (AN)	Gage
14	2		Chapman-Jouguet (CJ)	Nitromethane (NM)	TIGER
16	1		Nitropropane Nitrate (NPN)	Nonideal	ANFO

19. ABSTRACT (Continue on reverse if necessary and identify by block number)

In support of the Defense Nuclear Agency (DNA) Silo Test Program, the planar steady detonation processes were characterized and initial JWL (Jones-Wilkins-Lee) equation of state (EOS) coefficients were developed for two chemical high explosives (HEs), NA/NP and NPN. NA/NP is a liquid explosive composed of weak (Baumé 42) aqueous nitric acid (NA) and the solvent nitropropane (NP). The NA/NP studied here was 3.158 parts NA to 1 part NP, by weight, and its density was 1.25 Mg/m^3 at 29°C. NPN (nitropropane nitrate) is a damp granulated blasting agent composed of ammonium nitrate (AN), NP, and methyl alcohol (MA). Our study material was 0.848 AN, 0.075 NP, 0.075 MA, and 0.002 methocel (an added antimigratory agent), by weight, and had a density of 1.01 Mg/m^3. These unusual explosives are being considered by DNA for use in various nuclear weapons effects simulators because of their potential for producing desired pulse shapes at competitive costs.

SRI large-scale multiple Lagrange particle velocity gage experiments, in combination with Lagrange analyses, quantified the early stages of the steady planar detonation process in

20. DISTRIBUTION/AVAILABILITY OF ABSTRACT	21. ABSTRACT SECURITY CLASSIFICATION
☐ UNCLASSIFIED/UNLIMITED ☒ SAME AS RPT. ☐ DTIC USERS	UNCLASSIFIED
22a. NAME OF RESPONSIBLE INDIVIDUAL Betty L. Fox	22b. TELEPHONE (Include Area Code) (202) 325-7042
	22c. OFFICE SYMBOL DNA/STTI

DD FORM 1473, 84 MAR

83 APR edition may be used until exhausted
All other editions are obsolete.

SECURITY CLASSIFICATION OF THIS PAGE
UNCLASSIFIED

18. SUBJECT TERMS (Continued)

Characterization	Nitropropane	JWL
Detonation	Lagrange	BKW
Initiation	Lagrange Analysis	NA/NP
Equation of State	Particle Velocity	JCA3
Nitric Acid	SDT	SRI Large Scale Legrange Gage and Analysis Technique

19. ABSTRACT (Continued)

each material. Thermodynamic equilibrium calculations, performed with the SRI TIGER code, extended the adiabatic release paths to pressures approaching atmospheric.

NA/NP exhibited ideal detonation with a pressure-relative volume (p-V) adiabatic release path slightly above that of nitromethane (NM) and a resolved reaction zone of surprisingly long duration, 0.2-0.6 μs. A single experiment indicated that the shock-to-detonation transition (SDT) may occur over unusually long buildup distances.

The NPN detonation process was nonideal in that not all the AN reacted to support the steady detonation. The p-V release adiabat was very close to that for ANFO over a large relative volume range, but lay somewhat above it at and near the detonation state. (At higher initial densities, the NPN performance advantages near the detonation state would be greater.) Two possible two-step AN reactions were postulated to model the nonideal detonation process in NPN.

A new JWL fitting procedure was developed based on the detonation state release isentrope and three hydro-thermodynamic constraints. The procedure is intended to provide JWL EOS parameters suitable for use in DNA hydrocode calculations to estimate high explosive performance in various nuclear weapons effects simulators. The procedure was used to determine JWL EOS parameters for each material.

Five recommendations, three strong, are made to DNA in the areas of HE use and characterization:

(1) NA/NP is a very promising liquid HE; we strongly recommend considering its use in NWE simulators, as a low cost alternative to NM.

(2) Although NPN compacts irreversibly, especially at low densities, we recommend its consideration in NWE applications calling for an HE similar to ANFO but with the ability to do somewhat more work at high pressures and/or with more rapid kinetics.

(3) We strongly recommend Lagrange gage SDT experiments to characterize the buildup and propagation of detonation in NA/NP.

(4) We recommend further research to confirm the presumed charge size independence of the present NPN experimental results.

(5) We strongly recommend further experimental and computational efforts to improve the understanding of, and ability to model, nonideal detonation processes in AN-rich HEs such as NPN and ANFO.

SUMMARY

Two unusual chemical high explosives (HEs), a liquid explosive called NA/NP and a blasting agent called NPN, are of interest to the Defense Nuclear Agency (DNA) for possible use in various nuclear weapon effects (NWE) simulators in the Silo Test Program and other programs. These novel HEs may be able to produce desired pulse shapes at competitive cost in such applications. In the present research, SRI International investigated NA/NP and NPN to (1) experimentally and computationally characterize the planar steady detonation process in each HE at large charge diameters and (2) develop initial JWL (Jones-Wilkins-Lee) equation of state (EOS) parameters suitable for DNA hydrocode calculations predicting the performance of each HE in various NWE simulators.

METHODS

SRI large-scale multiple Lagrange particle velocity gage experiments, in combination with Lagrange analyses, were used to quantify the early stages of the steady planar detonation processes in each material. In the experimental technique, thin metallic foil gages were embedded at various depths within the explosive to provide the velocity histories of particles (Lagrange histories) during the shock compression and early expansion phases of the detonation process.

Thermodynamic equilibrium calculations were used to complete the quantification of the detonation process by extending the adiabatic expansion path determined experimentally to pressures approaching atmospheric. These calculations assume chemical, mechanical, and thermal equilibrium among the detonation products and determine the composition and state variables for proscribed thermodynamic processes modeling the adiabatic expansion. The calculations were performed with the SRI TIGER code and used the BKW and JCZ3 EOSs for individual detonation product gases.

A new fitting procedure was developed to determine JWL EOS parameters from the adiabatic release path through the CJ (Chapman-Jouguet) detonation state. The procedure provides unique values for the JWL parameters by minimizing the RMS deviation between the CJ release adiabat and the JWL CJ isentrope subject to three hydro-thermodynamic constraints. The procedure is quite general and is believed to have applications beyond the present program. Initial JWL parameters were developed for each material by applying this procedure to the release adiabat determined from the Lagrange gage experiments and extended by the TIGER calculations.

NA/NP CHARACTERIZATION

NA/NP is a liquid explosive composed of Baumé 42 nitric acid (NA), a weak aqueous nitric acid solution containing 67.18 wt% pure nitric acid, and nitropropane (NP), a solvent. The NA/NP composition studied here was 3.158 parts NA to 1 part NP, by weight, and had a density of 1.25 Mg/m^3 at 29°C. This composition is oxygen balanced to CO_2. Despite its acid and solvent components, we found NA/NP to be relatively easy to handle.

Two successful Lagrange gage detonation experiments were performed in NA/NP. The second had more precise instrumentation settings and produced high quality reproducible particle velocity data that were Lagrange analyzed to determine the compression and initial adiabatic release states of a particle in the steady detonation process. NA/NP exhibited ideal detonation conforming to the ZND (Zeldovich, Von Neumann, Doering) model with a clearly resolved reaction zone of surprisingly long duration, 0.2-0.6 μs. At the CJ state the pressure was 13.3 GPa, the detonation velocity was 6.48 km/s, the particle velocity was 1.64 km/s, the specific volume was 0.5986 m^3/Mg, and the adiabatic exponent was 2.99.

A single Lagrange gage experiment with a reduced amplitude input shock was also performed to examine the shock-to-detonation transition (SDT) in NA/NP. The resulting particle velocity histories, although not

reproducible across the target, indicate the possibility of an unusual SDT phenomenology with long buildup distances. If confirmed by further experiments, this effect should be accounted for in NWE simulator designs using NA/NP.

To extend the CJ adiabatic release path from the second Lagrange gage NA/NP detonation experiment to large volumes, we assumed the expansion to be isentropic and used TIGER with both the BKW and the JCZ3 EOSs to estimate the isentrope. The BKW calculations terminated prematurely at about 1 GPa, whereas the JCZ3 calculations extended to about 2 MPa. Therefore, the JCZ3 calculations were selected to characterize the NA/NP detonation product expansion to large volumes. The TIGER/JCZ3 isentrope through the experimental CJ state agreed very closely with the release adiabat from the Lagrange gage experiment in the regions of overlap.

NA/NP JWL EOS coefficients were calculated by applying the new fitting method to the CJ state determined from the Lagrange gage detonation experiment and the release path through it from the TIGER/JCZ3 calculations. The resulting coefficients are as follows: $A = 7.554$ Mbar, $B = 0.1962$ Mbar, $C = 0.012717$ Mbar, $R_1 = 6.366$, $R_2 = 1.810$, and $\omega = 0.285$. These coefficients are the major result of the present NA/NP characterization effort. They are judged appropriate for use in hydrocode calculations to evaluate NA/NP performance in a variety of NWE simulator applications.

The NA/NP JWL CJ release isentrope determined here is close to, but slightly above, that for nitromethane (NM) determined from cylinder test data. Therefore, NA/NP performance in NWE simulators is expected to be very similar to that of NM, although its material cost is much less. We conclude that NA/NP is a very promising liquid HE offering an attractive low cost alternative to NM.

NPN CHARACTERIZATION

NPN (nitropropane nitrate) is a damp granulated blasting agent composed of ammonium nitrate (AN), NP, and methyl alcohol (MA). The NPN studied here was, by weight, 0.848 ground porous AN prills, 0.075

NP, 0.075 MA, and 0.002 methocel (an added anti [illegible]ory agent) and had a density of 1.01 Mg/m^3. This composition is very slightly overfueled relative to CO_2 balance. The NPN was selected to be close to that examined previously for DNA in an airblast experiment. We found that careful handling was required to keep NPN in a uniform state because it easily undergoes irreversible compaction at these low densities.

Special procedures were developed to uniformly load the NPN in the Lagrange gage experiment target chambers without distorting the embedded particle velocity gages. Two NPN multiple Lagrange particle velocity gage experiments were performed, but despite the precautions, some gage displacement occurred in the first experiment. Therefore, only data from the second experiment, in which slightly modified loading procedures were used, were analyzed quantitatively.

For the valid recording duration of the experiment (about 8 μs), the reactive flow in the NPN consisted of a uniform particle velocity pulse propagating at a velocity of 5.08 km/s. The steady particle velocity history profile is idealized as consisting of a shock compression to a peak amplitude of about 2.4 km/s in 0.2 μs, a decay to about 0.6 of the peak amplitude in about 2 μs, and a very slow further decay, or a constant state, for about 6 μs. The steady flow and slow final decay rate observed in the NPN have not been observed in the other HEs we have studied with this technique and suggest that the detonation process in NPN may be nonideal.

Because the flow observed in the NPN detonation experiment was steady, the Lagrange analysis could be performed by application of the Rankine-Hugoniot relations for shocks and steady flows. The resulting pressure history has the same shape as the idealized particle velocity history, and the pressure-relative volume path consists of compression and expansion along the Rayleigh line.

An extensive effort was required to simulate and extend the experimental results with TIGER. Initial calculations performed with both the BKW and the JCZ3 EOSs revealed that the detonation process was indeed nonideal in that not all the AN reacted to support the detonation. BKW

predicted that 51.5 wt% of the AN did not support the detonation and estimated the CJ pressure at 5.44 GPa. JCZ3 predicted that only 14.5 wt% of the AN was inert and estimated the CJ pressure at 6.48 GPa.

Because of the different calculated amounts of unreacted AN at the CJ state and because a BKW procedure had been developed previously for treating nonideal detonation in ANFO (an HE similar to NPN), we postulated different secondary AN reaction processes to calculate adiabatic release paths to large volume with the two EOSs. In the BKW calculations, following the previous treatment for ANFO, we assumed that the remaining 51.5 wt% of AN was consumed in an irreversible reaction spread over a large pressure-volume range starting at the CJ state and that the subsequent expansion was isentropic. However, in the JCZ3 calculations, because of the nearly constant state observed in the latter part of the experimental records, we assumed that the small remaining amount of AN reacted slowly at a pressure and volume near that of the CJ state and that the subsequent expansion was isentropic. Because only the JCZ3 results extended to large enough relative volumes to permit application of the new JWL fitting procedures, we used the JCZ3 calculations to represent the NPN CJ release adiabat.

Initial JWL EOS parameters were calculated for NPN by applying the new fitting procedures to the CJ release adiabat consisting of the Rayleigh line determined from the Lagrange gage experiment and the isentrope through its final state from the TIGER/JCZ3 calculations. The resulting coefficients are as follow: $A = 6.783$ Mbar, $B = 0.1824$ Mbar, $C = 0.007212$ Mbar, $R_1 = 7.628$, $R_2 = 2.305$, and $\omega = 0.345$. These coefficients are judged appropriate for use in hydrocode calculations to evaluate NPN performance in a variety of NWE simulator applications.

The NPN JWL release isentrope determined in this work is very close to that for ANFO from cylinder tests, over the full relative volume range examined, but lies somewhat above it at and near the detonation state. At higher initial densities, the NPN performance advantages over ANFO would be expected to be greater. The enhanced high pressure performance of NPN may outweigh its handling and cost disadvantages relative to ANFO in some DNA applications.

The nonideal AN reaction phenomenology is presumed to be similar in NPN and ANFO, but the findings of this study indicate that this phenomenology is not yet defined or quantified. Therefore, the ability to accurately predict the performance of either material in specific applications is suspect. This is an important conclusion since ANFO will probably be the HE used by DNA in forthcoming large airblast simulations.

RECOMMENDATIONS

The results of the NA/NP and NPN characterization efforts lead us to make five recommendations to DNA in the areas of HE use and characterization. Recommendations (1), (3), and (5) are recommended strongly.

(1) We strongly recommend the use of NA/NP in NWE simulation applications calling for low cost liquid explosives similar in performance to NM.

(2) We recommend that the use of NPN be considered in NWE applications calling for an HE similar to ANFO but with the ability to do somewhat more work at high pressures and/or with more rapid kinetics. Its relative performance advantages over ANFO, and the ease of keeping it uniform, probably both increase at higher intial densities than studied here.

(3) We strongly recommend support for Lagrange gage shock-to-detonation transition experiments to characterize the buildup and propagation of detonation in NA/NP.

(4) We recommend further research to confirm the presumed charge size independence of the present NPN experimental results.

(5) We strongly recommend support for further experimental and computational efforts to improve the understanding of and ability to model, nonideal detonation processes in AN-rich HEs such as NPN and ANFO.

PREFACE

This is one of two reports on investigations performed for the Defense Nuclear Agency under Contract DNA001-82-C-0103 during the period 11 January 1982 to 31 March 1984. Technical monitors for this work were Major M. E. Furbee (now at BMO) and Dr. K. Goering.

We are pleased to acknowledge and thank the many individuals who provided valuable support and assistance in the work described in this report. From outside SRI, we thank Mr. Joseph L. Trocino, Trocino and Associates, for information on NA/NP and its components; Dr. H. Dean Mallory, Naval Weapons Center, for sharing his results and experiences with NA/NP; Mr. John R. Post, General Energy Company, for advice and information on NPN; and Dr. Roland Franzen, Ford Laboratories, Inc., for discussions on NPN.

Within SRI, we thank Mr. Darwin R. Henley for constructing the targets, Mr. Daniel F. Walter for operating electronic instrumentation, Mssrs. Hugh E. Hanna, George S. Cartwright, and Kennard E. Nelson for assistance at the tests site, and Ms. Bonnie Y. Lew for extensive computational assistance. A special debt of gratitude is owed Dr. Michael Cowperthwaite for many illuminating discussions.

TABLE OF CONTENTS

LIST OF ILLUSTRATIONS

LIST OF TABLES

SECTION 1

INTRODUCTION

The Defense Nuclear Agency (DNA) is using chemical high explosives (HEs) to simulate various nuclear weapon effects (NWEs) including direct and airblast induced ground shock and airblast effects on structures. In such simulations, kilotons of HE and/or very precise blast pulse shapes, amplitudes, and durations may be required. These simulations have generated the need for new HEs offering lower cost, improved performance, or different properties than conventional HEs previously developed for military or mining purposes.

In this work we examined two new HEs of interest to DNA: a liquid explosive here called NA/NP and a blasting agent called NPN. The overall objective was to generate initial JWL (Jones-Wilkins-Lee) equation-of-state parameters for each HE to allow hydrocode calculations for evaluating the performance of each material in NWE simulators.

NA/NP is mixture of aqueous nitric acid (NA) and the solvent nitropropane (NP). NA/NP offers performance similar to nitromethane (NM) at a much lower material cost. NPN (nitropropane nitrate) is composed of ammonium nitrate (AN), NP, and methyl alcohol (MA). NPN is similar to the commercial blasting agent ANFO (ammonium nitrate and fuel oil) used in the mining industry, but has a higher detonation velocity and pressure and a somewhat greater cost. Both materials are being studied for the DNA Silo Test Program, but have potential for many other DNA applications as well.

The present work included both experimental and theoretical characterization techniques. The SRI large-scale Lagrange particle velocity gage method was used to measure particle velocity histories within each HE as it underwent steady detonation. Lagrange analyses of these data provided histories of the other flow variables including propagation velocity, pressure, specific volume, and specific internal energy during

the chemical reaction and the initial adiabatic expansion of the detonation products for each material. Thermodynamic equilibrium calculations performed with the SRI TIGER code modeled the Lagrange gage and analysis results and extended the adiabatic product expansion data to large volumes. Initial JWL coefficients suitable for hydrocode calculations were developed for each material from the results of the Lagrange gage experiments and the TIGER calculations.

Section 2 of this report describes the techniques we used, including a valuable new procedure for obtaining JWL coefficients consistent with a specified detonation state and the release isentrope passing through it. Sections 3 and 4 present the results of the NA/NP and NPN characterization efforts, respectively. Section 5 gives our recommendations for the use and further characterization of NA/NP and NPN.

SECTION 2

METHODS

Three methods were used to quantify the detonation state and the subsequent adiabatic expansion states generated in HE reaction products by steady planar detonations: the SRI large-scale Lagrange particle velocity gage technique, GUINSY uniaxial flow Lagrange analysis calculations, and TIGER thermodynamic equilibrium calculations. These methods are reviewed below. A new technique developed to calculate unique JWL equation-of-state (EOS) parameters from the detonation state and the release isentrope centered on it is described here for the first time.

2.1 SRI LARGE-SCALE LAGRANGE PARTICLE VELOCITY GAGE TECHNIQUE

The objective of this technique is to measure histories along particle paths (Lagrange histories) of the particle velocity at several depths within an explosive undergoing steady planar detonation. Here and throughout this report we use as the basis for discussion the well-known ZND (Zeldovich-VonNeumann-Doering) model for ideal steady planar detonation with an explicit reaction zone. In this model the detonation process experienced by a particle is idealized as consisting of (1) nonreactive shock compression, resulting from a shock propagating at the detonation velocity D, to a state on the Hugoniot of the unreacted explosive ("spike" state), (2) chemical reaction and expansion, produced by a steady rarefaction (steady-state reaction zone) also propagating at the detonation velocity D, terminating at a state on the detonation products Hugoniot (CJ [Chapman-Jouguet] detonation state), and (3) nonreactive isentropic expansion to ambient pressure, resulting from a dispersive rarefaction (Taylor wave) in the detonation products.

The representation of the ideal ZND detonation process in the pressure-specific volume (p-v) plane and the corresponding Lagrange

particle velocity (u) histories are shown schematically in Figure 1. The objective of the present Lagrange particle velocity gage experiments is to measure the actual particle velocity histories analogous to those in Figure 1 so that the real detonation process and associated parameters can be determined.

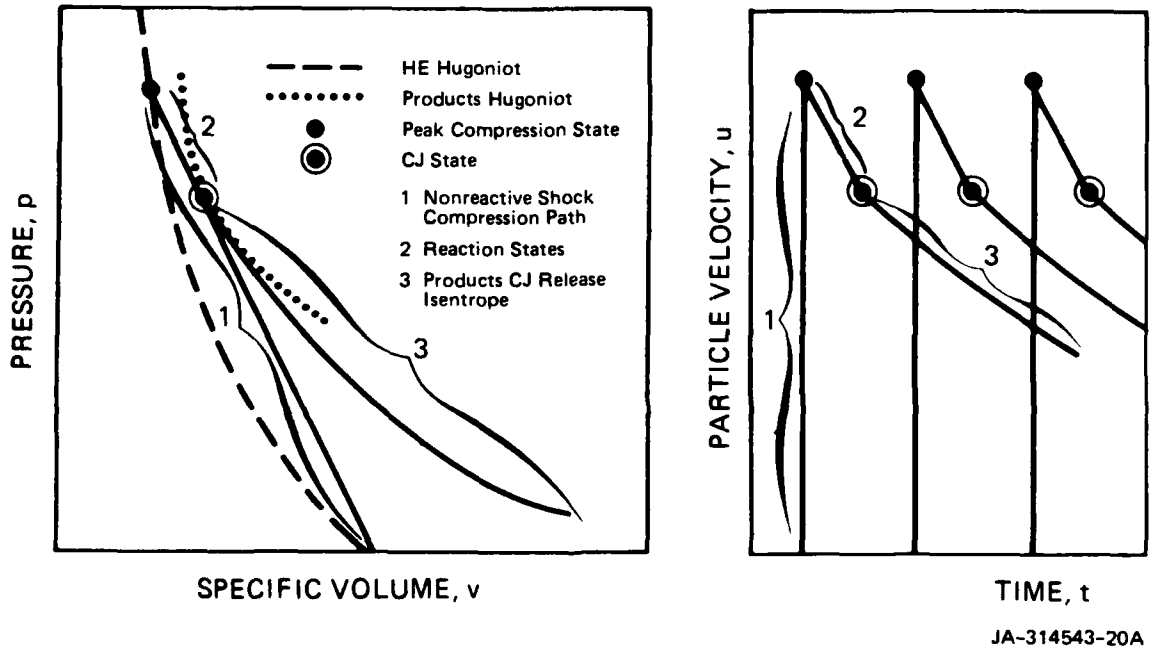

Figure 1. Pressure-specific volume paths and corresponding particle velocity histories for ideal detonation with resolved reaction zone.

The SRI large-scale Lagrange particle velocity gage technique used here has been described previously.[1,2] The basic experimental configuration is shown in Figure 2. The HE target is a right cylinder typically 0.2-0.3 m in diameter by about 0.13 m in height. A plane-wave lens and appropriate HE driver are used to initiate steady planar detonation in the target HE. A number of electromagnetic particle velocity (EPV) gages,[3,4] described below, are embedded at various depths

(Lagrange coordinates) in the target to record the particle velocities at these Lagrange coordinates. Expendable Helmholtz coils wound on plywood frames, and powered by a capacitive discharge system with a time constant of several milliseconds, provide a uniform uniaxial magnetic induction of 400-500 gauss in the region of the EPV gages. The magnetic induction is essentially constant during the measurement interval, about 10 μs. The configuration in Figure 2 is termed large-scale in comparison to Lagrange gage gas gun experiments performed in other laboratories, typically with 0.05-m-diameter targets, to study shock initiation of detonation for shorter times.[5,6]

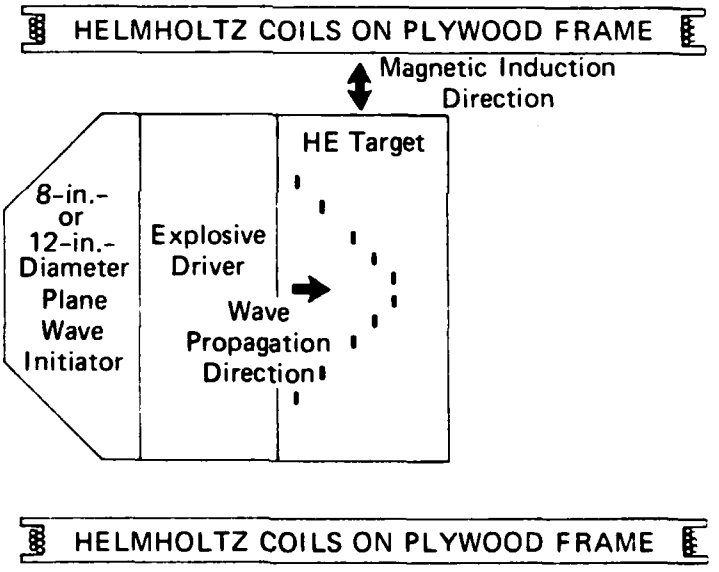

Figure 2. Configuration of SRI large-scale Lagrange particle velocity gage experiments.
Heavy dashes in the HE target indicate the active elements of the embedded particle velocity gages.

The principle of the EPV gage is that an electrical conductor moving in a fixed magnetic field will generate a motional electromotive force (EMF) proportional to its velocity. If the conductor, motion, and

magnetic induction are each uniaxial and mutually orthogonal, as in the present case, then by Faraday's law of induction for moving circuits

$$E(t) = B\ell u'(t) \qquad (1)$$

where E is the EMF, t is time, B is the magnitude of the magnetic induction, ℓ is the length of the conductor, and u' is its velocity.

The EPV gages used in this work are formed from aluminum strips nominally 0.15 mm thick by 3 mm wide. The strips are bent into rectilinear U-shapes, and ten are mounted on a standard linen phenolic gage block for embedding in a target as shown in Figure 3. The crossbar of the U is the active element of the gage and is nominally 25.4 mm long. The sides of the U, electrical leads that carry the signal out the back of the target, do not contribute to the signal because they are strictly parallel to the direction of particle motion in the target. The gages are anodized and sealed to provide an electrical insulating layer 5-10 μm thick. Because the active elements of the EPV gages are only 0.15 mm thick in the wave propagation direction and because of the reasonable impedance match between the aluminum gage material and the HE detonation products, the gages reach close mechanical equilibrium with instantaneous changes in the surrounding flow in the products in less than 0.1 μs. Therefore u'(t) is taken equal to the local particle in the reactive flow, u(t), everywhere except at the spike state, which generally cannot be fully resolved with the present EPV gages.

A high frequency recording circuit, consisting of RG 213 or RG 58 coaxial cables and a 51-Ω viewing-and-termination resistor in series with the EPV gage, monitors each gage. Tektronix 7000 series oscilloscopes, time correlated by a repetitive beam-blanking pulse simultaneously applied to each oscilloscope, record the potential drops across the viewing resistors. Typical peak potential drops are 2 V. E(t) is determined from the potential drop across the viewing resistor, and u'(t), interpreted as u(t), is then determined from Equation (1).

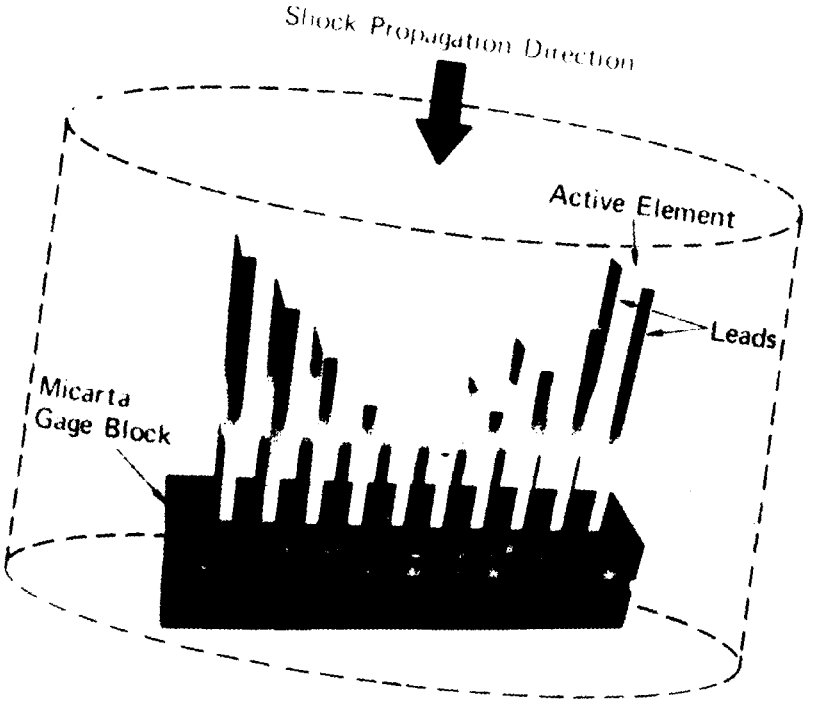

Figure 3. Gage block and gages used in SRI large-scale Lagrange particle velocity gage experiments.

The gage block shown contains ten anodized aluminum gages. The configuration of the HE target is indicated by dashed lines.

Our standard ten-gage gage block (Figure 3) was used in this work. The gage numbering system and dimensions in the wave propagation direction, that is, along the Lagrange coordinate axis, are shown in Figure 4. The gages are numbered sequentially from one end of the block to the other. The ten gages consist of two symmetrically placed 5-gage sets, 1 through 5 and 6 through 10. Thus there are two replicate gages, one from each 5-gage set in each of five planes (Lagrange positions) orthogonal to the detonation propagation direction. Adjacent gages are separated by 12.7 ± 0.1 mm in the propagation direction and by 12.0 ± 0.2 mm, center-to-center, in the lateral direction.

2.2 GUINSY UNIAXIAL FLOW LAGRANGE ANALYSIS CALCULATIONS

The Lagrange analysis for uniaxial flow is a method for determining p, v, and e (specific internal energy) histories and cross plots from the experimentally measured u(t) data obtained at different Lagrange coordinates h. The analysis numerically integrates the differential form of the conservation relations for momentum, mass, and energy in uniaxial one-dimensional (1D) flow. These relations, in a form ready for integration from particle velocity gage data, may be written as

$$p - p_0 = -\frac{1}{v_0}\int_{H(t)}^{h} \left(\frac{\partial u}{\partial t}\right)_h dh \qquad (2)$$

$$v - v_0 = v_0 \int_{\tau}^{t} \left(\frac{\partial u}{\partial h}\right)_t dt \qquad (3)$$

$$e - e_0 = -v_0 \int_{\tau}^{t} p \left(\frac{\partial u}{\partial h}\right)_t dt \qquad (4)$$

where τ = Lagrange time (the time a particle h enters the flow), H(t) is the shock path in the h-t plane, and the subscript 0 denotes the undisturbed state in the unreacted explosive ahead of the shock.

The SRI GUINSY code[7] solves these relations using the experimental u(t) data at various h to approximate the required spatial and time

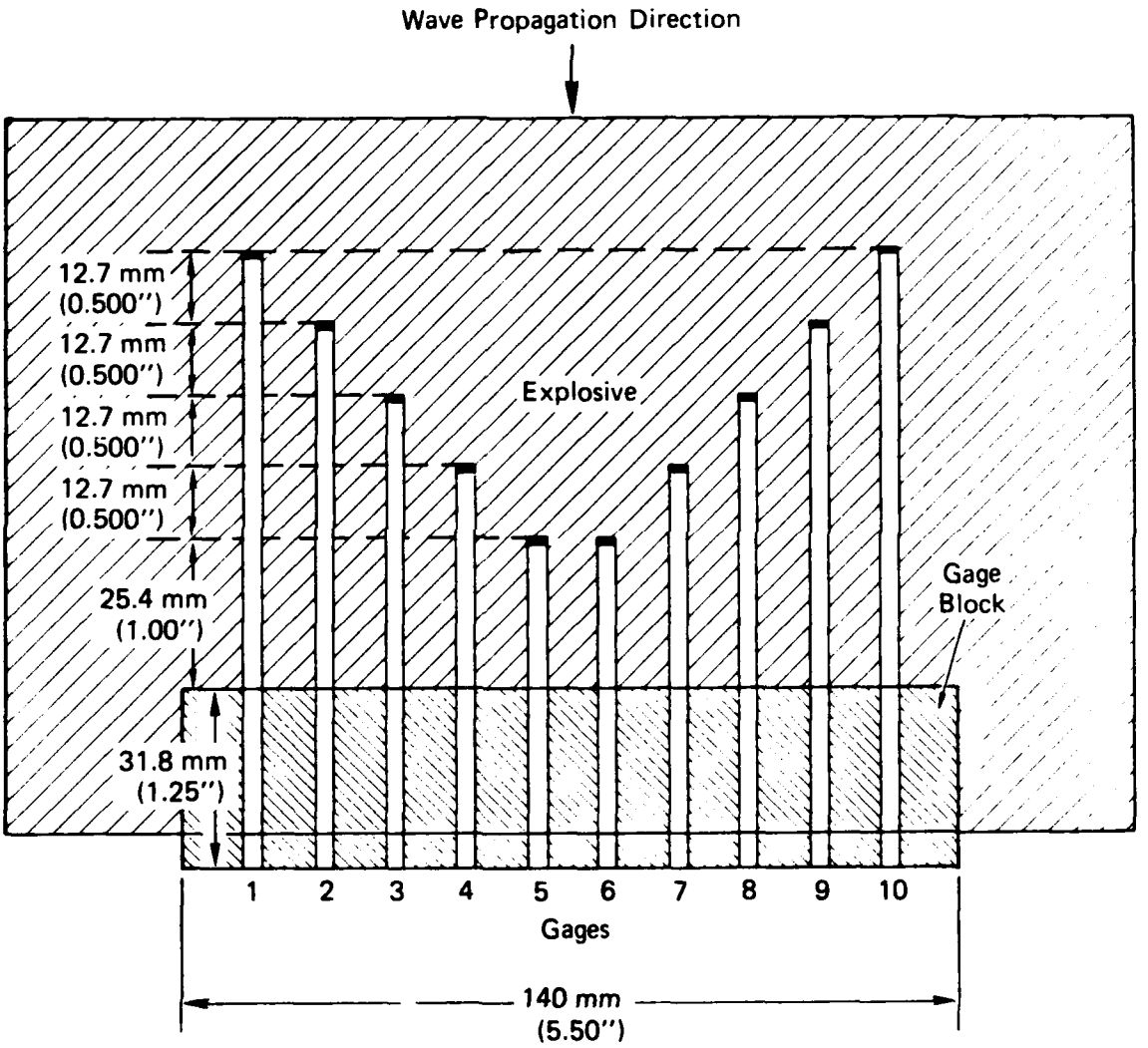

Figure 4. Side view of gage block showing gage numbering system and gage separations.

The gages are numbered sequentially as indicated, so, for example, 4 and 7 are at the same depth in the explosive. The locations of the active elements of the gages are indicated by heavy lines.

derivatives of particle velocity. GUINSY results based on particle velocity histories for steady detonation have been shown to be accurate by comparison with analytical solutions.[7]

Because the uniaxial flow Lagrange analysis is based on solution of the fundamental conservation relations without recourse to constitutive relations, it is general and applies, without restrictions, to any reactive or nonreactive uniaxial strain flow. Because the measurements used to obtain the solutions are made within the unperturbed flow rather than at a free surface or in a witness material, no unfolding procedures are necessary to relate the results to the basic detonation process. The Lagrange gage and analysis technique is the most direct and accurate method we know to determine CJ parameters.

2.3 TIGER THERMODYNAMIC EQUILIBRIUM CALCULATIONS

TIGER is a thermodynamic equilibrium code developed at SRI[8] for calculating the equilibrium thermodynamic properties of a heterogeneous system of known atomic composition governed by an arbitrary equation of state. Assuming thermodynamic equilibrium (mechanical, thermal, and chemical) for the product species and conservation of numbers of atoms of each element between reactants and products, TIGER calculates the product composition (specific mole numbers of each allowed species) and the remaining thermodynamic state variables if two state variables such as p and v are specified. Furthermore, under the same assumptions, TIGER calculates the thermodynamic state variables and the product composition along paths on the equation of state surface corresponding to well defined thermodynamic processes such as shocks, CJ detonation, and isentropic expansion. Thus, in this work we are able to estimate Hugoniots, CJ parameters, and isentropes through specified p-v states using TIGER.

Two equations of state for gaseous species are commonly used in TIGER caculations: BKW (Becker-Kistiakowsky-Wilson) and JCZ3 (Jacobs-Cowperthwaite-Zwisler). These are both nonideal gaseous p-v-T-n_i equations of state, where T is temperature and the n_i are the mole numbers

of the various species present in the products. Such EOSs that contain the product composition as independent variables are often said to have explicit chemistry.[9] Both BKW and JCZ3 represent the state of the art in such EOSs. JCZ3, however, has been formulated to predict a lattice pressure at 0 K and BKW has not. In practice, there are quantitative differences, often small, between their predicted values for detonation parameters. We find that TIGER/JCZ3 predictions are usually closer to experimental values, especially for detonation velocity. Further examples and discussion are given by Finger et al.[10]

In this work TIGEk calculations using both BKW and JCZ3 are used to model and extend the results obtained for each of the two study materials with the Lagrange gage and analysis techniques. Procedures vary considerably in the two cases and are described in Sections 3 and 4.

2.4 JWL CJ ISENTROPE FITTING PROCEDURE

JWL is an empirical detonation products EOS without explicit chemistry. The form of the EOS is

$$p = A\left(1 - \frac{\omega}{R_1 V}\right)e^{-R_1 V} + B\left(1 - \frac{\omega}{R_2 V}\right)e^{-R_2 V} + \frac{\omega E}{V} \qquad (5)$$

and the corresponding JWL form for an isentrope is

$$p_S = Ae^{-R_1 V} + Be^{-R_2 V} + CV^{-(\omega+1)} \qquad (6)$$

where E is specific energy/volume ($E = e/v_0$) measured with respect to the energy level of fully expanded (v = infinity) products; V is relative volume ($V = v/v_0$) and is dimensionless; A, B, and C are the linear JWL coefficients, with C being an integration constant assigned the appropriate value to specify the CJ isentrope; and R_1, R_2, and ω are the nonlinear JWL coefficients.

JWL is an E(p,V) EOS of the Mie-Grüneisen type with the reference curve being the CJ isentrope, Equation (6), and the Grüneisen parameter being the constant ω. The form of the JWL CJ isentrope is such that,

for large V (in practice, V > 6-8), the exponential terms become completely negligible. Therefore, for large V the JWL CJ isentrope takes the form of the polytropic gas CJ isentrope, pV^{γ} = const, where the polytropic constant γ is the ratio of specific heats at constant pressure and volume and from Equation (6), $\gamma = (\omega + 1)$.

Thus, the value of the nonlinear coefficient ω strongly affects the detonation product behavior predicted by JWL both for large V on the CJ isentrope (the low pressure polytropic limit) and for all V off the CJ isentrope (the constant Grüneisen parameter). Along the CJ isentrope, the R_1 term often dominates behavior for $V_{CJ} < V < 1$, and all terms are significant for $1 < V < \sim 5$.

The present form of JWL was developed by Lee et. al.[11] to accurately predict the metal pushing behavior of HEs in spherical and cylindrical geometries to large V. The six parameters are usually fit to reproduce the results of cylinder tests[11,12] to expansions approaching 10 as well as to satisfy certain thermodynamic, CJ state, and available energy constraints described in reference 11. General properties of JWL are reviewed by Fickett and Davis,[9] and JWL parameters for a number of HEs are given by Dobratz.[12]

The objective of our work was to develop initial JWL parameters for certain new HEs so that hydrocode calculations could be performed to evaluate the behavior of these HEs in various NWE simulators. In any one application, the detonation products may undergo different amounts of volume expansion and experience different energy exchange mechanisms with the surroundings than they do in another or in the cylinder test. Therefore, the present characterization results were not based on the results of cylinder tests or other experimental or computational simulations of a specific potential DNA application. Rather, to generate broadly applicable JWL parameters, we performed experiments and computations to obtain an estimate of the general CJ isentrope over as large a range of volume expansions as possible and then developed a procedure, described below, to uniquely fit the JWL form to this whole estimated CJ "basis isentrope."

If more accurate JWL parameters are desired for a specific application, the CJ basis isentrope estimate can be improved in the range of interest, for example, by performing a relevant simulation experiment to constrain the specification of isentropic release states in this range. The fitting techniques developed here can then be readily adapted to the new characterization range to uniquely determine JWL EOS parameters optimized to the application.

Fitting Procedure

The objective of the fitting procedure is to determine values for the six JWL EOS coefficients: A, B, C, R_1, R_2, and ω and to specify the four CJ state coefficients with which they are mathematically consistent: p, D, Γ, and E_0.

Γ is the adiabatic exponent at the CJ state defined as the logarithmic derivative $(d \ln p_S/d \ln V)_{CJ}$. It serves to specify V_{CJ}, the relative volume of the products at the CJ state since, as a result of the tangency of the CJ isentrope and the products Hugoniot at the CJ state, $V_{CJ} = \Gamma/(\Gamma + 1)$.

E_0 is defined by the equation $E_{CJ} = E_0 + (p_{CJ}/2)(1 - V_{CJ})$. In the cylinder test approach, E_0, which is closely related to the maximum useful work-potential of an HE in a detonation,[9] is chosen consistent with available chemical energy as determined either from detonation calorimetry or from thermodynamic calculations. Through its defining equation, E_0 then specifies E_{CJ} and provides one of the constraints used to determine the JWL parameters.[11] In the present approach, E_0 is also consistent with thermodynamic calculations, but is a derived quantity determined from the JWL parameters as described below.

The basis for the present fitting procedure is the set of points in the p-V plane defining the estimated CJ isentrope between V_{CJ} and some maximum relative volume, V_f. Call this "basis" isentrope $p_S(V)$, defined for $V_{CJ} \leq V \leq V_f$. (Values of a variable pertaining to the basis isentrope are now written without superscript; values of that variable pertaining to the JWL fit are written with the superscript J. The

subscript S denotes the CJ isentrope.) Let $\Delta = E_S(V_{CJ}) - E_S(V_f)$ and note that we can determine Δ from the basis isentrope using the first law of thermodynamics for an adiabatic process

$$\Delta = -\int_{V_f}^{V_{CJ}} p_S(V)\, dV$$

In fitting the JWL CJ isentrope form, Equation (6), to the basis CJ isentrope, we impose three strict mathematical constraints. First,

$$p_S(V_{CJ}) = p_S^{\,J}(V_{CJ}) \tag{7}$$

The CJ pressure-relative volume points on the basis and JWL CJ isentropes coincide. Second,

$$\frac{p_S(V_{CJ})}{1 - V_{CJ}} = \frac{d\, p_S^{\,J}(V_{CJ})}{d\, V} \tag{8}$$

The JWL CJ isentrope and the basis Rayleigh line (locus of material states in shock and steady-state reaction zone) are, by Equations (7) and (8), tangent in the p-V plane at the CJ state. Third,

$$\Delta = E_S^{\,J}(V_{CJ}) - E_S^{\,J}(V_f) \tag{9}$$

The volumetric internal energy differences on the JWL and the basis CJ isentropes between the CJ relative volume and the final "basis" relative volume are equal.

In addition to these mathematical constraints, following Lee et al.,[11] we impose two further restrictions on allowed fits. First, ω must be in the range $0.2 \leq \omega \leq 0.4$, and second, the linear coefficients must be positive.

The following solution procedure provides unique values for the six JWL EOS parameters; these values constitute a fit that closely reproduces the basis CJ isentrope and precisely satisfies the three constraints above subject to the two cited restrictions. First, we

select a threshold relative volume V_t in the range $10 < V_t < V_f$ such that for $V > V_t$, $p_S(V)$ is well represented as a constant γ gas with $1.2 < \gamma < 1.4$. Since $V_t > 10$, we know that for $V > V_t$ the exponential terms in $P_S^J(V)$, Equation (6), are completely negligible. Therefore, for $V_t < V < V_f$, we perform a least squares fit of the final term for $P_S^J(V)$ in Equation (6) to the basis isentrope and thereby determine C and ω. The resulting value for ω satisfies the first restriction stated above, assuring a reasonable value for the low pressure adiabatic exponent.

To determine the remaining four JWL EOS parameters, we next use constraining Equations (7) and (8) to express the two undetermined linear coefficients, A and B, as functions of the two unknown nonlinear coefficients R_1 and R_2, and known quantities. We use these expressions and the third constraint, Equation (9), to obtain an implicit equation for R_1 as a function of R_2. In this step we make use of the fact that $E_S^J(V_f)$ is a calculable number because $V_f > V_t$ and C and ω have been evaluated. To obtain an additional relation between R_1 and R_2 completing the system of equations and allowing us to determine the four unknown coefficients, we require that the RMS deviation between the basis and JWL CJ isentropes be a minimum.

The solution procedure described above determines the six JWL EOS coefficients. The only step that is not objective is the selection of V_t. The fitting procedure is completed by calculating E_0 from its defining equation and verifying that all the linear coefficients are positive. Negative coefficients were not encountered with this fitting procedure and the basis CJ isentropes used in this work, but they can arise. If they do, appropriate modifications must be made either to the basis isentrope or to the fitting procedure.

Discussion

Although the present fitting procedure provides unique values for the JWL EOS coefficients and closely reproduces the basis CJ isentrope, other equally valid procedures producing different unique fits are

possible. For example, another measure of goodness of fit between pressures on the basis and JWL CJ isentropes could be invoked or, more fundamentally, a different property of the basis CJ isentrope such as the adiabatic exponent could be matched. In the present approach the γ - V behavior is not controlled; it is a result of the fitting procedure. The motivation for the present approach is our belief that the locus of the CJ isentrope is the most important parameter for estimating the performance of an HE in a simulator.

The first two constraints, Equations (7) and (8), are the same as those used in fitting the JWL EOS parameters from cylinder test data.[11] The energy constraint, Equation (9), however, is different. The resulting E_0 value in our procedure is completely consistent with the JWL EOS form and, in the cases to which it is applied here, with thermodynamic equilibrium calculations to V_f. However, we do not invoke the condition that E_0 be equal to the available chemical energy estimated from the product composition at some point in the equilibrium calculations and from standard heats of formation of the products and reactants. In fact, our E_0 may be less or more than the available chemical energy. This difference between the present technique and the cylinder test techniques for fitting JWL parameters reflects the behavior of the products between $V_f \approx 200$–1000 and $V = \infty$, occuring mostly at $p < 1$ atm, and is judged to be of no concern in DNA NWE simulator hydrocode calculations with JWL fits from either method.

The fitting procedure developed here is believed to be general and useful in a number of situations. The optimization approach generates unique values for all the JWL EOS parameters and can be adapted to other characterization data bases such as cylinder test results. The specific method used here with the CJ isentrope is independent of the source of the basis CJ isentrope and is rapid and straightforward to apply. Thus, it provides a convenient means for transforming the results of thermodynamic calculations based on nonideal EOSs with explicit chemistry into the computationally preferable nonexplicit JWL form. The resulting JWL EOS is as consistent as possible with the explicit EOS in the important

region on and near the CJ isentrope and provides a good initial computationally convenient characterization for a new HE in the absence of experimental data.

SECTION 3

NA/NP CHARACTERIZATION

Initial JWL coefficients were developed for a representative member of the NA-NP family, liquid explosives similar in performance to nitromethane (NM). The specific composition selected for study was a blend identified in prior commercial studies[13-15] as offering a favorable combination of initiation, performance, cost, and handling properties. Throughout this report, we use the term NA/NP to refer to this baseline blend, the present study material.

The tasks performed in developing JWL coefficients for NA/NP included development of initial properties and handling procedures for the study material; Lagrange gage detonation and shock initiation experiments and Lagrange analysis to determine peak, CJ, and initial CJ release isentrope states; TIGER calculations to extend the CJ release isentrope to large volumes; and determination of JWL coefficients. The following subsections present the results of these tasks and conclude with a discussion.

3.1 DESCRIPTION OF MATERIAL

Background

NA/NP belongs to a family of liquid solutions consisting of nitric acid, nitropropane (NP), and water. It is convenient for this report, and in practice, to treat the nitric acid and the water as a single component, an aqueous solution of nitric acid referred to here as NA. The properties of the NA-NP family relevant to its potential use as an HE were initially examined by Mallory under contract to Trocino and Associates.[13,14] Trocino later compiled Mallory's results as well as practical data and handling requirements for NA and NP in a very useful reference on NA-NP as an HE for military and commercial applications.[15]

Mallory's investigations, briefly summarized below, are the only research on NA-NP of which we are aware other than this work.

For NA-NP blends oxygen-balanced to CO or CO_2, Mallory first examined the effect of NA concentration, over the practical range from 60 to 90 wt%, on properties including gap test sensitivity, plate dent, detonation velocity, and NP separation temperature (solubility limit).[13] This work indicated that the CO_2 balanced compositions with acid concentrations near or slightly greater than 65% were stable solutions at normal temperatures and had detonation velocities and gap sensitivities slightly greater than neat NM. Increasing acid concentrations led to lower separation temperatures, greater detonation velocities, and much greater gap sensitivities, with the last apparently exceeding that of tetryl for some blends with NA concentrations of 90%. A major conclusion was that the abundant, inexpensive, manageable NAs with relatively low acid concentrations near 65%, in CO_2 balanced mixtures, produced NA-NPs with a collection of good HE properties.

In his second report,[14] Mallory focused on the low concentration NAs and examined NA-NP properties including cap and booster sensitivity, mixture variation effects, calculated CJ pressure and detonation velocity based on the Kamlet and Jacobs Ruby code approximation method,[16] and performance in shaped charges. This work identified Baumé 42 NA (concentration = 67.18 wt%) and NP, CO_2 balanced by blending 2.24 parts NA and 1 part NP by volume, as the most promising from all aspects. This blend, described below, is NA/NP, the present study material.

The results of the detonation experiments and calculations performed here are in good agreement with Mallory's results. Specific comparisons are given as the results are presented.

Present Study Material

The present study material is Baumé 42 NA and NP blended to be oxygen balanced to CO_2. Note that our specification of the composition of this blend is slightly different from Mallory's. Below we discuss

Baumé 42 nitric acid, the NP used in this work, the NA/NP oxygen balance condition and resulting composition, the mixture precision for our NA/NP, the initial density of our NA/NP, and our calculated heats of formation and detonation for NA/NP.

Baumé 42 nitric acid is an industrial grade aqueous solution of nitric acid and is available from several manufacturers. In a Du Pont technical bulletin,[17] it is termed weak nitric acid, technical; at 15.6°C (60°F) it is stated to be (nominally) 67.18 wt% nitric acid with a specific gravity of 1.4087 and a temperature correction factor of 0.00084/°F. (Because the Baumé scale is a measure of density, the correspondence between an actual Baumé reading and the associated acid concentration is a function of temperature; however, in this case the Baumé 42 value is being used simply as a label for NA of concentration 67.18 wt%, and this association is therefore valid at all temperatures.)

On the basis that Baumé 42 NA is 0.6718 by weight pure nitric acid and 0.3282 water, we calculated the following molecular composition and heat of formation. Using the 1959 atomic weight scale (O = 16) in conformity with Mallory's procedures, there are 1.7088 molecules of water per molecule of pure nitric acid in Baumé 42 NA. The heat of formation, including heat of dilution, is -162.63 kcal/mole, in agreement with Mallory's value less the heat of dilution.

Baumé 42 NA appears to be one of the least expensive and most easily handled forms of nitric acid. We encountered no difficulties in storing or handling it, although NAs of higher or lower concentration might present additional problems related to toxicity or activity respectively. In the Lagrange gage experiments at our remote site, it was convenient to perform the NA handling operations outdoors while wearing conventional protective gear including gloves, face shields, and disposable overgarments. Over the preparation periods for our experiments (24 hours or less), we detected no reaction between the NA and our anodized aluminum gages or the polyethylene vessels we used for temporary NA storage or weighing containers.

The NP used here was furnished by the International Minerals and Chemical Corporation, IMC Chemical Group, 666 Garland Place, Des Plaines, IL 60016 (sample number DP-8562-TD). It is described as a mixture of the two stable isomers for each of which properties are given in two technical notes.[18,19] We attributed the following properties to the mixture by averaging values for the isomers. Specific gravity at 25°C = 0.992. Density correction/°C = 0.0011 Mg/m^3°C. Heat of formation = -41.7 kcal/mole. (In some TIGER calculations, we used the value for the isomer NP-2, namely, -43.2 kcal/mole, estimated to have a negligible effect on the results.)

We found NP to be easy to handle. In our preshot preparations performed outdoors, no special procedures were used other than preventing contact between the NP and those polymers for which it is a strong solvent. We stored it in polyethylene containers and used PVC or polyethylene foil or wax in our experimental assemblies to isolate it from components it could dissolve.

NA/NP is said to be oxygen balanced to CO_2 in that the reactant composition is chosen to produce only the stable detonation products CO_2, H_2O, and N_2. For NA/NP, including the water in the NA, the CO_2 oxygen balance equation is

$$3HNO_3 + 3(1.7088)H_2O + C_3H_7NO_2 \rightarrow 3CO_2 + [5 + 3(1.7088)]H_2O + 2N_2$$

Given the CO_2 oxygen balance equation, the molecular weights of pure nitric acid and NP, and the concentration of pure nitric acid in Baumé 42 NA, we can calculate the composition for NA/NP. The result is that NA/NP is 3.158 parts NA to 1 part NP, by weight. Alternatively, the weight fraction of NA in NA/NP is 0.7595.

We prefer to specify the NA/NP composition by weight because these values are independent of temperature. The composition by volume, as given by Mallory, has a slight temperature dependence. For example, at the temperature of our experiments, 29°C, the composition by volume, calculated from the density and specific gravity information cited above for NA and NP, is 2.251 parts NA to 1 part NP.

We mixed our NA/NP from preweighed stocks of NA and NP having the weight ratios given above. The stocks were weighed on an electronic balance with a precision of 0.1 g. The balance was calibrated after each weighing with a collection of standard weights chosen to have an aggregate weight about equal to the stock plus container weight. These aggregate weights were between 1 and 5 kg. We estimate that the weights of each component stock were controlled to accuracies better than 0.1% by this method. Therefore, the present NA/NP study material is judged to be well within 0.5% of the calculated oxygen balance condition. (The densities of the NA and the NP were checked and agreed with the nominal values given previously within 0.3%.)

We measured the density of the mixed NA/NP in the Lagrange gage experiments to be 1.252 ± 0.005 Mg/m^3 at 29°C. We used this value in our calculations although the last significant figure is not reliable. From the nominal densities, specific gravities, and correction factors for NA and NP, and ignoring mixing effects on volume, we calculate a density of 1.260 Mg/m^3 at this temperature, in good agreement with our measurement. If we use the measured rather than nominal densities for NA and NP and apply the temperature corrections, the calculated density is 1.256 Mg/m^3 in even better agreement with the measurement. From this we conclude that the present solution of Baumé 42 NA and NP is essentially ideal, although Mallory reports a detectable volume interaction on mixing. The calculated NA/NP density given by Mallory is 1.272 Mg/m^3, which is higher than our calculations but pertains to NA/NP at a lower temperature.

From the heats of formation for reactants given previously, we calculate a heat of formation of -176.53 kcal/g and a maximum heat of detonation of 911 kcal/g. Because NA/NP is oxygen balanced to CO_2, the detonation product composition is nearly constant throughout the product expansion; thus the maximum heat of detonation is close to the effective heat of detonation of NA/NP.

3.2 LAGRANGE GAGE EXPERIMENTS

Three large-scale multiple Lagrange particle velocity gage experiments were performed on NA/NP. Two were detonation experiments, and the third was a shock initiation experiment. The targets, initiation systems, and results for these experiments are described below.

NA/NP Target Chambers

The target chamber design used in all the NA/NP experiments is shown schematically in Figure 5. The chambers were fabricated from Pyrex beakers and were approximately 0.19 m in inside diameter by 0.12 m high. Precision ground parallel surfaces on the tops and bottoms ensured that the gage elements were parallel to the HE driver face to within 0.02 mm. The joints and the tops of the linen phenolic gage blocks were sealed with wax to protect against the solvent effects of the NP. A 1.42-mm-thick PMMA plate, protected on the inside by 0.01-mm-thick PVC foil, separated the NA/NP from the driver HE. Each chamber contained a fill tube and a bleed tube to remove air bubbles. A photograph of one of the chambers is shown in Figure 6.

The filling procedure was to mix the preweighed stocks of NA and NP at the time of the experiment. The target chamber was filled, and the experiment performed, in the orientation indicated in Figure 5, that is, with the gage block down. Therefore, it was critical to avoid entrapped air. Air bubbles were removed through the bleed tube, and fluid heads were left in each tube to account for possible leaks, though none were detected.

The EPV gages in the NA/NP experiments were hard anodized. Anodization was considered particularly important in these experiments because NA/NP, unlike other HEs we have examined, is an electrical conductor in the unreacted state. Because of difficulties encountered by the vendor in making good connections to each of the gages premounted on the gage block, the gages had to be anodized and stripped twice before satisfactory coatings were obtained. Consequently, the gages in these experiments were somewhat thinner and more embrittled than

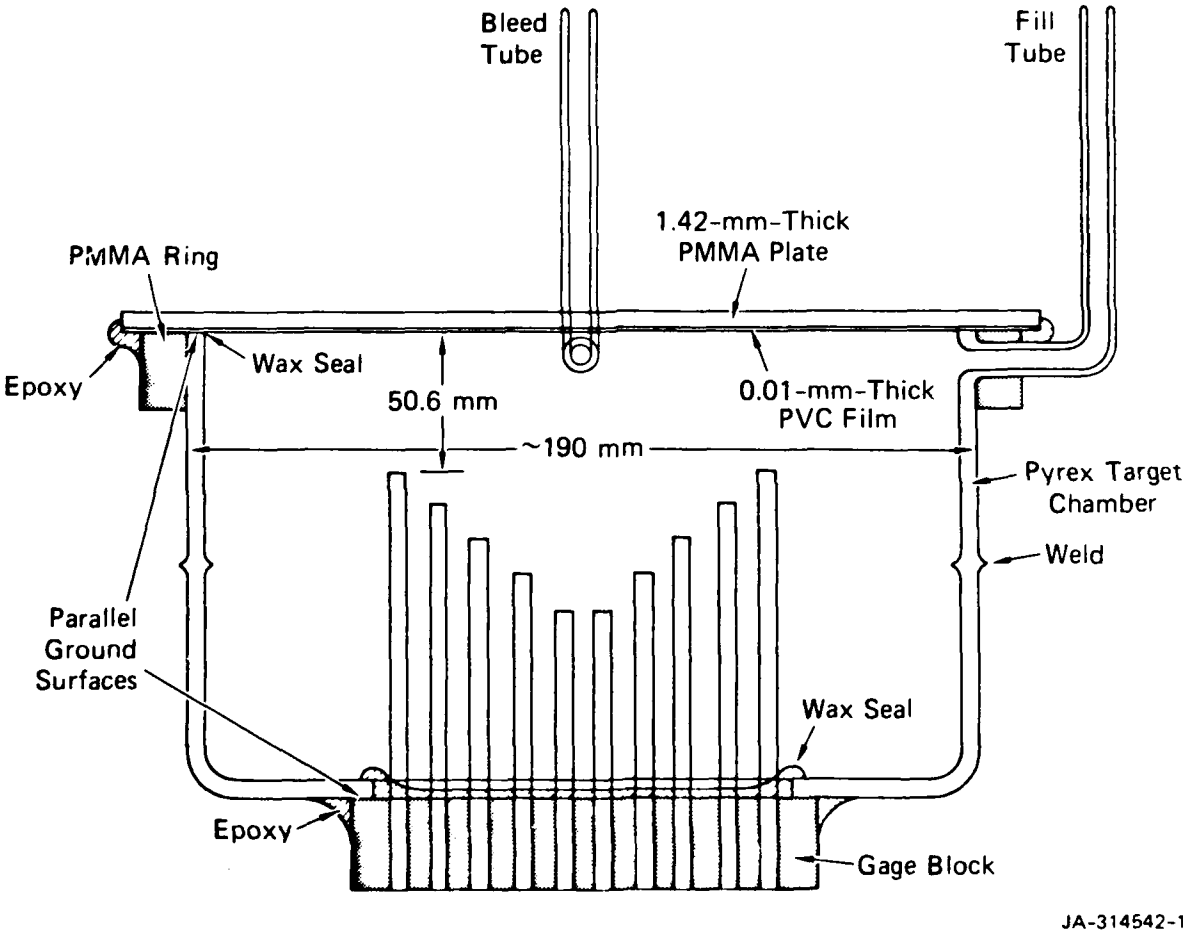

Figure 5. NA/NP Lagrange gage target chamber design (schematic). Additional gage block details are shown in Figures 3 and 4.

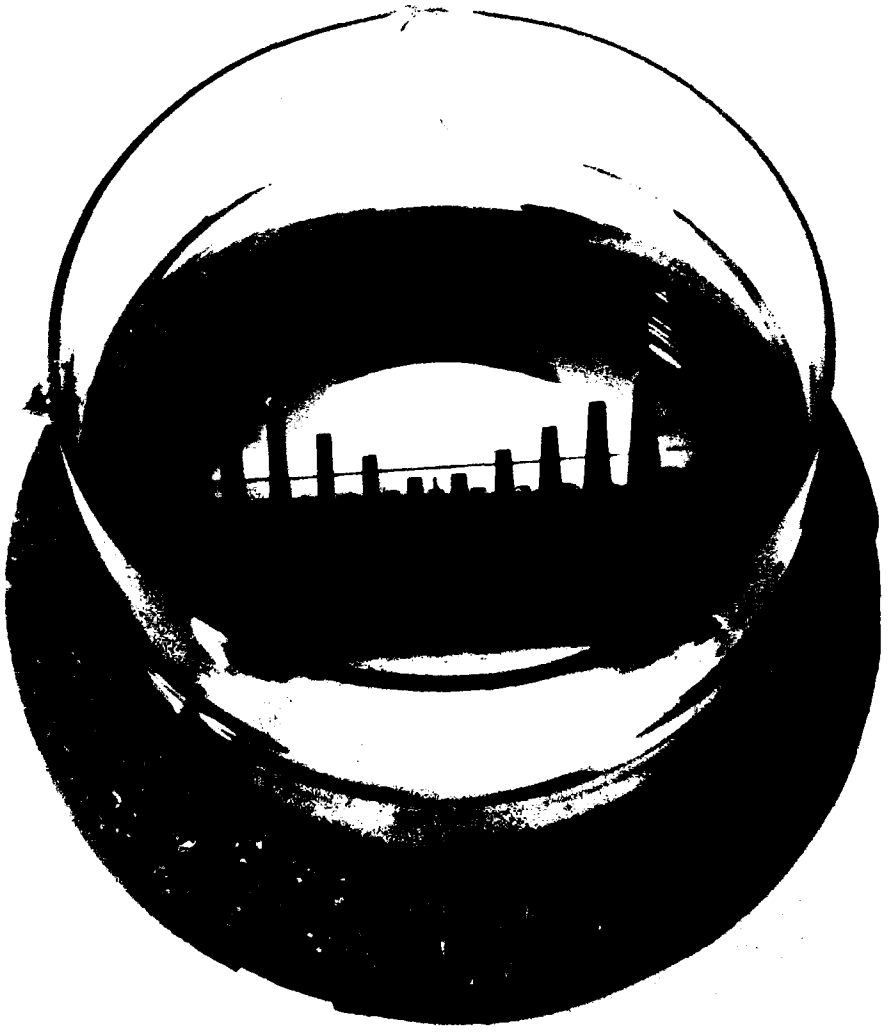

JP-4015-78

Figure 6. NA/NP Lagrange gage target chamber.

normal. In the later NPN experiments, a special holding fixture was built and the gages were anodized before they were attached to the precision gage blocks. No difficulties were encountered with this system.

Initiation Systems

The NA/NP experiments were performed with 0.2-m-diameter (8 inch) HE drivers and P-80 plane wave lenses. We selected the driver HE as follows. We assumed that, for rapid and reliable initiation of steady detonation in NA/NP, the pressure amplitude of the initial shock induced in the unreacted NA/NP by the driver (ignoring the spike in the driver) should be approximately equal to the predicted CJ pressure. This condition is discussed further in regard to the NPN experiments in Section 4.2.

We very approximately estimated a Hugoniot for unreacted NA/NP by scaling the Hugoniot pressures of unreacted NM according to the density difference between NA/NP and NM. We then graphically performed an impedance mismatch calculation for TNT and Baratol drivers using their estimated products CJ release isentropes, as shown in Figure 7. The shock amplitude estimated for a TNT driver was 158 kbar. (The CJ pressure estimated by Mallory with the Ruby code approximation method of Kamlet and Jacobs was 152.84 kbar.[14]) We therefore selected TNT for the driver HE for the detonation experiments. The effect of the 1.42-mm-thick PMMA plate was neglected because of the approximate nature of these calculations.

By the same techniques, a Baratol driver was estimated to induce a much lower shock pressure, well below 100 kbar, in unreacted NA/NP (see Figure 7). A Baratol driver was therefore used in the initiation experiment to generate initial information on the shock-to-detonation transition (SDT) in NA/NP.

Experimental Results

Three multiple Lagrange particle velocity gage experiments were performed on NA/NP. Shots 1 and 2 were detonation experiments to observe the shock compression, reaction zone, and initial adiabatic

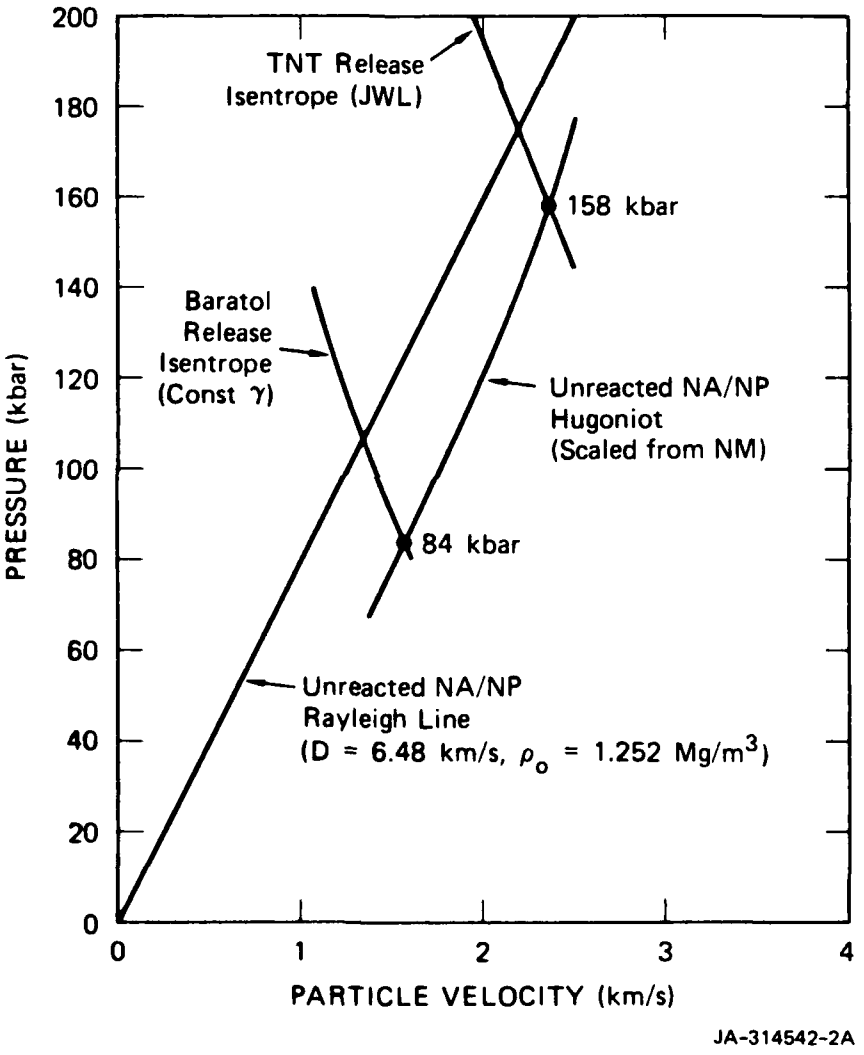

Figure 7. Pressure-particle velocity plots for estimating initiation pressures in NA/NP experiments.

All curves estimated; do not use for other applications.

expansion states during steady planar detonation in NA/NP. Shot 3 was a preliminary SDT experiment. The results of the detonation experiments are considered first.

Both detonation experiments provided a good data return. However, because improved instrumentation settings were used in the second experiment, only data from that experiment were selected for quantitative analysis. Data were obtained from all gages except 10, which was found to be open before the experiment. The oscillographs from the second NA/NP detonation experiment are shown in Figure 8.

Vertical sensitivities for the oscillographs in Figure 8 are 500 mV/division; horizontal sensitivities are 1 μs/division. Short gaps in the profiles are the repetitive beam blanks used to time-correlate the records.

For the first several microseconds after shock arrival, the quality of the gage signals from this experiment is the best that we have seen with this technique (see discussion in Section 4.2). The records contain exceptionally little noise either before or after shock arrival.

There are only two negative features in these data from a measurement point of view. First, some of the records (for example, those from gages 2, 3, and 8) show a slight ramping before shock arrival. The cause is not known, but may have to do with the conductivity of the unreacted NA/NP. Second, exceptionally large perturbations occur on a given record when the next downstream gage enters the flow about 2 μs later. This effect is so pronounced that it determines the useful recording time of the EPV gages in this experiment. The cause is again not known, but may be partial breakdown of the anodizing.

The nine particle velocity histories calculated from the oscillographs in Figure 8 are shown in a composite plot in Figure 9. For clarity, the histories from each half of the target are also shown separately in Figure 10. The structure of these histories is considered in the analysis presented in the next subsection.

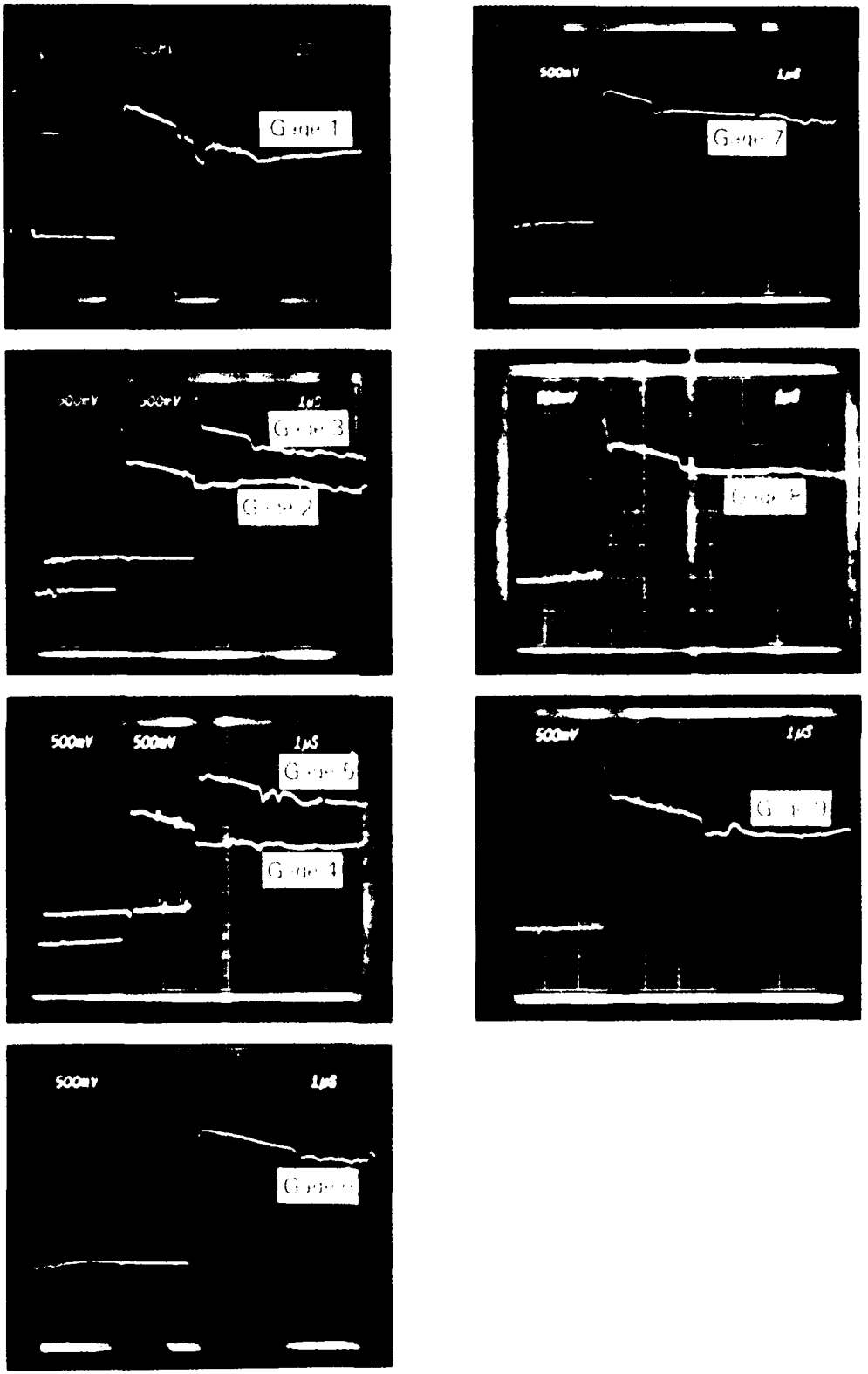

JP-4015-79

Figure 8. Lagrange particle velocity gage records from second NA/NP experiment.

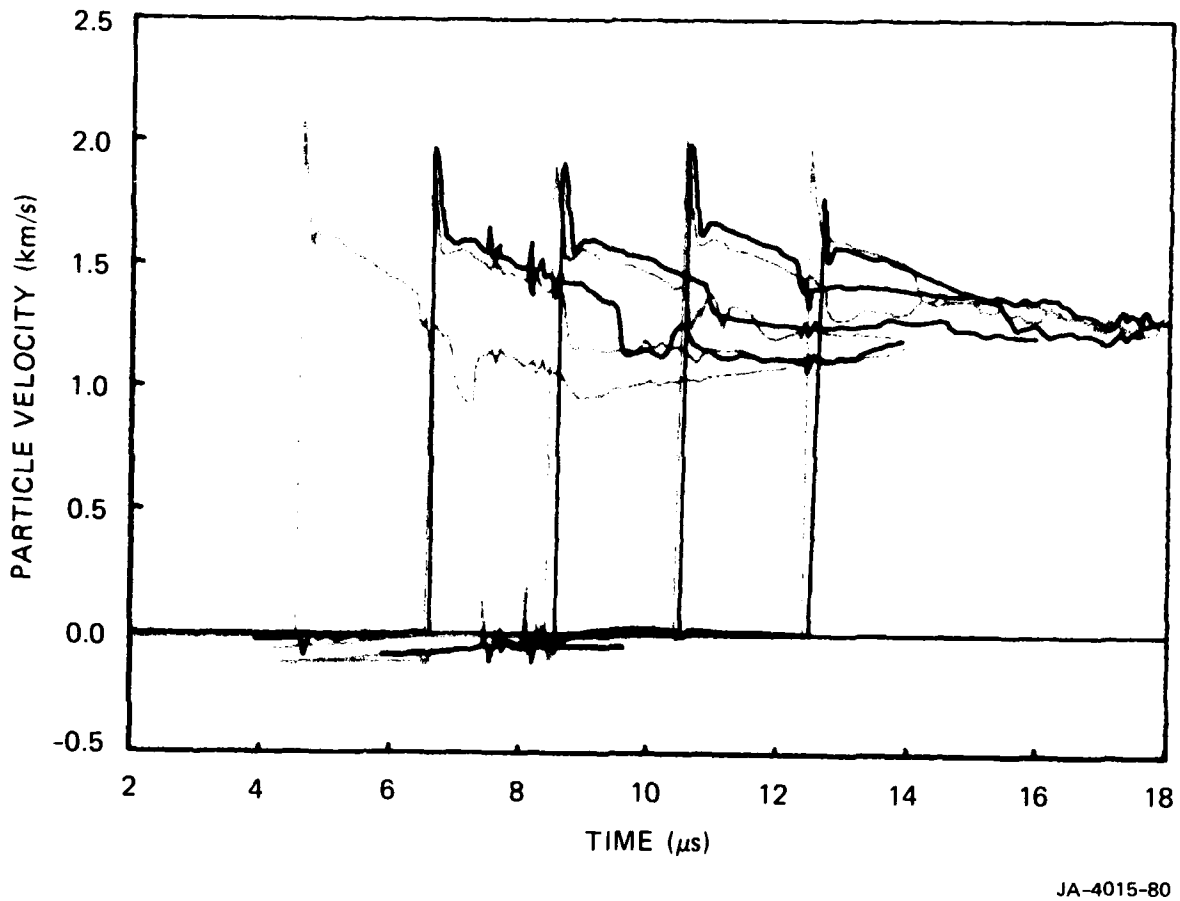

Figure 9. Lagrange particle velocity histories, gages 1-9, second NA/NP detonation experiment.

The histories for gages 6-9 are shown gray.

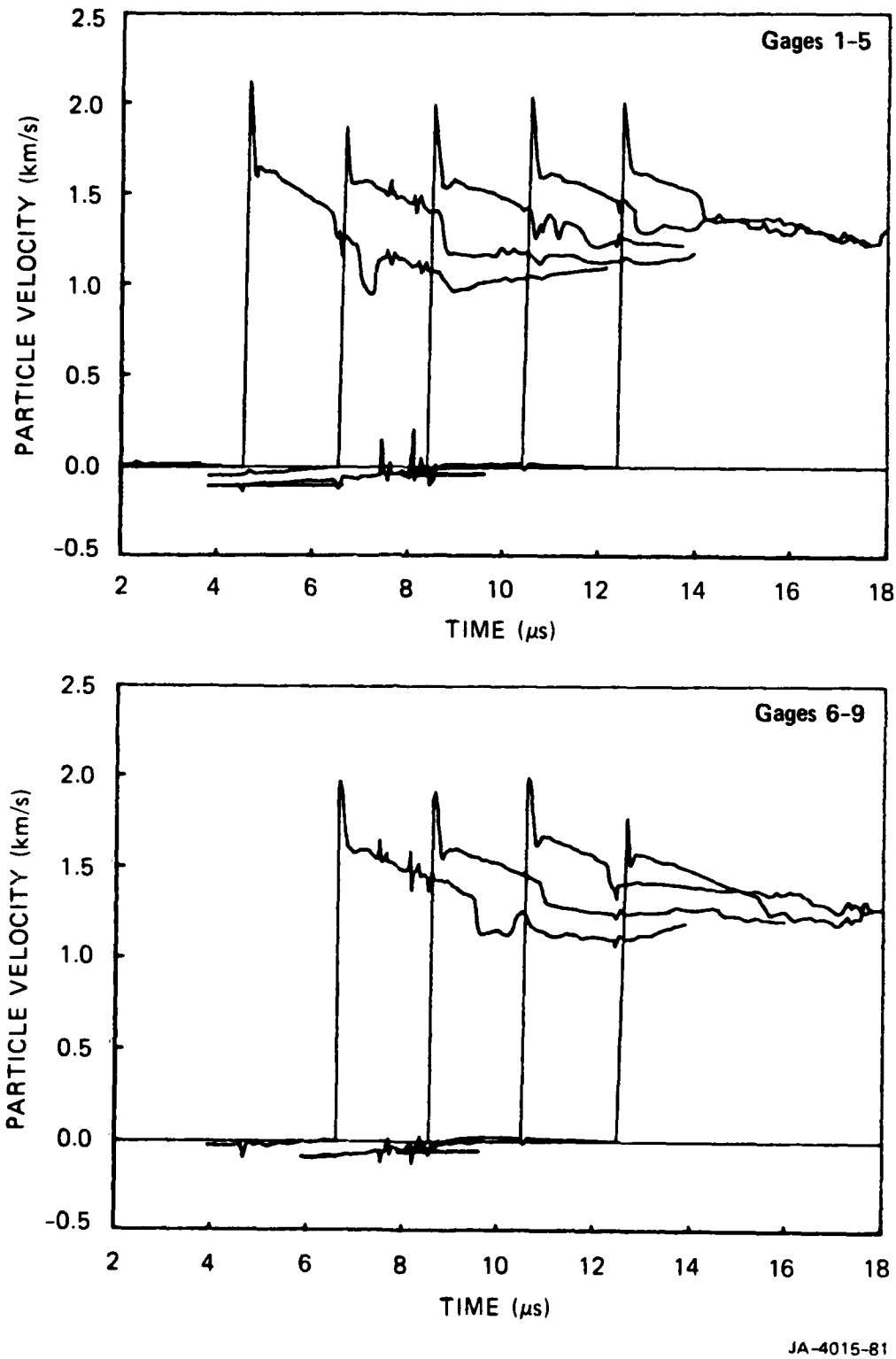

Figure 10. Lagrange particle velocity histories for each half of target, second NA/NP detonation experiment.

The SDT experiment produced unusual results. The particle velocity histories are shown in a composite plot in Figure 11 and for each half of the target in Figure 12. These histories clearly are not reproducible across the target, perhaps indicating nonuniform or marginal initiation. The peak particle velocity amplitudes are less and the structures of both the individual profiles and the flow evolution are qualitatively different from those for the detonation experiment. The histories from gages 1-5 show no obvious pattern; those from gages 6-10 seem to consist of a fairly steady spike followed by a growing pulse. Histories 6-10 could be argued to be tending toward the shape of the profiles in the steady detonation experiments.

The SDT experiment is not analyzed further here because the data are ambiguous and because the primary objective of this task was to generate JWL coefficients for NA/NP. However, the results indicate that the SDT process in NA/NP may have unusual features, such as a surprisingly long time to reach steady detonation and possibly a complex hydrodynamic phenomenology. These features could be significant in DNA NWE simulator applications and should be investigated.

3.3 LAGRANGE ANALYSIS

The particle velocity histories from the second NA/NP detonation experiment, Figures 9 and 10, were compared to obtain a single data set for Lagrange analysis. The first step was to discard the history from gage 1 because this record is anomalously higher than the other records, and there is no redundant gage history to corroborate it. The remaining records were then combined and idealized as follows.

Data later than about three microseconds after shock arrival were discarded because of the cross talk from downstream gages discussed in the previous subsection. (The profiles were extrapolated slightly beyond the first occurrence of the perturbations if we judged the data warranted it.) Redundant profiles were then averaged and smoothed by hand. Finally, the four resulting histories were idealized in two ways. In the first, the dip occurring after the first rapid spike was included; in the second, it was omitted. (The dip was omitted by

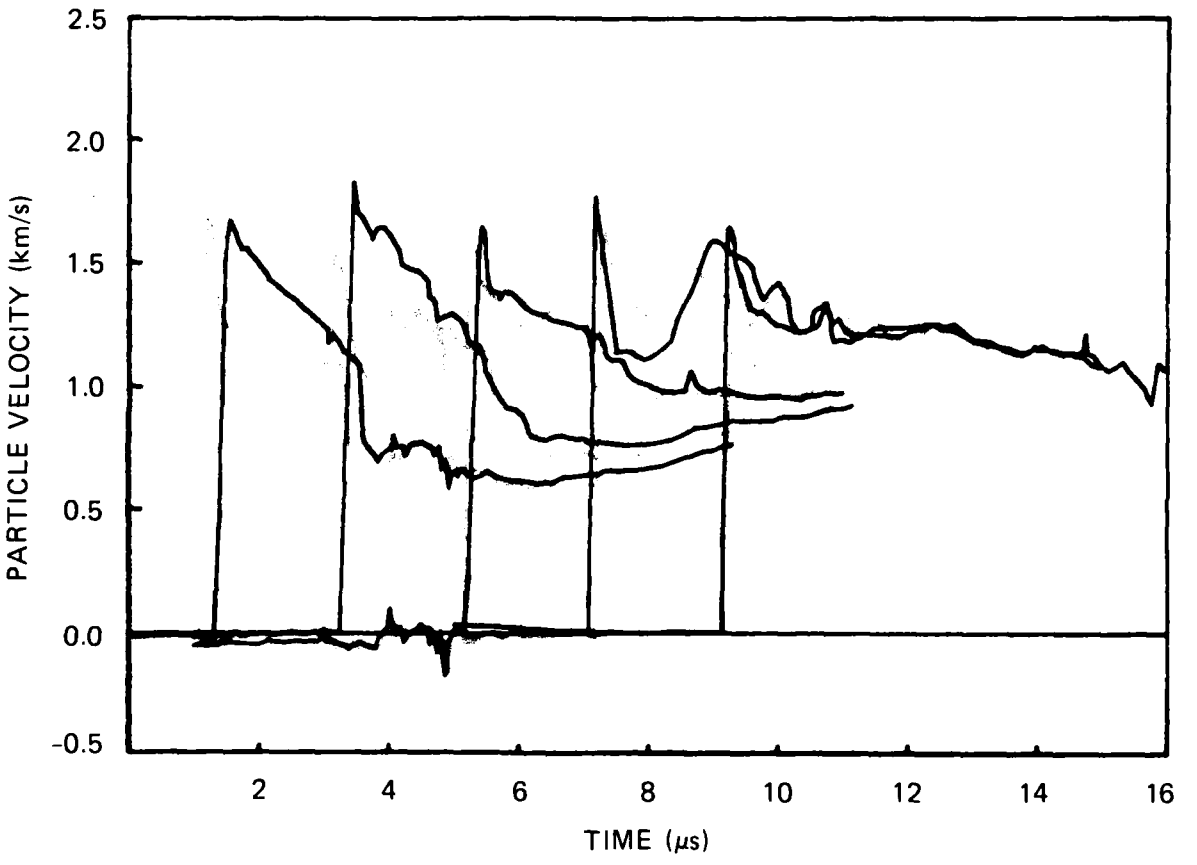

Figure 11. Lagrange particle velocity histories, gages 1-10, NA/NP initiation experiment.

The histories for gages 6-10 are shown gray.

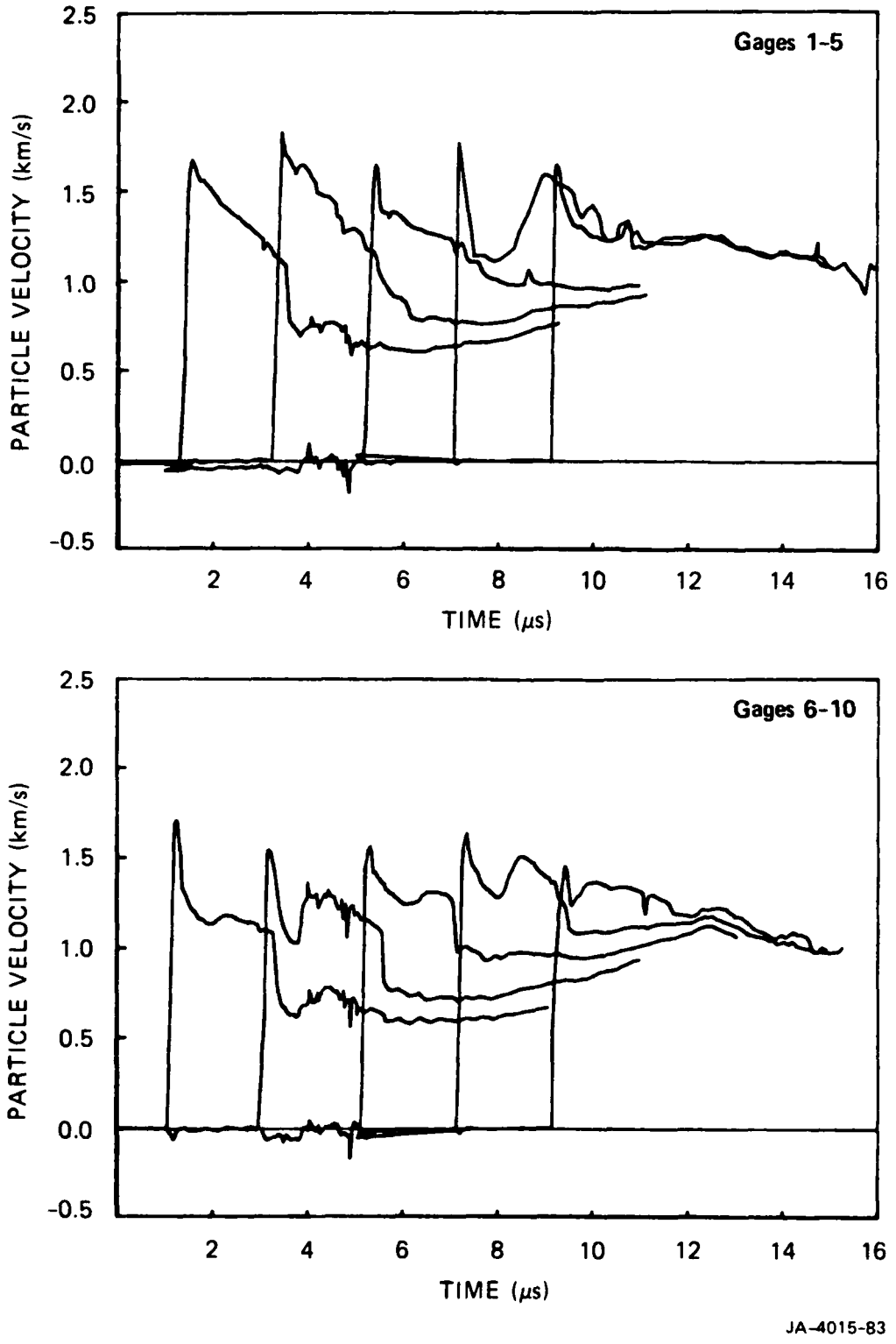

Figure 12. Lagrange particle velocity histories for each half of target, NA/NP initiation experiment.

extrapolating the late time, slow decay portion of the history backward in time until the falling edge of the spike was intersected.) Although the dip is quite apparent in the original oscillographs (Figure 8) and the digitized histories (Figures 9 and 10), we chose to omit it in one idealization because we were not sure we would be able to incorporate it in a reactive hydrodynamic model of the detonation process in NA/NP. The resulting profiles for both idealizations are shown in Figure 13.

We were now in a position to characterize the reactive flow observed in NA/NP. Both idealizations included a spike propagating at the steady velocity of 6.48 km/s followed by a slightly dispersive rarefaction, in conformity with the qualitative behavior expected based on the ZND detonation model. The detonation velocity of 6.48 km/s is in excellent agreement with the value of 6.50 km/s inferred from a plot of detonation velocity versus acid concentration presented by Mallory.[13]

The precise starting point for the nonsteady flow, that is, the CJ point, cannot be resolved. Therefore, for the idealization including the dip, we arbitrarily select it to be the maximum particle velocity reached after the dip, and for the idealization omitting the dip, we choose it to be the apparent discontinuity in decay rate after the spike. A surprising result was that NA/NP has a significant reaction time: 0.2 μs for idealization omitting the dip and 0.55 μs with the dip included and interpreted as being in the reaction zone.

The two idealized data sets shown in Figure 13 were Lagrange analyzed using the SRI GUINSY code discussed in Section 2.2 The results are shown in the p-v plane in Figure 14. This figure represents the loci of p-v paths followed by four different particles having the Lagrange coordinates of the last four gage planes in the second NA/NP experiment. The CJ point indicated is an average of the values on the middle two gage planes for the two idealizations.

Figure 14 represents the results of the present Lagrange gage and analysis characterization of the steady detonation process in NA/NP. It shows the Rayleigh line followed in the shock compression to the maximum pressure resolved by the gages (less than the ZND spike pressure because

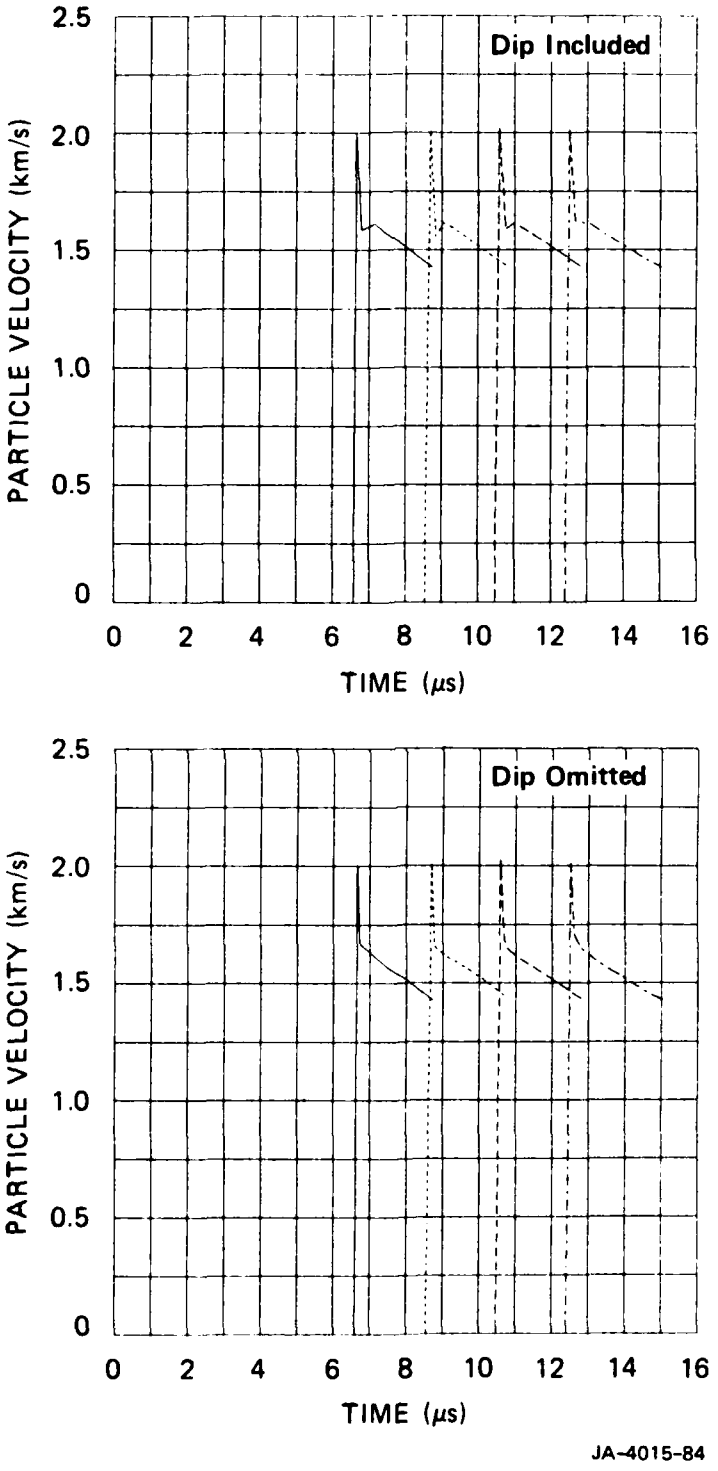

Figure 13. Idealized particle velocity histories for Lagrange analysis, second NA/NP detonation experiment.

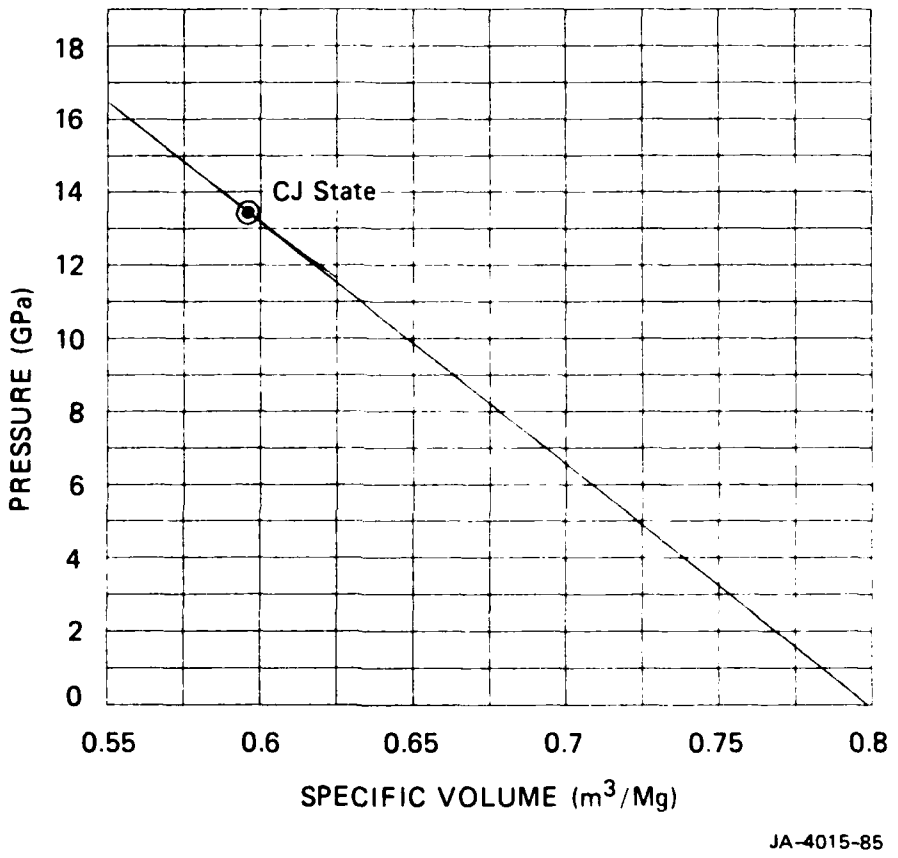

Figure 14. Lagrange analysis calculations of pressure-specific volume compression and release paths at four Lagrange coordinates, second NA/NP detonation experiment.

of the response time of our EPV gages), the reactive release states also lying on the Rayleigh line, the CJ state, and the initial adiabatic release states. The CJ state variables are D = 6.48 km/s, p = 13.3 GPa, v = 0.5986 m^3/Mg, V = 0.7494, u = 1.64 km/s, and the adiabatic exponent (logarithmic derivative of isentrope) γ = 2.99.

3.4 TIGER CALCULATIONS

TIGER calculations using the BKW and the JCZ3 EOSs were performed to extend the NA/NP CJ adiabatic release path to large volumes by modeling the release process as being isentropic. First, we used both EOSs to predict the CJ state as well as the CJ release isentrope. The results in the p-v plane are shown in Figure 15, on a log-log scale, along with the Lagrange gage and analysis CJ state and a release path discussed later in this section.

The CJ state variables from the two calculations are listed below. From the BKW calculation, D = 7.14 km/s, p = 16.40 GPa, v = 0.5937 m^3/Mg, u = 1.83 km/s, and γ = 2.90. From the JCZ3 calculations, D = 6.12 km/s, p = 11.30 GPa, v = 0.6060 m^3/Mg, u = 1.48 km/s, and γ = 3.14.

The CJ state calculated by JCZ3 more closely matches the Lagrange gage and analysis results. A more significant difference, however, for our purposes, is that the JCZ3 calculation extends to large volume expansions so we can apply the JWL fitting procedures described in Section 2, whereas the BKW calculation does not. The difference is believed to result from the construction of TIGER and its interaction with this particular detonation problem and not to reflect any difficulty with the BKW EOS. Because of the limited range of the present BKW calculations, we elected to use JCZ3, in the manner described below, to match the Lagrange gage and analysis results and extend the CJ release adiabat to large volumes.

We matched the experimental results simply by initiating the TIGER/JCZ3 isentrope calculations at a p-v point on the experimental release path. We used both the CJ point and the final point on the CJ

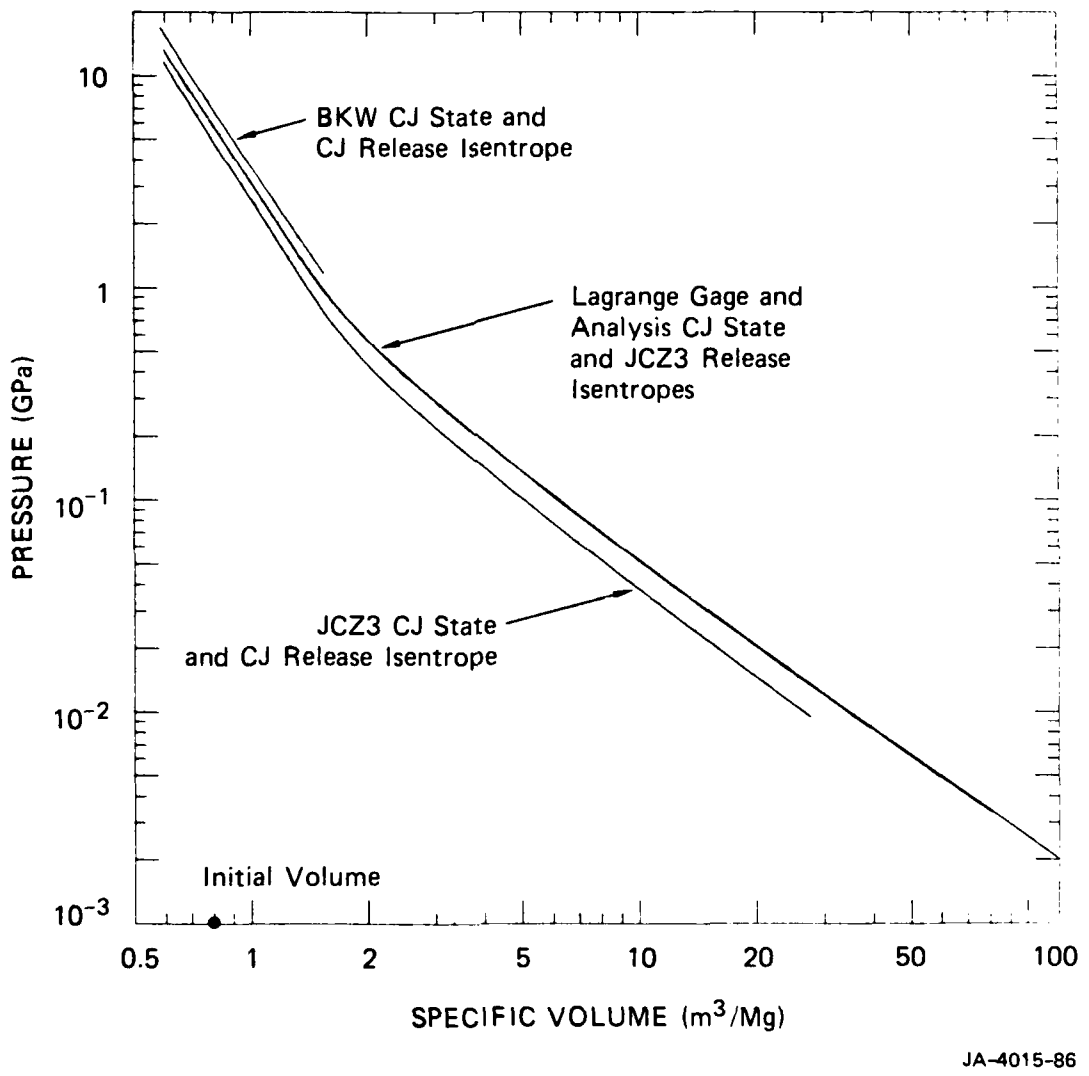

Figure 15. TIGER BKW and JCZ3 calculations of NA/NP CJ state and release isentrope.

release adiabat. In the regions of overlap there was no detectable difference between either isentrope or the experimental release path. Both isentropes are shown in Figure 15 and are indistinguishable. For computational convenience, we selected the isentrope centered on the experimental CJ state to generate initial JWL coefficients for NA/NP.

3.5 CALCULATION OF JWL COEFFICIENTS

Initial JWL coefficients for NA/NP were calculated by applying the method described in Section 2 to the basis NA/NP CJ release adiabat taken to be the JCZ3 CJ isentrope through the experimental CJ state (Figure 15). The V_t value was 30. The resulting JWL coefficients are listed in Table 1.

Table 1. NA/NP JWL coefficients.

Initial State	CJ State				Equation-of-State Parameters					
ρ_0 (Mg/m^3)	p (Mbar)	D (cm/μs)	E_0 (Mbar)	Γ	A (Mbar)	B (Mbar)	C (Mbar)	R_1	R_2	ω
1.252	0.133	0.648	0.0697	2.991	7.554	0.1962	0.012717	6.366	1.810	0.285

The JWL and basis CJ release paths in the p-V plane are shown in Figure 16. Figure 17 shows the adiabatic expansion coefficients, γ, the logarithmic derivatives of the release paths in Figure 16. The correlation between the isentropes in Figure 16 is controlled by the fitting process; the behavior in the γ-V plane, Figure 17, is not constrained.

The NA/NP JWL coefficients in Table 1 are the major result of the research described in this section and can be used in DNA hydrocode calculations to predict the performance of NA/NP in NWE simulators. Additional discussion is given in the next subsection, and recommendations regarding the use of NA/NP and further research are given in Section 5.

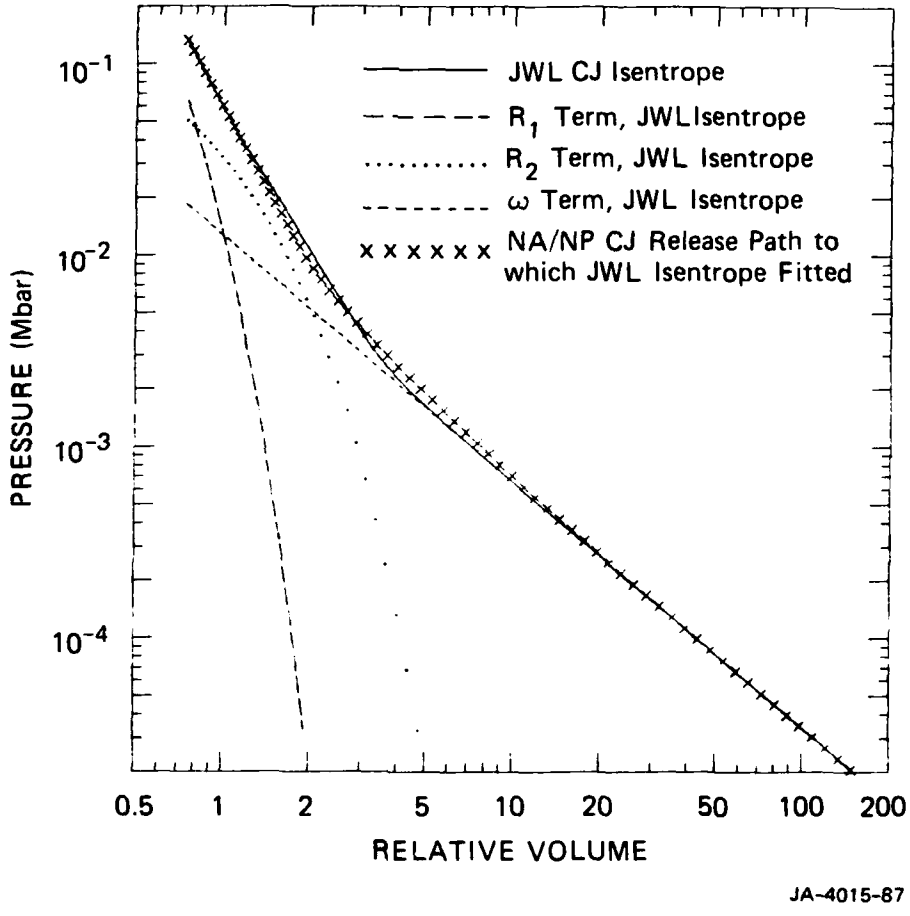

Figure 16. JWL CJ release isentrope for NA/NP.

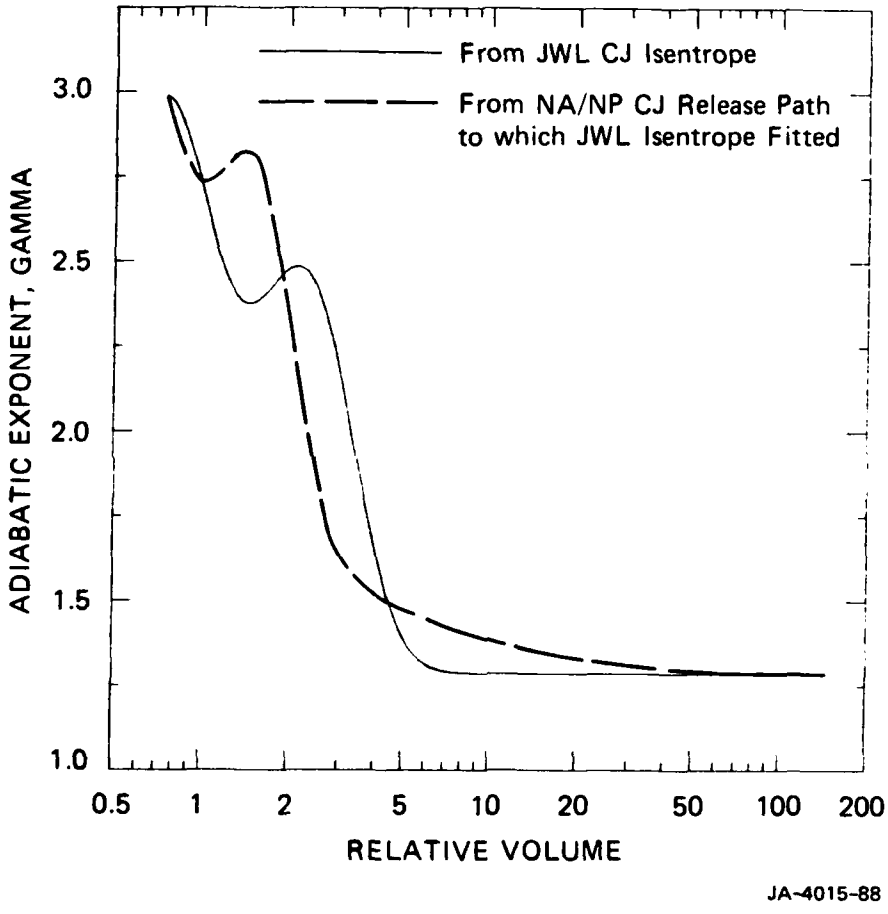

Figure 17. Gamma versus relative volume for NA/NP JWL CJ release isentrope and NA/NP CJ release isentrope being fitted.

3.6 DISCUSSION

The present work indicates that the performance of NA/NP in many applications can be expected to be comparable to, or slightly better than, that of NM. This conclusion is based on a comparison between the JWL CJ isentrope from this work and that of NM from cylinder tests.[12] These isentropes are shown in Figure 18, and the corresponding JWL coefficients are given in Table 2.

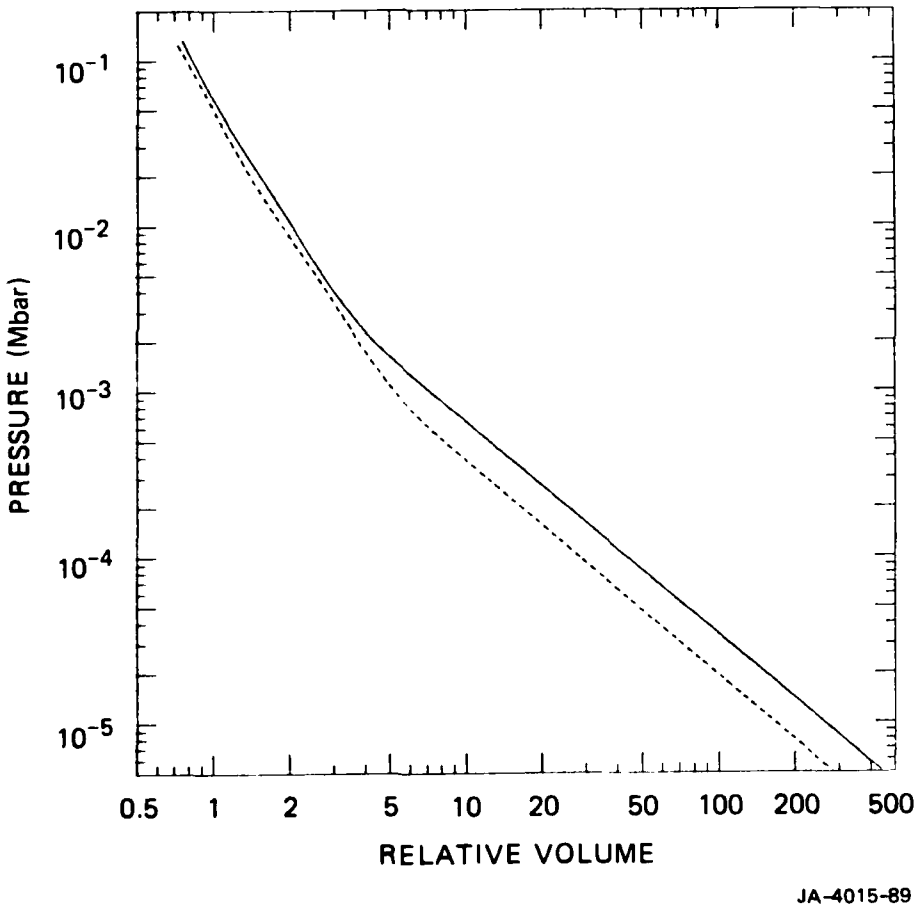

Figure 18. NA/NP (solid) and nitromethane JWL CJ isentropes.

Table 2. Comparison of NA/NP and NM JWL coefficients.

NA/NP

Initial State	CJ State				Equation-of-State Parameters					
ρ_0 (Mg/m^3)	p (Mbar)	D (cm/μs)	E_0 (Mbar)	Γ	A (Mbar)	B (Mbar)	C (Mbar)	R_1	R_2	ω
1.252	0.133	0.648	0.0697	2.991	7.554	0.1962	0.012717	6.366	1.810	0.285
NM[a]										
1.128	0.125	0.628	0.0510	2.538	2.092	0.05689	0.00770	4.40	1.20	0.30

The JWL coefficients generated here for NA/NP differ from typical cylinder test values in that the nonlinear coefficients, R_1 and R_2, are larger. We believe this is because of the larger expansion range over which the isentrope is constrained here and possibly because of the difference in the energy constraints between the two methods. The present coefficients are within the range of results from cylinder tests and are believed to be appropriate for a range of DNA applications as intended. For specific applications, specialized coefficients could be generated from dedicated experiments simulating the application, if necessary.

The Lagrange gage and analysis results indicated a surprisingly long reaction zone, between 0.2 and 0.6 μs, apparently with resolvable structure, for NA/NP undergoing steady planar detonation. This may result from the effects of the water in the reactants, which may impede the kinetics of the chemical reaction and will also undergo a phase change and affect the temperature distribution in the products.

The SDT experiment was ambiguous. The results were not reproducible in that gage records 1 through 5 differ from gage records 6 through 10. Also, over the range spanned by the gages (50 to 100 mm from the initiator system) the input shock had neither built to steady detonation nor decayed. Some of the particle velocity histories showed a late time pulse building with depth in the target, behind a narrow

[a]From Reference 12.

relatively constant initial spike. This structure has a qualitative resemblance to the profiles observed in the steady detonation experiment. The results indicate that the shock initiation of detonation in NA/NP may be unusual, and in some cases sluggish, and should be investigated further.

We believe that NA/NP is a good liquid HE offering an attractive low cost alternative to NM. Neither the Baumé 42 weak nitric acid nor the nitropropane presented undue handling problems.

SECTION 4

NPN CHARACTERIZATION

Initial JWL equation-of-state parameters were developed for the detonation products of NPN, a blasting agent somewhat like ANFO. The specific composition and initial density of the NPN selected for characterization were chosen to be similar to those for the NPN investigated previously for DNA in an airblast performance test by Franzen and Wisotski.[20]

The tasks performed included selection and fabrication of a particular NPN study material; Lagrange gage experiments and analysis to determine shock compression, CJ, and initial CJ adiabatic release states; TIGER calculations to interpret the experiments and extend the experimental CJ release adiabat to large volume expansions; and determination of JWL coefficients. The results of these tasks are described in the following subsections.

4.1 DESCRIPTION OF MATERIAL

Background

NPN (nitropropane nitrate) is composed of the solid oxidizer ammonium nitrate (AN) and the liquid fuels nitropropane (NP) and methyl alcohol (MA). The material was developed initially by John R. Post as an alternative blasting agent to ANFO with improved performance for mining applications.[21] Basic NPN physical characteristics and initial performance data, as well as a fairly standardized baseline composition, were described by Post in 1977[22] and are summarized below.

The baseline NPN composition given by Post was 87 wt% AN and 13 wt% fuel (NP and MA in equal volumes). This composition was reported to be oxygen-balanced and could be loaded to densities ranging from about 1 to 1.4 Mg/m^3 depending on the degree of compaction induced by the loading procedures and by its own weight. Approximate detonation velocities

observed by Post were between 4.5 and 6 km/s depending on initial density and confinement.

We are aware of only two experimental investigations of NPN other than Post's work cited above. In 1977 Mallory measured the detonation velocity in thick-wall 1-inch-ID steel pipes for the baseline composition at an initial density of 1.298 Mg/m^3.[23] He observed a detonation velocity of 5.206 ± 0.028 km/s. In 1983 Franzen and Wisotski[20] performed a 100-pound quasi-spherical airblast test for an NPN composition slightly modified from the baseline material (see next subsection) at an initial density of 1.05 Mg/m^3. They observed propagation velocities between 2.8 and 4.1 km/s in the detonation buildup regime.

In addition to the specific investigations cited above, two recent DNA reports review useful NPN information. The first is an informal report prepared by Franzen summarizing available documents on NPN.[24] The other is a technical report by McMullan[25] containing an evaluation of the properties of a number of explosives, including those of NPN summarized by Franzen[24], for large-scale DNA air blast tests.

Present Study Material

The composition of the present study material, like the material studied by Franzen and Wisotski, is 84.8 wt% AN, 0.2 wt% methocel (a stabilizer to prevent migration or puddling of the liquid fuels,[26] and 15.0 wt% fuel. However, the present study material differs slightly from that investigated by Franzen and Wisotski in that the relative proportions of the fuel components, MA and NP, are equal by weight, not volume. Both compositions, which can be considered equivalent for most purposes, have a slightly higher fuel concentration than the oxygen-balanced baseline material. Post[26] recommended this overfueling for both this study and the previous study by Franzen and Wisotski to increase the dampness-induced cohesiveness and therefore the achievable initial density in the NPN. In both studies, the fragility of the embedded sensors precluded the use of heavy tamping to achieve the high NPN loading density characteristic of field applications.

The NPN tested in this work was constructed from the following materials. The AN was crushed, porous, uncoated, fertilizer-grade prills. Crushing the rather uniform spherical AN prills increases both packing densities and intimacy of mixing of the AN and the fuels. Because degree of crushing and prill porosity are AN parameters that may affect performance and/or sensitivity of NPN, we purchased the crushed AN (premixed with methocel) directly from Post, who also supplied these materials for the work by Franzen and Wisotski. The approximate screen analysis provided by Post for our crushed AN, and described as representative of that obtained for AN crushed in the field with commercial hammer mills, is tabulated below.[26]

Mesh	wt%
+20	30.5
-20 +60	40.5
-60 +100	11.8
-100	17.2

The NP was furnished by International Minerals and Chemical Corporation, IMC Chemical Group, and is a mixture of the two stable isomers. The MA was standard reagent grade material.

Procedure for Producing Uniform Density Specimens

Before the Lagrange particle velocity gage experiments were performed, a significant effort was made to identify a method of loading the NPN specimen material into the Lagrange gage target chamber so that:

(1) The NPN, which is highly compactible, would have a constant density throughout the chamber, particularly in the vicinity of the gages.

(2) The density would be close to 1.05 Mg/m^3.

(3) The fragile particle velocity gages would not be distorted and would be in intimate contact with the NPN.

To this end, a "sampling densitometer" was constructed in the shape of a cylindrical chamber with an inside diameter of 0.124 m and a height

of approximately 0.30 m. The densitometer incorporated thin steel sheets positioned at four heights in the cylinder that could be pulled across guillotine-style to physically separate the NPN into a set of shorter cylindrical chambers with minimal sample disturbance. These sections could be weighed separately after various trial loading procedures to obtain the average NPN densities at heights within the densitometer corresponding to the heights of the gage elements in the Lagrange gage test chamber.

Figure 19 shows the densitometer results for the five filling methods methods that were evaluated:

(1) Strong vertical shaking of the densitometer during and after loading the NPN through a large funnel.

(2) Pneumatically vibrating the chamber during and after loading the NPN through a large funnel.

(3) Drop loading the NPN through a vibrating mesh screen located about one meter above the chamber.

(4) Same as method (3), followed by vertically compressing the sample approximately 2.5 cm.

(5) Same as method (3), followed by deadweight compressing the sample to a predetermined density, while pneumatically vibrating the chamber.

As seen from Figure 19, the first two methods resulted in bulk densities averaged over the entire densitometer that were reasonably close to 1.05 Mg/m^3, but with large density gradients from top to bottom. The last three methods resulted in lower average densities, presumably because the screen mesh reduced the initial compacting tendencies of the material. Method (5), in which the deadweight compression during vibration reduced the pressure gradient in the sample while allowing the material to flow, resulted in a very low density gradient, at an average density of 1.01 Mg/m^3. Attempts to increase the bulk density while retaining a low density gradient were unsuccessful. Method (5) was chosen as the basis for filling the chambers for the particle velocity gage tests.

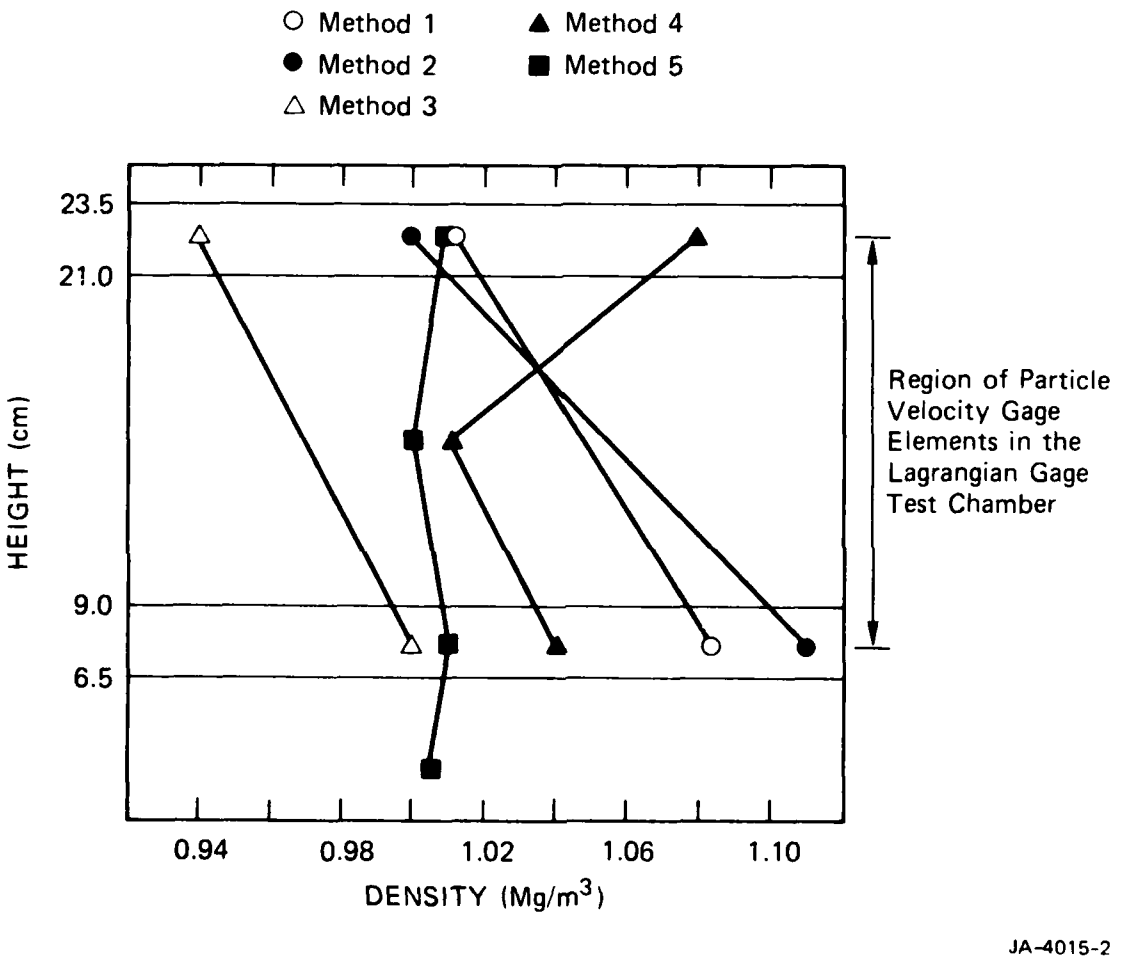

Figure 19. Density of NPN at various heights in the densitometer chamber for five filling procedures.

4.2 LAGRANGE GAGE EXPERIMENTS

Lagrange Gage Target Chambers and Filling Procedures

The Lagrange gage target chambers, Figure 20, were PVC cylinders approximately 0.30 m OD, 0.28 m ID, and 0.15 m high. The chambers were sealed at the bottom with a PMMA base plate containing a standard particle velocity gage block of the type described in Section 2 (see Figures 3 and 4) and used in the NA/NP experiments described in Section 3. An auxiliary 0.105-m-diameter filling hole with a cap (for use in the filling operation described below) was cut in the cylindrical wall of each PVC chamber in line with the axis of the gage block.

The gage blocks, each containing the usual five pairs of 0.15-mm-thick aluminum foil particle velocity gages, were mounted in the base plates so that the active elements of the gages were parallel to the top surface of the chambers to within ±0.025 mm. The active elements of the tallest gage pair (that is, the first pair to enter the flow) were located 82.5 mm below the upper NPN surface, and the active elements of the shortest gage pair (the last pair to enter the flow) were 50.8 mm below that. (The difference in heights between successive gage pairs is 12.7 mm as discussed in Section 2.) The inner surface of the base plates and the tops of the gage blocks were coated with paraffin for protection from the solvent action of the NP. Each target chamber was loaded immediately before the experiment and covered with a 1.7-mm-thick PMMA plate to prevent evaporative loss of the fuel and to separate the driver charge from the NPN solvents.

The target chamber filling procedure was based on the principle of method (5) developed with the sampling densitometer, modified to minimize disturbance to the particle velocity gages. The preweighed components were mixed to produce a slightly damp compressible powder as before. Approximately 90% of the material required to achieve the desired density was drop loaded into the pneumatically vibrated test chamber from the top through a mesh screen. The top of the chamber was then sealed with the PMMA cover plate and a temporary PMMA backing plate. The chamber was rotated 90° until the long dimension of the gage

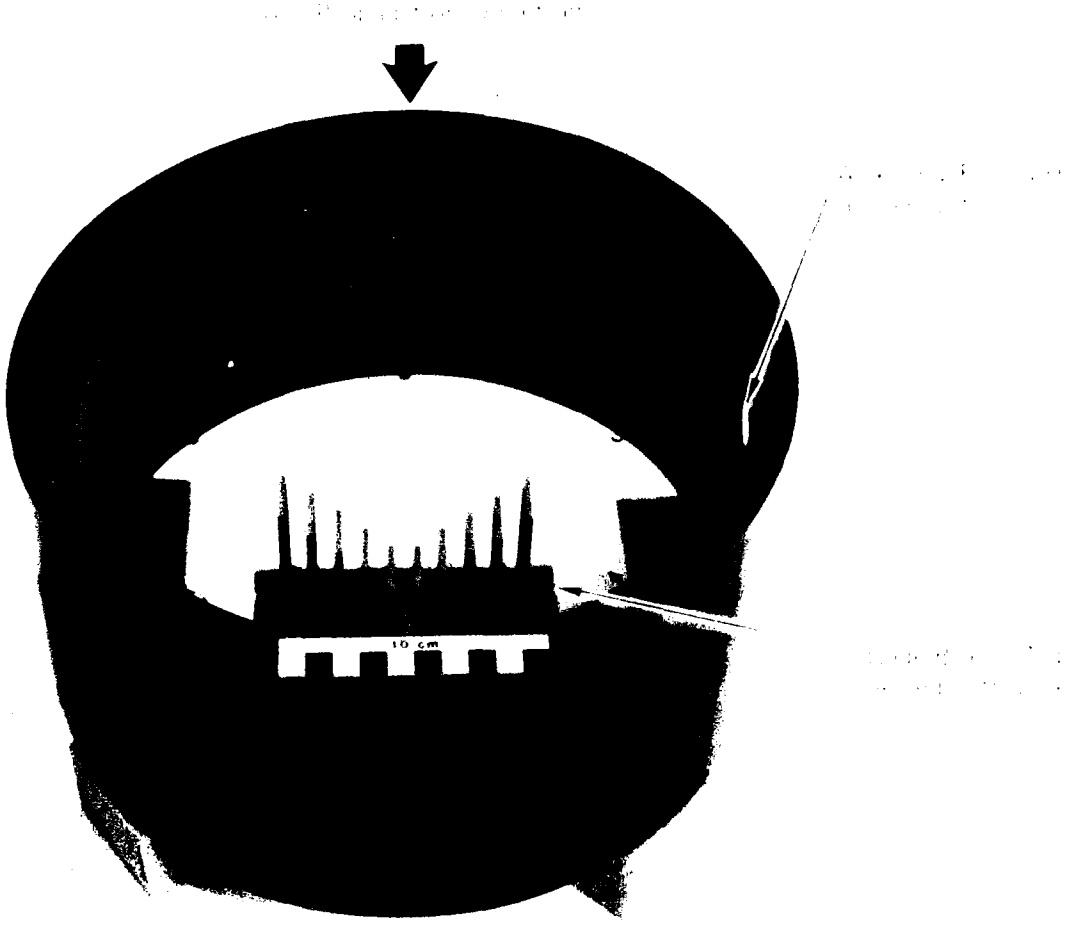

JP-4015-61

Figure 20. NPN Lagrange gage target chamber (PVC)
(Top and bottom are sealed with PMMA plates. The four blocks beneath chamber are temporary supports for this photograph.

block was vertical, and the remaining material was then deadweight compressed through the auxiliary fill hole as in method (5). The motion of the dense NPN in the final stages of filling was thus in the direction of maximum gage element rigidity (parallel to the plane of the gage foil).

For the first Lagrange gage experiment, the chamber was subjected to planetary pneumatic vibration while the main portion of the NPN was added and before the chamber was rotated 90°. After the experiment we discovered that the planetary vibration caused bulk rotation of the NPN within the circular cross-section chamber and severely distorted the gages. For the second experiment, linear vibration was used before the chamber was tilted, and no gage distortion was detected or is believed to have occurred.

The NPN specimen uniformity in the Lagrange gage experiments is estimated from the results of the sampling densitometer study, from visual inspection of the specimen material through the transparent target chamber cover during and after loading, from experience gained in trial loadings of the target chambers, and from the results of the Lagrange gage experiments themselves. The final average (bulk) density was 1.01 Mg/m^3, and we estimate that the density variation throughout the majority of the chamber was less than ±2%. The NPN appeared to be in intimate contact with the gages.

During the final step of the chamber loading operation for the second experiment, we noted that small gaps developed along the upper portion of the cylindrical interface between the NPN and the target chamber wall, immediately adjacent to the filling tube. These resulted from the combined effects of settling and nonhydrodynamic rheology in the NPN. We believe these gaps had a very small effect on the bulk properties of the NPN; however, they did asymetrically alter the target width such that the effective target radius was smaller on the side near the filling hole than on the other side. In spite of this difficulty, we believe that the specimen density in the Lagrange gage experiments is probably more uniform than could be achieved in the field.

Initiation System

We selected Baratol as an appropriate driver for rapidly initiating steady detonation in NPN. Slight underdriving was assumed to be the optimal condition for initiating steady detonation in the present Lagrange gage experiments. We assumed that the reaction time in any candidate military HE driver was negligible compared with that in the NPN. We then sought a driver for which the shock impedance mismatch between the driver detonation products and the unreacted NPN produced a pressure in the unreacted NPN about equal to the expected NPN CJ pressure. Because this pressure on the unreacted NPN Hugoniot is well below the expected spike pressure on the Hugoniot during steady detonation and because of the long postulated NPN steady reaction time, this initiation pulse is taken to underdrive NPN detonation. However, because of the long duration of the driver induced pulse and its significant percentage of the expected NPN steady detonation spike amplitude, this initiation pulse was estimated to satisfy any threshhold criteria for shock initiation of detonation and thus to provide the slight underdriving but reliable initiation we sought.

We estimated by an impedance mismatch calculation that Baratol would generate an input shock pressure in unreacted NPN of about 7.0 ± 1 GPa. For this estimate we very roughly approximated the Hugoniot for unreacted NPN from unreacted AN data.[12] Since 7 GPa was the CJ pressure we estimated for NPN at a density of about 1 Mg/m^3 from data by Post, we selected Baratol for the HE driver.

Experimental Results

Two NPN Lagrange gage detonation experiments were performed. The purpose of the first was to evaluate gage/specimen compatibility and to determine optimal instrumentation settings. In this experiment a 20-cm-diameter P-80 plane wave lens was used to initiate detonation. Since the base charge in our P-80 lenses is Baratol, the amplitude of the shock initiation pulse driven into the NPN target is that resulting from the impedance mismatch between Baratol detonation products (considering the reaction zone in Baratol to be negligible) and unreacted NPN.

Data were obtained from all gages in the first experiment, resulting in good time-of-arrival information for optimizing oscilloscope sweep speeds and delays in the second experiment. However, the shapes of the recorded profiles were irregular and inconsistent, preventing quantitative analysis of the detonation process in NPN. As discussed previously, these anomalous profiles are attributed to the gage distortions resulting from the planetary vibration used in filling the target chamber for this experiment. Modified filling procedures were used in the second experiment.

The purpose of the second Lagrange gage experiment was to provide data on the detonation process in NPN. In this experiment, a 30-cm-diameter plane wave lens (P-120) and a 10-cm-thick by 30-cm-diameter Baratol pad were used to initiate the NPN to increase the uniaxial strain recording time at the gage locations.

Records were obtained from all particle velocity gages. The oscillographs are shown in Figure 21. For these oscillographs, vertical sensitivities are 500 mV/division and horizontal sensitivities are 1 μs/division. Short blanks on all the scope records are simultaneous fiducial marks generated by a repetitive "z-axis blanking" beam intensity modulation system used to time-correlate the oscillographs.

The NPN gage records in Figure 21 are judged to be better than average detonation records in two ways but worse in a third. We have previously used this gage design to observe detonation in higher performance explosives including Composition B,[27] Amatex 20,[28] and the eutectic explosive EAK,[29] as well as in the NA/NP experiments described in Section 3. Typical results, Composition B records from reference 27, are reproduced in Figure 22. The records in Figure 21 show considerably less high frequency noise on the first gage plane than the records from the other materials such as the Composition B data in Figure 22 (the NA/NP results, Figure 8, are also free of this noise). In addition, the records in Figure 21 contain considerably smaller perturbations on upstream records when downstream gages enter the shock front than we see in the other materials. These two improvements may result from the

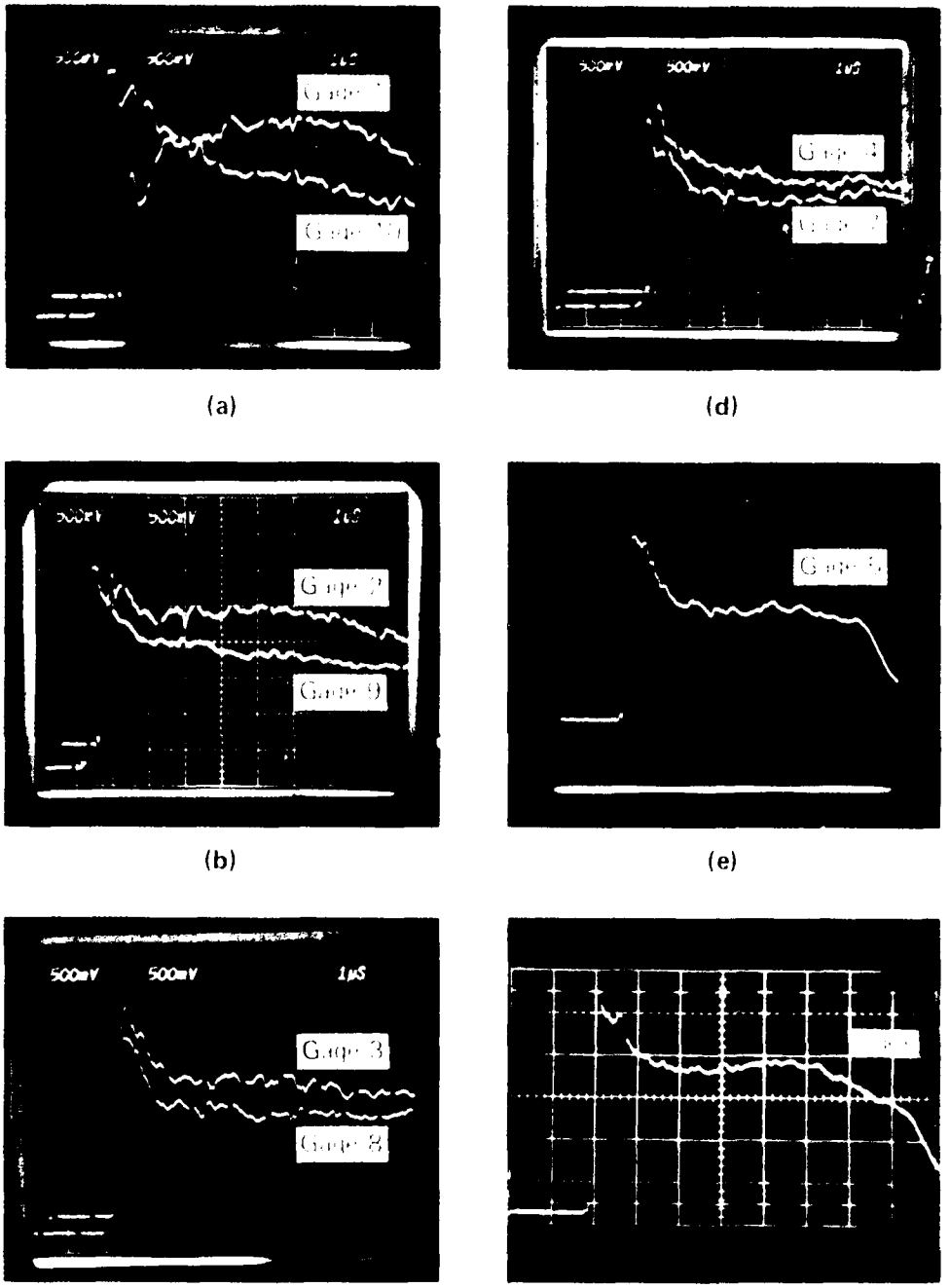

Figure 21. Lagrangian particle velocity gage recc. Js from second NPN experiment.

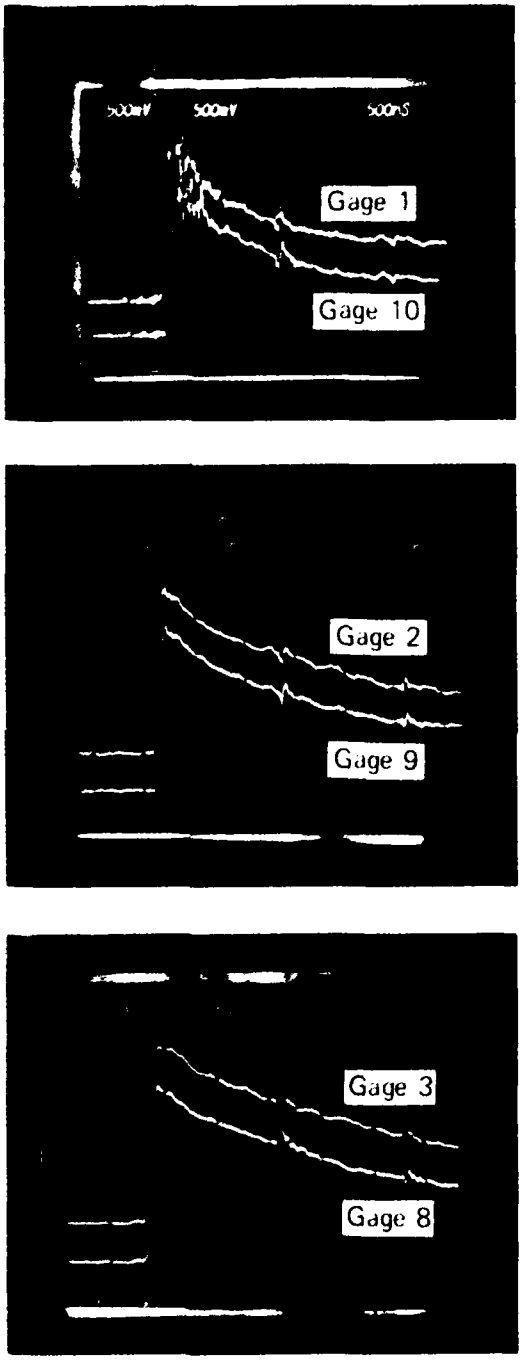

JP-1764-3

Figure 22. Lagrange particle velocity gage records composition B, shot 1764-4 (Reference 27).

lower temperatures, pressures, and conductivities expected in the NPN reaction zone than in the reaction zones of the higher performance materials.

However, the NPN records in Figure 21 contain more pronounced intermediate frequency, low amplitude oscillations during stress release than the records from the other materials in this region. The origin of this structure is unknown, but it may be related either to the particulate nature of the NPN or to the relatively large plastic strains experienced by the leads in the present experiments.

The ten particle velocity gage oscilloscope records in Figure 21 were digitized and reduced to the particle velocity histories shown together on a common time scale in Figure 23. This figure shows the overall nature of the flow in a single composite plot. In the following section these histories evaluated in various subgroups in which their individual features are more readily viewed.

Recall that the gages are numbered sequentially from one side of the gage block to the other (see Figure 4). Thus, each set of histories (1,10), (2,9), (3,8), (4,7), and (5,6) results from a pair of redundant particle velocity measurements at one Lagrange coordinate, and the five Lagrange coordinates at which the measurements are made are initially 12.7 mm apart in the wave propagation direction. The gage pair (1,10) is the closest to the driver and thus the first to enter the flow; the pair (5,6) is the closest to the rear boundary of the target and thus the last to enter the flow.

4.3 DATA ANALYSIS

The ten particle velocity records in Figure 23 were first compared to (1) obtain a best nonredundant set of histories for Lagrange analysis and (2) characterize the reactive flow in NPN. We performed three types of comparisons: intra-side, intra-pair, and inter-side. In the intra-side comparisons, we considered the five profiles from each side of the target as independent groups to evaluate the data and the flow in each half of the target as separate experiments. In the intra-pair

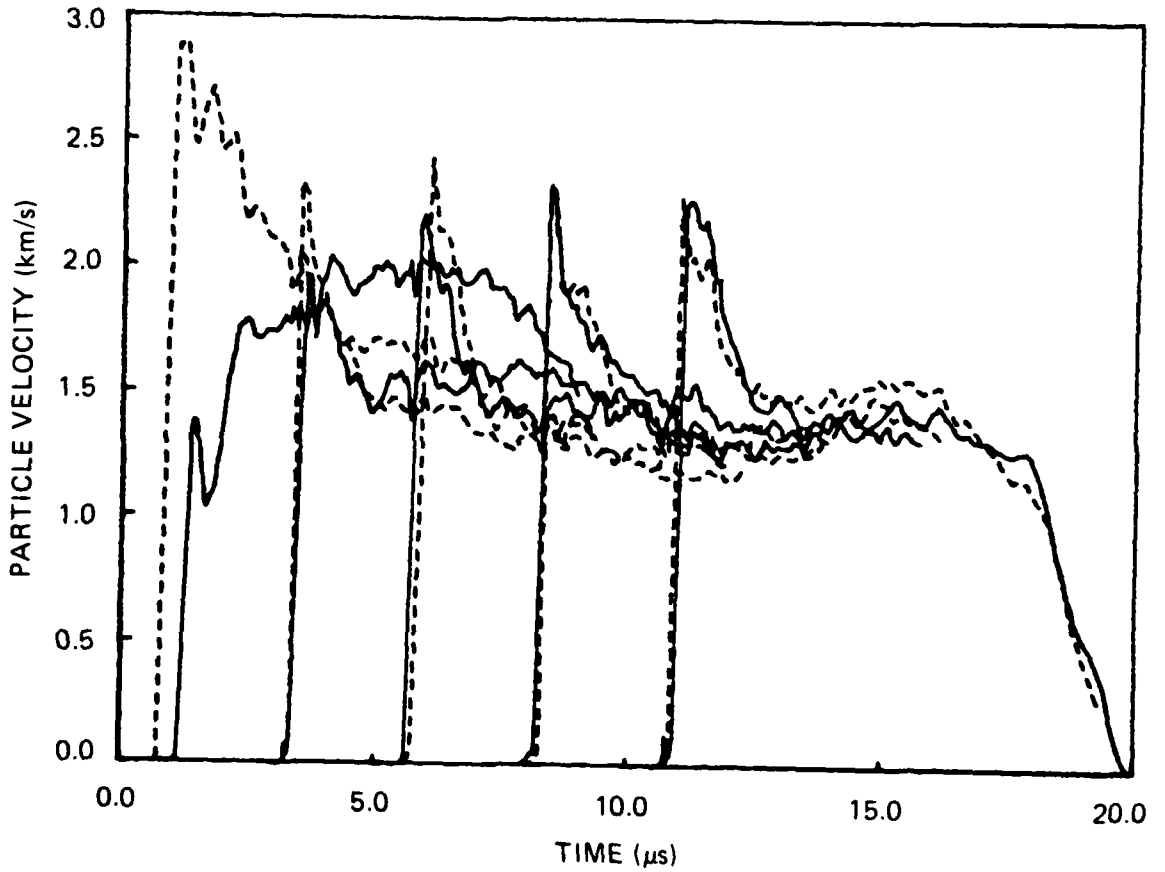

Figure 23. Lagrange particle velocity histories, gages 1-10, second NPN experiment. Solid lines used for gages 1-5, dashed for gages 6-10.

comparisons, we compared the two redundant measurements at each of the five Lagrange coordinates to determine measurement reproducibility at these locations. In the inter-side comparison, we compared the five records from one side of the target with those from the other to evaluate overall target response. Below we summarize the comparisons, select a data set for analysis, and give an initial characterization of the flow. Additional interpretation is given after the thermodynamic TIGER calculations are presented.

Intra-side Comparisons

Histories 1-5, recorded by the gages that were on the top side of the target chamber during the final filling operation, are shown in Figure 24. The peak particle velocity amplitudes increase monotonically with propagation distance in the region spanned by the first three gages (1-3) and remain constant, within experimental error, in the region spanned by the last three (3-5). This is consistent with steady flow beginning near gage 3.

The shapes of histories 3-5 are essentially identical within experimental error, again consistent with steady flow in the region spanned by these gages. (Experimental accuracy of the particle velocity measurements is estimated to be ±5%.) History 1 has an anomalous shape compared with histories 3-5 and, for the first microsecond after entering the flow, is almost 50% lower in amplitude than these histories. History 2 is for the most part similar in shape to 3-5, but is as much as 20% lower in amplitude during the first microsecond.

The histories from the bottom half of the target, 6-10, are shown in Figure 25. The peak amplitudes and shapes of the histories from the last four gages (9-6) are consistent with steady flow in the region spanned by these gages. No growth of peak amplitude is observed on the first gages; in fact, the first profile, 10, is anomalously large at early times.

The shock transit velocities between adjacent gages (not redundant gage pairs), for each side of the target, and the mean transit

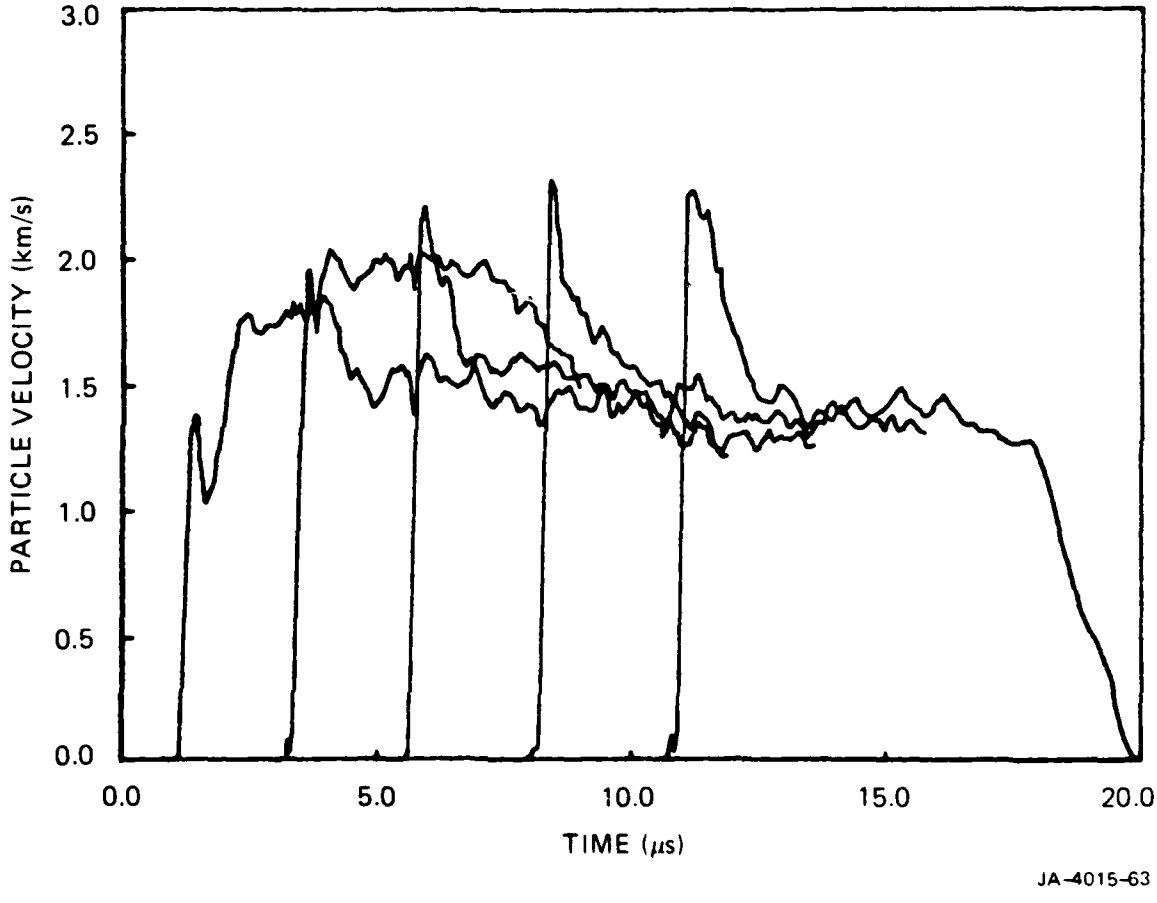

Figure 24. Lagrange particle velocity histories, gages 1-5, second NPN experiment.

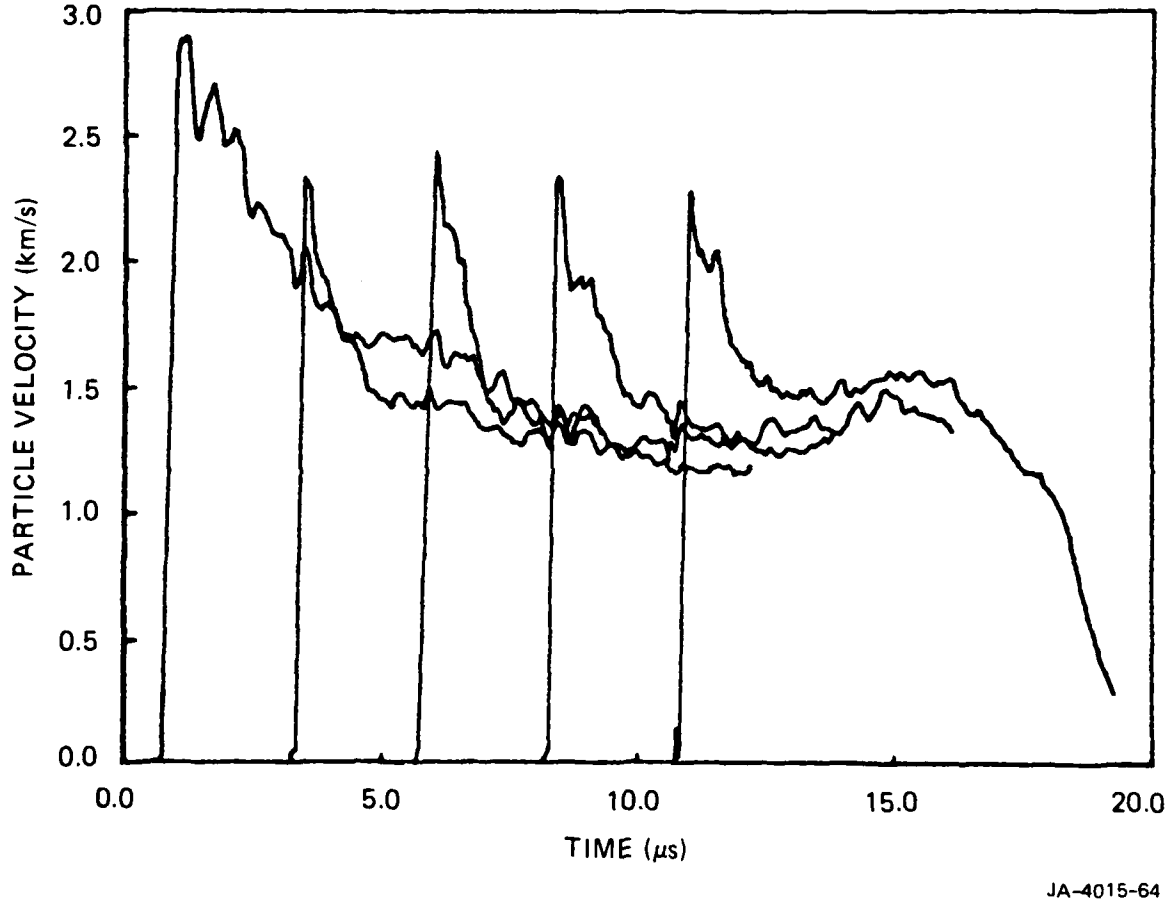

Figure 25. Lagrange particle velocity histories, gages 6-10, second NPN experiment.

velocities and standard deviations for each side, are listed in Table 3 along with the shock arrival times from which they were calculated. Here arrival times are for the midpoint of the leading edge of the compressive wave, following recommended shock wave practice. In the side of the target away from the auxiliary filler, the transit velocities agree within measurement accuracy (estimated to be 2%-3%). This is consistent with steady flow propagating at 5.07 km/s. (We note here, however, that for reasons presented in the following discussion, the steady velocity attributed to the detonation wave in NPN is 5.08 km/s.) In the side of the target nearer the auxiliary filling hole, the shock propagation velocity differences exceed experimental error, indicating less uniform flow.

Intra-pair Comparisons

Figure 26 shows the redundant pairs of histories measured at each of the five Lagrange gage coordinates. The two records from the first gage pair to enter the flow, 1 and 10, are qualitatively different. Note that history 1 is both lower in initial particle velocity amplitude and later in time of first motion than history 10.

The records in the remaining pairs are qualitatively similar to each other. However, in the second pair, 2 and 9, 2 is initially 15%-20% lower than 9 and later is higher by a similar percentage. These differences exceed the estimated experimental errors. In the third pair, 3 and 8, the differences during the shock compression also exceed the estimated experimental errors, but are the result of a time correlation difference rather than a profile shape difference. If 3 is shifted back approximately 0.1 microsecond, reducing the scatter in shock propagation velocity, these records agree to within experimental error everywhere. The records in each of the last two pairs to enter the flow generally agree to much better than ±5%, indicating that both the flow and the measurements are reproducible at these locations.

Table 3. Shock arrival times, transit velocities, and detonation velocity for second NPN experiment[a]

Shock Arrival Times at Gages		Gage Pair Transit Velocities			
		Side Near Filler		Side Away From Filler	
Gage	Shock Arrival Time[b] (μs)	Gage Pair	Transit Velocity (km/s)	Gage Pair	Transit Velocity (km/s)
1	(1.23)				
10	(0.90)	1-2	(5.75)	10-9	(5.04)
2	(3.44)				
9	3.42	2-3	(5.50)	9-8	5.14
3	(5.75)				
8	5.89	3-4	(5.00)	8-7	5.18
4	(8.29)				
7	8.34	4-5	(4.69)	7-6	4.92
5	(11.00)				
6	10.92				
		Mean	(5.24)	Mean	(5.07)
		Std. Dev.	(0.48)	Std. Dev.	(0.12)
				Detonation Velocity[a]	5.08 ±0.14

[a]Only gages 6-9 were used to characterize detonation process in NPN. Values relating to other gages are shown in parentheses. See text for explanation.

[b]Times are for midpoint of leading edges of compressive waves measured from a common arbitrary zero time.

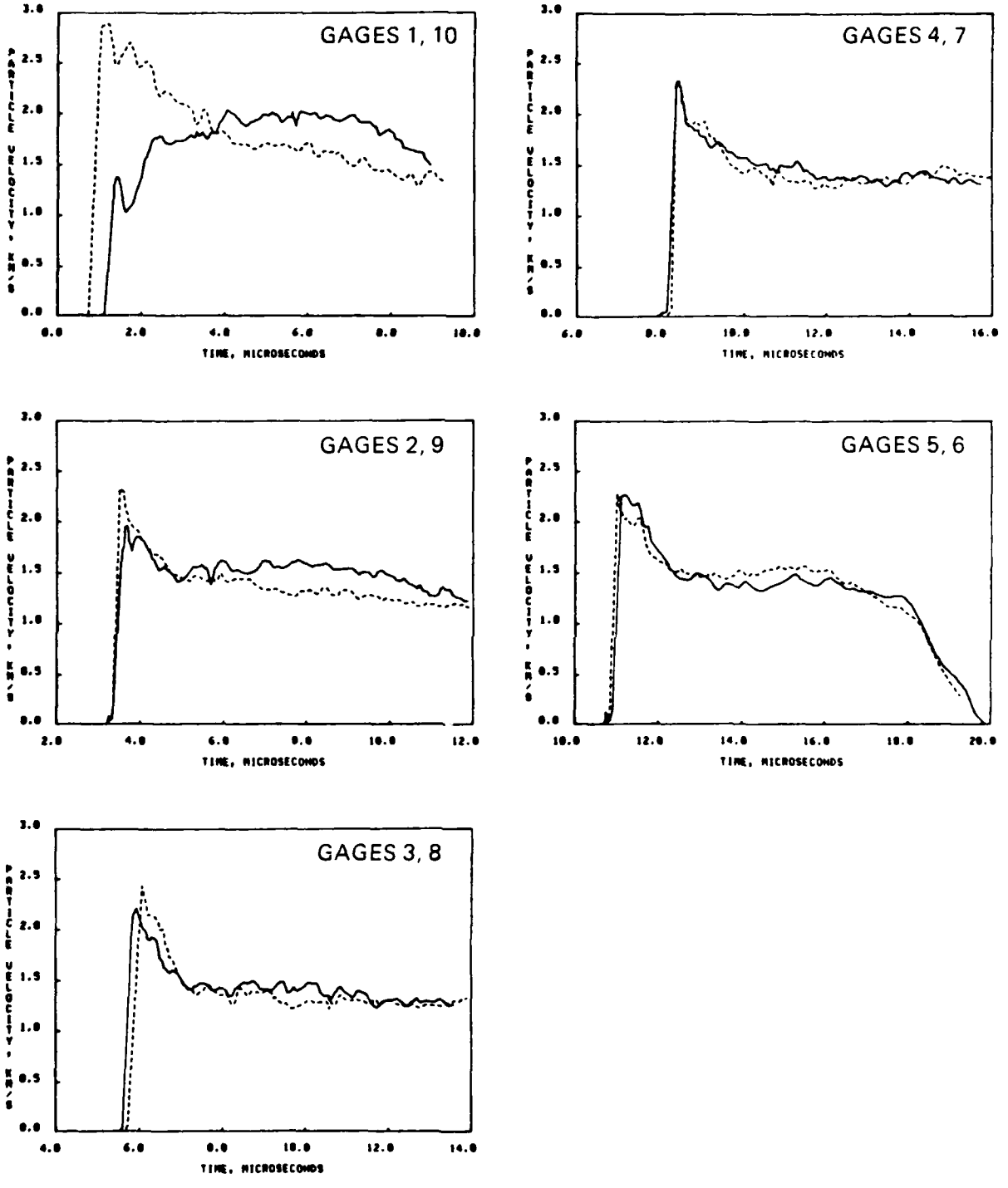

Figure 26. Lagrange particle velocity histories by pairs, second NPN experiment. Solid lines used for gages 1-5, dashed for gages 6-10.

Inter-side Comparisons

The histories from both halves of the target (all the records) were shown together in Figure 23. The same apparently steady flows were recorded in each half at the final two gage stations. In the upper half, however, the flow apparently builds in the region spanned by the first three gages, whereas in the lower half the flow is steady at all gage locations except the first where it is anomalously large. The shock velocity between adjacent gages is much more uniform in the lower half than in the upper half, even if gage 1 in the upper half is excluded. The shock velocity in the lower half of the target is consistent with steady flow at 5.08 km/s.

Data Selection

Histories 1 and 10, recorded by the longest and most fragile gages, are anomalous by all three comparisons. Because they do not reproduce each other and neither provides information on the steady detonation process in NPN, these histories are not included in the Lagrange analysis.

Histories 2-5 from the upper half of the target show an unexpected flow structure in which an apparent buildup occurs over the first gages and steady state is not reached until the third gage location. We attribute this to a target asymmetry resulting from the filling procedure described previously. In the final step of the filling procedure, NPN was added through the auxiliary filling hole in the side of the chamber. During this step, voids developed in regions of the target chamber near, but not directly under, the filling tube. Attempts to flow NPN into these regions were only partially successful, effectively decreasing the NPN specimen diameter in the upper half of the target.

We consider it likely that the reduced particle velocity amplitudes recorded by the first several gages in the upper half of the target, which are those nearest the voids along the side boundary, are a result of rarefactions originating from these regions. The late arrival of the shock at gage 1 is consistent with this interpretation. Because of this

target asymmetry, we excluded the records from the top half of the target, 1-5, from the Lagrange analysis and from the characterization of the detonation process in NPN.

The histories recorded by gages 9-6 from the bottom half of the target appear to be high quality records of the detonation process in NPN. These records were therefore selected as the nonredundant data set for flow characterization and Lagrange analysis. The following discussions are based on these records. As indicated in Table 3, the NPN detonation velocity calculated from particle velocity histories 9-6 is 5.08 km/s.

Flow Characterization

Histories 6-9 are shown superimposed in Figure 27. (The histories were superimposed by adjusting the zero times for records 6, 7, and 8 so that their "midpoint" shock arrival times were the same as that given for record 9 in Table 3.) The profiles are the same to well within the estimated experimental error, confirming the previous hypothesis of steady flow. Although history 6 shows a slight increase above the others beginning about 3 μs after shock arrival, we do not attach physical significance to it because it does not occur on the redundant gage record 5 nor on the other histories.

History 9 lies within the envelope defined by the superimposed profiles in Figure 27 and therefore is a convenient representation of the steady-state particle velocity profile. The steady-state profile can be idealized as consisting of three parts: a shock compression to a peak amplitude of 2.4 km/s in about 0.2 microseconds, a relatively rapid decay to 1.4 km/s occurring in about 2 μs, and then a much slower, nearly linear decay, to 1.2 km/s in about 6 μs.

The decay rate is so slow in the third region that an alternative idealization is to consider the particle velocity within it to be constant at 1.3 km/s. The significance of these alternative interpretations is considered during presentation of the results of the thermodynamic calculations.

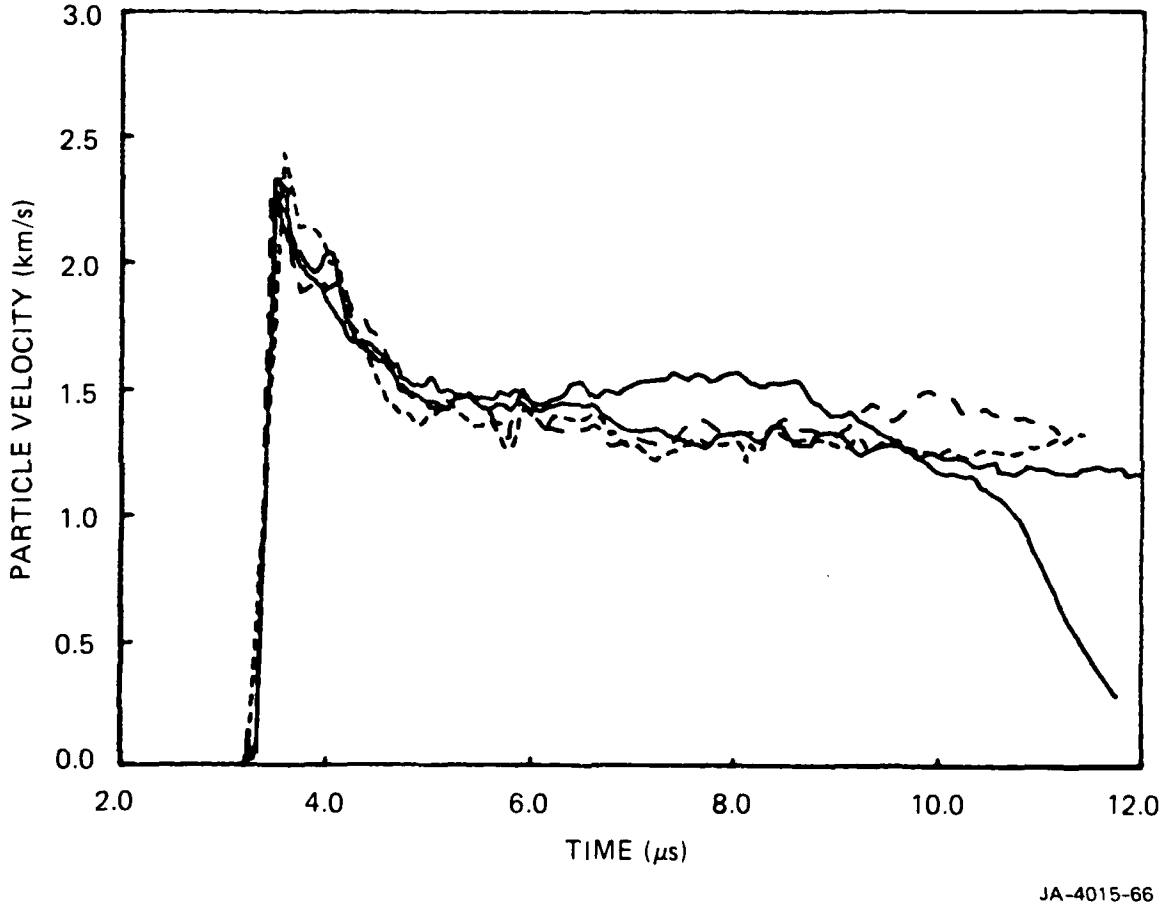

Figure 27. Superimposed Lagrange particle velocity histories, gages 6-9, second NPN experiment.

The experimental results may now be summarized. NPN in 30-cm-diameter charges exhibits a steady detonation wave propagating at 5.08 ±0.1 km/s. The idealized steady-state particle velocity profile consists of a shock compression to 2.4 km/s in about 0.2 μs, a decay to about 60% of the peak amplitude in about 2 μs, and a very slow further decay or constant state until the termination of the experimental data about 6 μs later. The steady profile is well represented by particle velocity history 9.

Lagrange Analysis

Because the flow is steady, the Lagrange analysis can be performed by application of the Rankine-Hugoniot shock-jump equations expressing conservation of momentum and mass:

$$p = [Du]/v_0 \tag{10}$$

$$v = v_0[1 - u/D] \tag{11}$$

where p is pressure, D is detonation velocity, u is particle velocity, v is specific volume (reciprocal density), and the subscript 0 denotes the initial state into which the steady wave propagates.

The Lagrange pressure history in the steady-state region was calculated by applying Equation (10) with D = 5.08 km/s and $v_0 = 0.99$ m^3/Mg to particle velocity history 9. The result is shown in Figure 28. The p-u and p-v paths are the well-known Rayleigh lines, which may be represented analytically from Equations (10) and (11) as:

$$p/u = [D/v_0] \tag{12}$$

$$p/(v - v_0) = [D/v_0]^2$$

or,

$$p/(V - 1) = D^2/v_0 \tag{13}$$

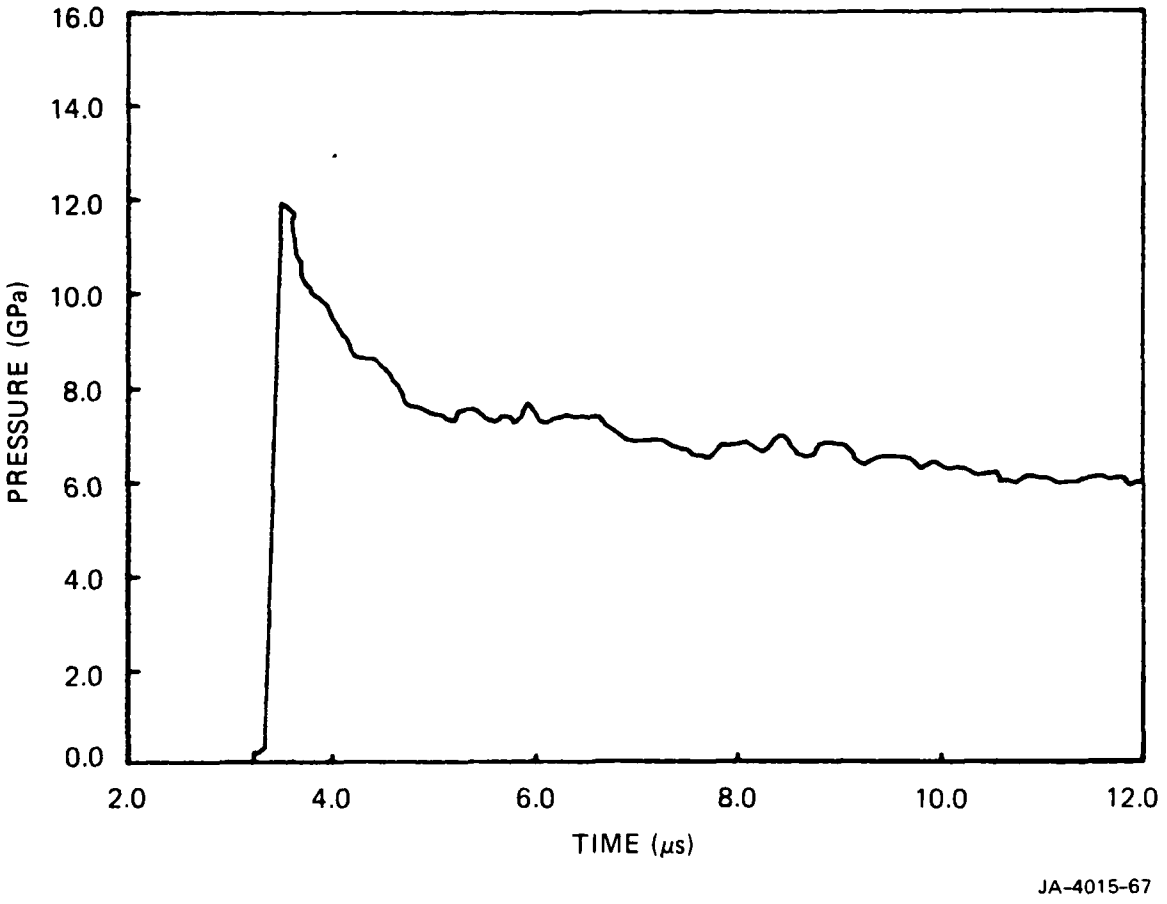

Figure 28. Lagrange pressure history calculated from particle velocity history, gage 9, second NPN experiment.

where V is relative volume, $V = v/v_0$. In the remainder of this section it is convenient to give volumes in terms of relative volume and pressures in Mbar (1 Mbar = 100 GPa), following normal JWL conventions, since the results will be used to generate JWL parameters.

The p-V path (Rayleigh line) calculated for NPN from the second experiment is shown in Figure 29. This figure summarizes the experimental results.

4.4 TIGER CALCULATIONS

Calculations were performed with the thermodynamic equilibrium code TIGER to interpret and extend the experimental results in Figure 29. Specifically, the TIGER calculations were used to investigate the ideality (see following paragraphs) of the NPN reaction process, to calculate the CJ state, and to extend the experimentally determined release path to relative volumes approaching 1000. The TIGER calculations used both the BKW and the JCZ3 equations of state for gaseous detonation products. These two equations of state will be shown to suggest rather different interpretations of the detonation process in NPN.

The term ideality is commonly used to refer to two properties of detonations: (1) charge size dependence and (2) completeness of the chemical reaction supporting steady detonation. Consider first charge size dependence. A real, quasi-1-D detonation process is said to be nonideal if the observed detonation parameters such as CJ pressure and detonation velocity are not essentially independent of charge size. Size dependence occurs when 2-D (lateral) effects within the reaction zone are so significant that the reaction zone is not well represented as a plane wave. This type of nonideality is believed to occur in all reactive materials when the ratio of charge size to reaction zone length is small enough and to become negligible when the ratio is large enough. In the latter case we say that "infinite diameter" behavior is attained. The present TIGER calculations are inherently 1-D and can be sensibly compared only with results from "infinite diameter" experiments.

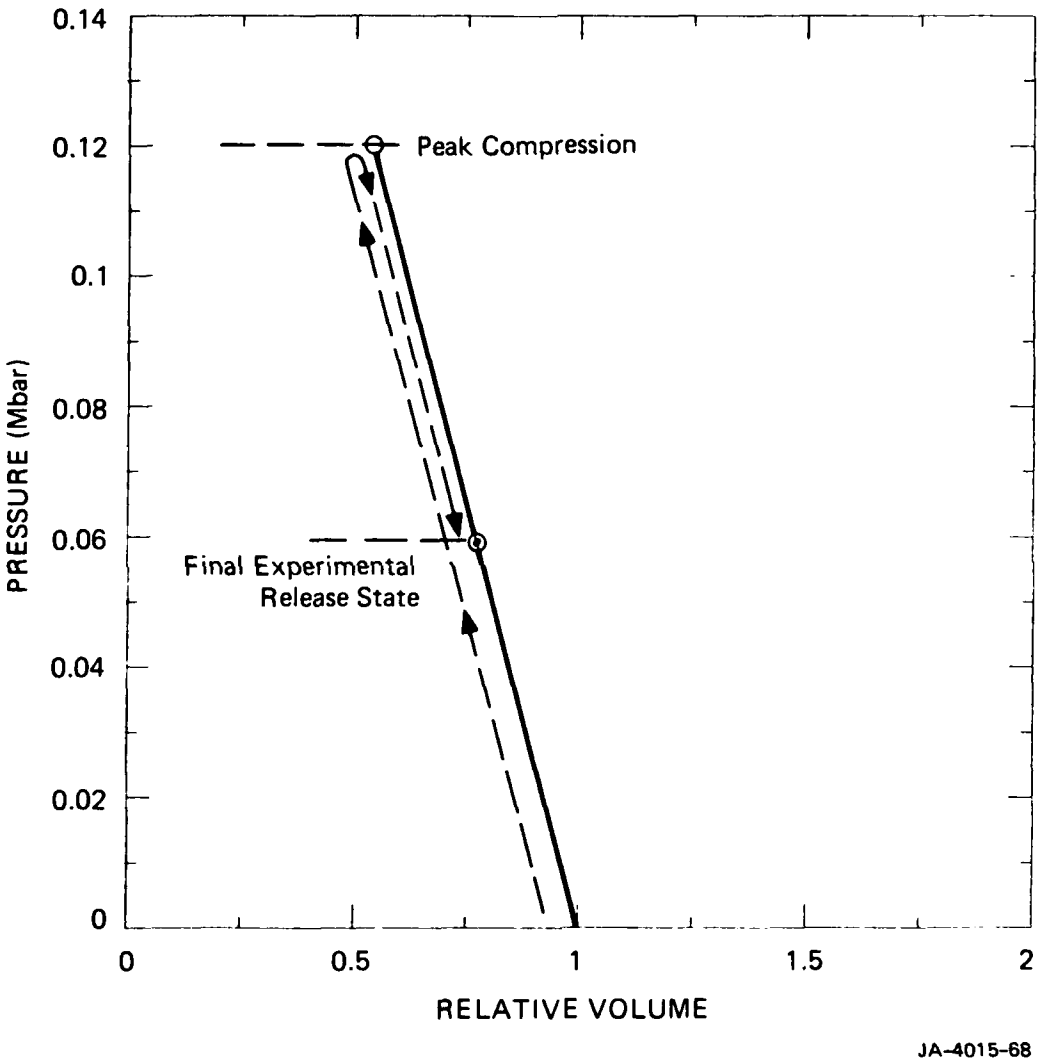

Figure 29. NPN pressure-relative volume compression and release paths, second NPN experiment.

The locus of Lagrange p-V states calculated from particle velocity records 6-9.

Some reactive materials such as NPN have longer reaction zones than conventional military explosives. These materials are sometimes called "nonideal" because they do not exhibit infinite diameter behavior except for relatively large charges. In fact, like other reactive materials, they may support either ideal or nonideal detonations depending on charge size and confinement. In the present work, we assume that the 0.3-m-diameter contained NPN charges studied here are large enough to exhibit "infinite diameter" behavior. This assumption is reasonable because ANFO data reported by Finger et al.[30] indicates that this would be a good approximation for ANFO and because NPN is expected to have a shorter reaction zone because of its finer particle size, greater intimacy of mixing, and enhanced detonation pressures and temperatures. The NPN results reported by Franzen and Wisotski[20] are also consistent with this assumption. We therefore interpret the results of the present NPN experiments as infinite diameter behavior and do not consider this type of nonideality further.

The other detonation property referred to by the term ideality is the completeness of the chemical reaction supporting the detonation. Kinetic constraints may prevent the completion of the chemical reaction minimizing free energy and the attainment of thermodynamic equilibrium at the back of the steady-state reaction zone. Then, as in the case of size dependent reactions, not all the thermodynamically predicted chemical energy is available to support the 1-D detonation and the process is called nonideal. Certain types of such "chemical nonideality" can be accounted for in thermodynamic calculations if the specific reaction phenomenology resulting from the constraints is known.

In the remainder of this report we use the term ideality to refer to the effects of chemical reaction constraints rather than to size dependence. By this definition, a detonation process is ideal if the experimentally measured and the thermodymanically calculated values for the CJ state agree within the accuracies of the measurement and the calculation.

BKW Calculations

As the first step in interpreting the experimental results using BKW, we calculated the ideal NPN CJ state and CJ release isentrope using the SRI BKW parameters for the gaseous species and rejecting liquid water. The resulting CJ state values were D = 6.33 km/s, p = 10.9 GPa, v = 0.724 m^3/Mg, and u = 1.70 km/s. Figure 30 shows the p-V representations of this CJ state and the corresponding CJ release isentrope to a relative volume of about 2 (the complete calculated CJ isentrope is shown later in a log-log plot). Figure 30 includes the experimentally determined compression and release states for comparison with the ideal BKW calculations.

The BKW value for D is significantly greater than the experimentally observed steady propagation velocity, so the calculated CJ state does not lie on the experimental Rayleigh in Figure 30. Thus, on the bases of BKW/TIGER calculations and our definition of nonideality, the detonation process in NPN must be nonideal.

Assuming that the detonation process in NPN is nonideal and that the Lagrange gage experiment does not define the end of the initial steady-state reaction zone, we must postulate a specific calculable nonideal reaction phenomenology to determine a final detonation state and subsequent adiabatic expansion states in NPN with BKW/TIGER. The present experiments and the other available NPN information provide no guidance because they do not monitor the detonation product behavior in the regime where the nonideal behavior occurs.

For ANFO, however, Johnson et al.[31] and Mader[32] have reported the results of underwater cylinder expansion experiments (aquarium tests) and have presented methods, based on a specific nonideal reaction phenomenology, for numerically modeling such expansions with thermodynamic BKW calculations. In the present work, we assumed that the same qualitative phenomenology also applies to NPN. Our justification for this assumption is that we expect ANFO and NPN to react similarly and that the aquarium test provides ANFO product expansion data to volumes large enough to provide a relevant check against the predictions based on the

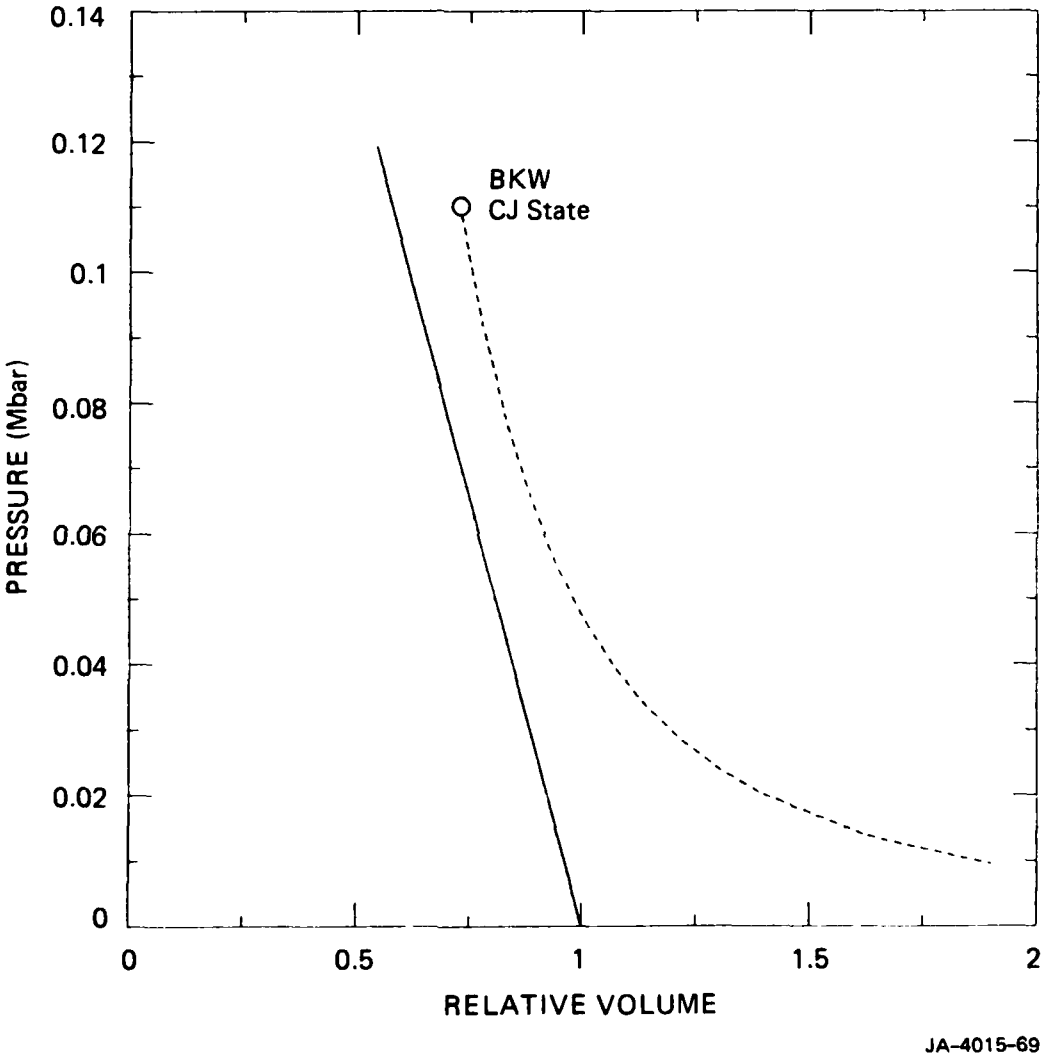

Figure 30. NPN BKW pressure-relative volume CJ state and partial release isentrope, NPN ideal.

The experimental results (solid line) from Figure 29 are included for comparison.

postulated phenomenology and BKW calculations. Following Johnson et al. and Mader, we made the following assumptions and calculations to model the nonideal detonation in NPN.

First, we assumed that only a portion of the ammonium nitrate reacts to support the steady-state detonation and determined the amount of AN that must be held inert to match the steady detonation velocity observed in the Lagrange gage experiments. We calculated a CJ detonation state based on this fraction of inert AN. Next we assumed that, in the initial part of a real adiabatic expansion from this state (such as might be observed in a very large Lagrange gage experiment), the remaining AN would be consumed irreversibly. Johnson et al. and Mader reported that the numerical simulations of the ANFO aquarium tests were insensitive to the assumptions used in modeling the secondary AN reaction. We postulated a specific irreversible process and calculated the corresponding p-V path and entropy increase. Finally, we assumed that the remainder of the expansion to atmospheric pressure that would be observed in an appropriate experiment would occur isentropically, and we calculated the corresponding isentrope. Details of the NPN calculations are given below.

We first calculated nonideal CJ detonation velocities for various fractions of inert AN. The inert AN was modeled as simply as possible within the options available in the TIGER solid equation of state. The AN was assumed to be incompressible and to have a constant specific heat = 32.82 cal/degree mole, a standard state heat of formation = -87.3 kcal/mole, and a standard state entropy = 33.8 cal/degree mole (estimated from values for related compounds). In these and the subsequent TIGER calculations for NPN, the methocel, which is only 0.2 wt% of the NPN and is a complex C-H-O molecule, was simply accounted for by increasing the amount of methyl alcohol by 0.2 wt%.

The experimental detonation velocity of 5.08 km/s was matched by BKW calculations with 51.5 wt% AN inert. Thus a nonideal CJ detonation with 51.5 wt% AN inert reproduces the experimentally determined Rayleigh line. The corresponding CJ state variables determined from the TIGER calculations are $p = 5.44$ GPa, $u = 1.08$ km/s, and $v = 0.780$ Mg/m^3.

The nonideal BKW/TIGER CJ pressure and particle velocity are less than the final values from the second NPN experiment, as expected. This is consistent with the interpretation that the flow observed in this experiment is entirely within the primary AN reaction zone. The calculated nonideal CJ detonation state then defines the end of the reaction zone.

We can now estimate a reaction time for the primary AN reaction by assuming the first steady-state particle velocity profile idealization discussed in the previous section. In this idealization, the final portion of the history is taken as a slow linear decay. We extrapolated the approximate decay rate to the calculated CJ state to estimate a primary AN reaction time of 11 ± 3 μs.

We noted in Section 4.2 that the last part of the experimental particle velocity history may also be idealized as a constant state. With this interpretation, the reaction time estimate above is clearly invalid. However, the constant state interpretation is not believed to be consistent with the present BKW calculations for the following reason.

The only plausible explanation we can provide for a steady wave followed by a truly constant state is that the NPN is overdriven. (This would occur if a constant particle velocity greater than the CJ particle velocity were applied to the rear boundary of the NPN; the driver input criteria discussed in the Section 4.2 suggest that this is extremely unlikely.) However, if NPN is overdriven, then its non-overdriven steady-state detonation velocity is less than our experimental value of 5.08 km/s. But for the BKW/TIGER calculations to be consistent with such a detonation velocity, essentially all the AN would have to be held inert. Because we consider this to be an unreasonable condition, on the basis of these BKW calculations we conclude that the NPN is apparently not overdriven, and in this section we discard the possibility of idealizing the last part of the experimental record as a constant state.

To calculate the expansion from the nonideal CJ state to the state where the remaining AN is consumed, we must define a specific secondary

reaction process. From the results of Johnson et al.,[31] the calculational simulations of the aquarium tests are not sensitive to the specific process chosen. We chose to model the process as a CJ deflagration centered on the nonideal detonation state.

This choice apparently implies a second steady reactive flow traveling slower than the steady detonation observed experimentally, with a constant state of growing duration between them. A constant state is compatible with our flow idealization. However, a growing constant state is not physically realistic because the later a particle enters the flow, the longer it will wait to undergo the secondary reaction even though it is preconditioned identically to particles entering the flow earlier. Nevertheless, the BKW/TIGER release path is intended to be used only as an intermediate step in generating a JWL isentrope through the CJ state. Because the JWL isentrope form always has a positive second derivative with respect to relative volume, the physically unrealistic hydrodynamic behavior will not be present in a JWL EOS fitted to the nonideal BKW CJ isentrope.

The p-V path for the postulated deflagration process is the Rayleigh line between the nonideal detonation state and the CJ deflagration state. From BKW/TIGER calculations, at the CJ deflagration state: $p = 2.96$ GPa, $v = 1.19$ m^3/Mg, and $S = 1.727$ cal/Kg, ($S_1 = 1.292$ cal/Kg), where S is specific entropy and the subscript 1 refers to the nonideal detonation state. The remainder of the release path is modeled simply as the BKW isentrope through this CJ deflagration state.

The nonideal BKW adiabatic release path generated as described above to model and extend the results of the second NPN experiment then consists of the Rayleigh line from the nonideal CJ detonation state for 51.5 wt% AN inert to an appropriately centered ideal (AN 100% active) CJ deflagration state and an ideal BKW isentrope through this deflagration state. Figure 31 shows the nonideal BKW detonation state and the adiabtic release path to a relative volume of about 2. Figure 31 also includes the experimental data and the ideal BKW CJ isentrope for comparison.

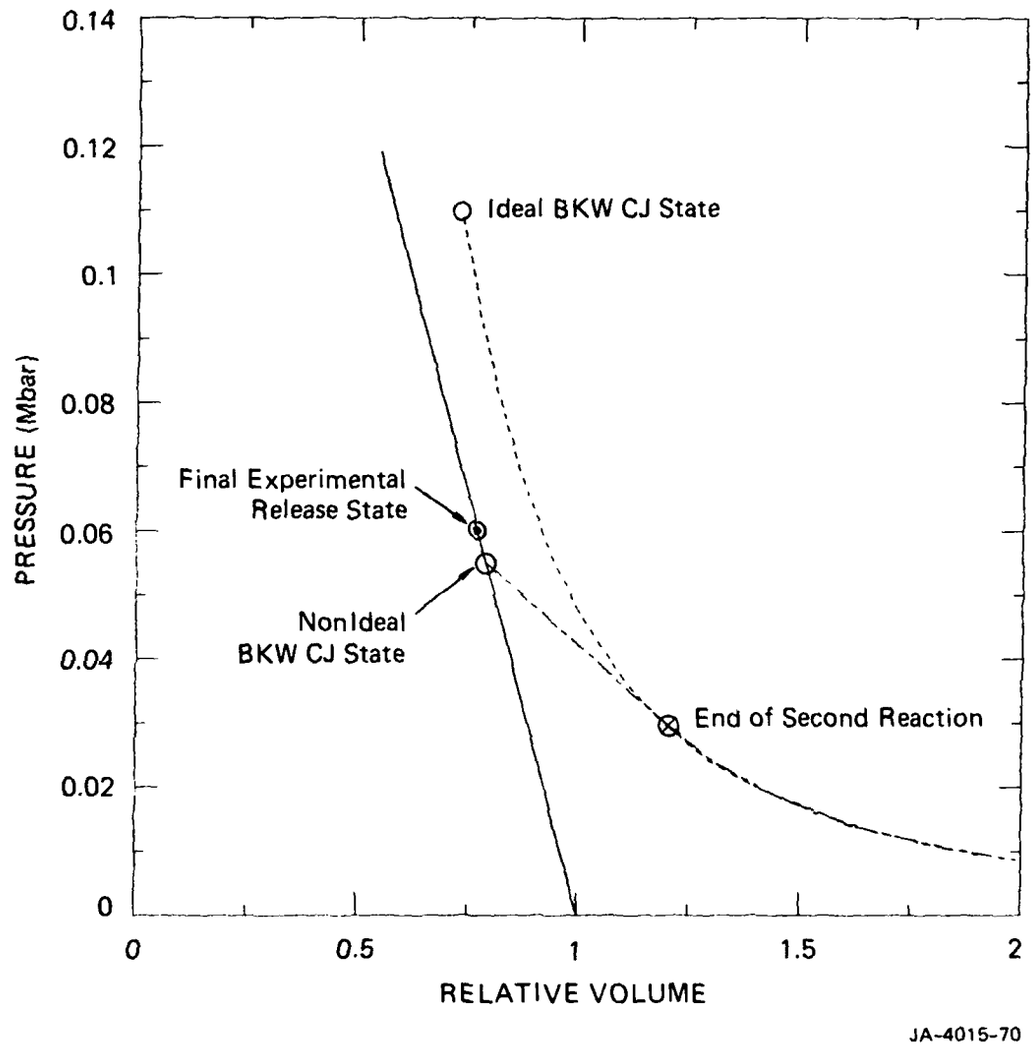

Figure 31. NPN BKW pressure-relative volume CJ state and partial release adiabat, NPN nonideal.

The experimental results from Figure 29 (solid line) and the ideal BKW results from Figure 30 (dashed line) are included for comparison. See text for details of nonideal two-reaction detonation process.

Figure 32 shows the CJ states and full release paths to the largest relative volumes calculated for the ideal and nonideal cases on a log-log scale. (The isentrope calculations were carried out to the largest volume expansions possible; the calculations terminated when temperatures dropped below the limits built into the EOS.) The ideal BKW CJ isentrope and the lower portion of the nonideal BKW CJ isentrope are indistinguishable in this figure because the entropy productions in the one-step and two-step AN reaction processes are nearly the same. The significance of these thermodynamic calculations is discussed after the JCZ3 calculations are presented.

JCZ3 Calculations

As the first step in interpreting the experimental results using JCZ3, we again calculated the ideal NPN CJ state and CJ release isentrope. We used the SRI JCZ3 parameters for the gaseous species, rejected liquid water, and assumed ideal detonation. The resulting CJ state values were D = 5.48 km/s, p = 7.93 GPa, v = 0.731 m^3/Mg, and u = 1.43 km/s. This CJ state and the ideal CJ release isentrope to a relative volume of about 1.8 are shown in Figure 33 along with the experimental Rayleigh line presented previously. (The full release isentrope is shown later.)

In sharp contrast to the BKW calculations, the JCZ3 CJ detonation calculation with AN fully active reproduces the experimentally observed detonation velocity within the estimated accuracies of the calculation and experiment. (The experimental measurement was previously estimated to have an uncertainty of ±0.1 km/s; the calculations are judged to have an uncertainty of about ±5%.) Therefore, by the definition given previously, with respect to the JCZ3 equation of state, the detonation process in NPN is ideal.

The conclusion that the detonation process observed in NPN in the Lagrange gage experiment is ideal with respect to JCZ3 follows from our definitions and is convenient for indicating that the ideal JCZ3 calculations much more closely replicate the observed NPN behavior than the ideal BKW calculations. It could, of course, be argued that the

AD-A166 462 SIMULATION DEVELOPMENT FOR SILO TEST PROGRAM (STP) 2/2
VOLUME 2 DETONATION CH (U) SRI INTERNATIONAL MENLO
PARK CA J T ROSENBERG ET AL 31 MAR 84
UNCLASSIFIED DNA-TR-84-219-V2 DNA001-82-C-0103 F/G 19/1 NL

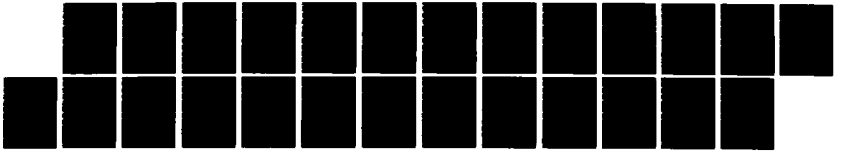

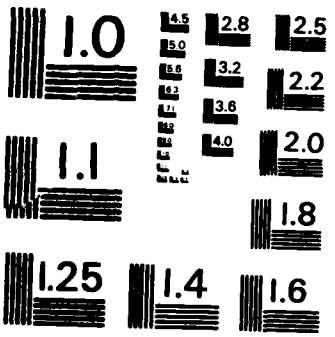

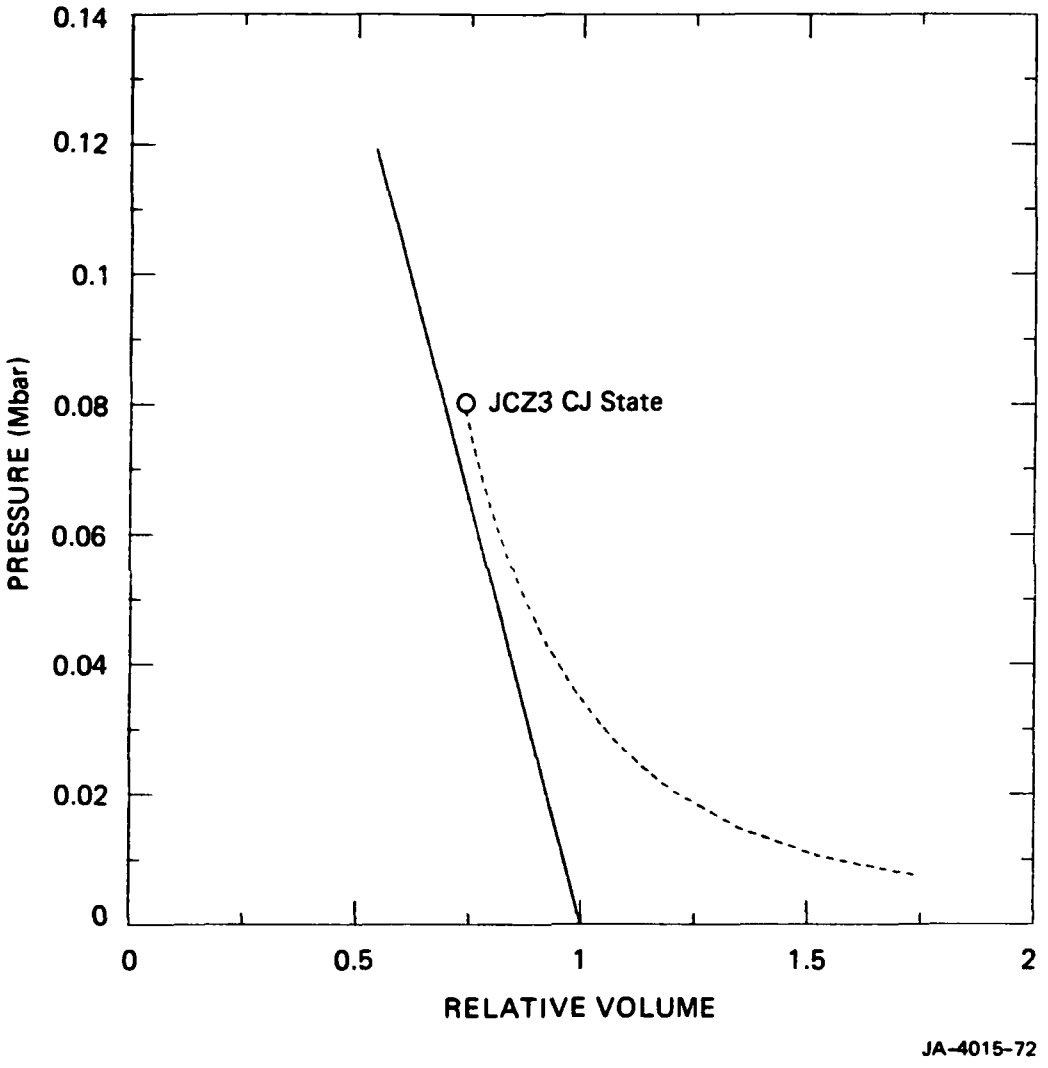

Figure 33. NPN JCZ3 pressure-relative volume CJ state and partial release isentrope, NPN ideal.

The experimental results (solid line) from Figure 29 are included for comparison.

discrepancy is significant and the NPN detonation process is nonideal. In fact, in the remainder of this section, to proceed toward our primary objective of developing initial JWL parameters for NPN, we improve the correlation between experiment and calculation by treating the NPN detonation process as nonideal.

To obtain precise agreement in CJ detonation velocity between the JCZ3 calculations and the experiment, we again assumed that not all the AN reacted to support the steady flow. We determined that agreement was obtained if 14.5 wt% of the AN was held inert in the calculations. The corresponding CJ state variables are p = 6.48 GPa, u = 1.26 km/s, and v = 0.744 Mg/m^3. We take this to be the nonideal JCZ3 CJ state in NPN.

The calculated nonideal JCZ3 CJ state is reached during the Lagrange gage NPN experiment, in distinction to the situation with the BKW calculations. The JCZ3 values for the nonideal CJ pressure and particle velocity are located on the corresponding experimentally determined histories either at the end of the first rapid rarefaction or early in the linear decay region. On this basis, we estimate the reaction time as 2 (+5 -1) μs for the primary AN reaction (the reaction that supports the observed detonation velocity).

The experimentally observed steady flow persists to lower pressures and particle velocities than the primary AN reaction, which terminates at the nonideal JCZ3 CJ point. This suggests either that (1) some secondary reaction occurs near the CJ state, maintaining the steady flow and causing the slow pressure and particle velocity decay rates, or that (2) the flow is not rigorously steady below the nonideal CJ state, although we failed to resolve the dispersion from our measurements. In the latter case we would still have to account for the unusually low decay rates of the Lagrange stress and particle velocity histories. This slow decay differs from the behavior we have observed in other explosives and is an interesting result. We consider these points further to calculate the JCZ3 nonideal adiabatic CJ release path.

In calculating a JCZ3 nonideal CJ release path, we must again postulate a calculable reaction phenomenology as we did in the case of

the BKW calculations. We choose not to use the ANFO BKW phenomenology itself, however, because it was developed and validated specifically for BKW calculations. To apply the method to JCZ3 calculations, we would have had to arbitrarily choose a secondary reaction process and a final pressure for terminating the process with no means of justifying the choice.

We calculated JCZ3 release isentropes for two assumed processes. In the first, the AN that did not support the steady detonation was assumed also to remain inert in the subsequent adiabatic release. This assumption is computationally convenient and, because most (85.5 wt%) of the AN is consumed in the primary reaction, may be sufficiently accurate. It fails to account, however, for the anomalously slow decay rates observed in the experimental records.

The second assumed release process was more complex and was motivated by the shape of the experimentally observed pressure and particle velocity histories. In developing our second postulated process from the nonideal CJ state, we were motivated by the experimental observation that the pressure decay rate was so slow that the pressure could be idealized as being constant. We now attribute this not to an overdriven detonation (which we consider highly unlikely because of the initiator selection criteria described earlier), but to a secondary AN reaction. Furthermore, if the particle velocity is also idealized as constant, then the particle velocity gradient is zero. Therefore, by the continuity condition for uniaxial flow (Equation 3, Section 2), the specific volume is constant. Thus, the experimental profiles suggest a secondary reaction occurring at nearly constant p and V. We therefore postulated that (1) such a reaction exists, (2) it consumes the remaining AN, and (3) the constant p and V values are those calculated for the nonideal CJ state. We do not argue the plausibility, or even possibility, of such a process, but only state that it is consistent with the experimental results.

We calculated JCZ3 isentropes for both postulated processes. In the first case, the JCZ3 isentrope is the frozen isentrope for 14.5 wt%

AN inert through the nonideal CJ state. In the second case, it is the ideal (all AN active) isentrope through the nonideal CJ state. These two isentropes plus the ideal JCZ3 CJ isentrope are shown in their entirety in Figure 34. Note that the JCZ3 calculations extend to relative volumes approaching 1000.

We selected the nonideal CJ release isentrope based on the second postulated process as the preferred JCZ3 representation for the NPN steady detonation and expansion. This path, to relative volumes of about 1.8, is shown in Figure 35 along with the Rayleigh line from the experiment and the ideal JCZ3 CJ state and release isentrope. We used this path to develop initial JWL parameters for NPN.

4.5 CALCULATION OF JWL COEFFICIENTS

Initial JWL coefficients were developed for NPN using the procedures described in Section 2. The nonideal JCZ3 CJ state and release path (Figure 34, dashed curve, and Figure 35) were selected as the basis characterization data for use in developing the JWL parameters. We had intended to also use the BKW nonideal CJ adiabatic release path for this purpose. However, the failure of the calculations to reach volume expansions large enough to define realistic low pressure limits for the slope of the CJ release adiabat prevented this.

The fitting procedures produced JWL parameters consistent with the nonideal JCZ3 CJ release adiabat as well as with the three constraints on CJ pressure, slope, and energy, Equations (7), (8), and (9). The only choice required was a value of V_t. We selected $V_t = 25$ and encountered no difficulties in completing the fitting process.

The JWL parameters calculated for NPN are listed in Table 4 in conventional JWL format and units. Note that in this format the CJ relative volume is determined from Γ. For convenience the values of the various CJ state flow parameters not given in Table 4 are summarized here: $u = 0.126$ cm/μs, $v = 0.744$ m^3/Mg, and $V = 0.7514$.

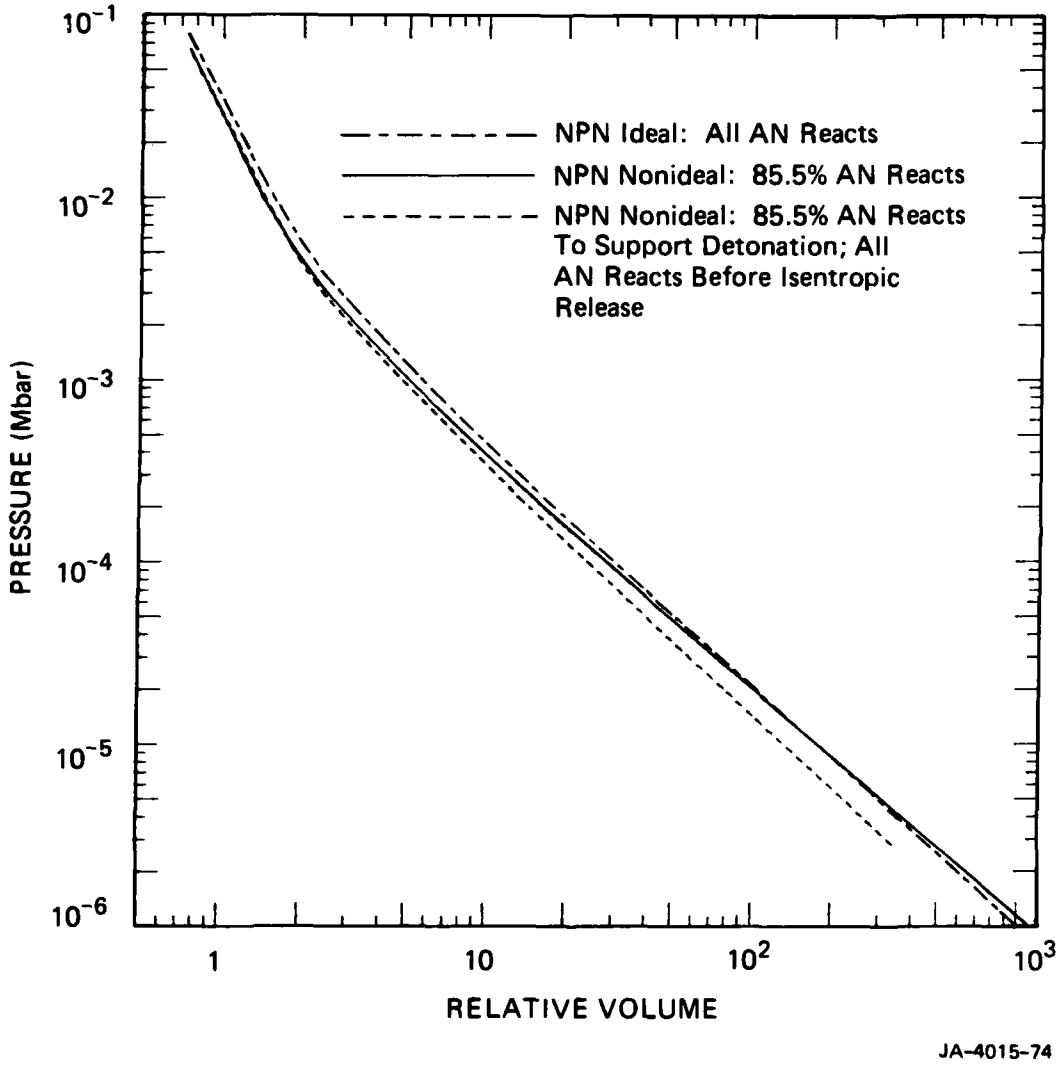

Figure 34. Three JCZ3 calculations of NPN pressure-relative volume CJ state and release isentrope.

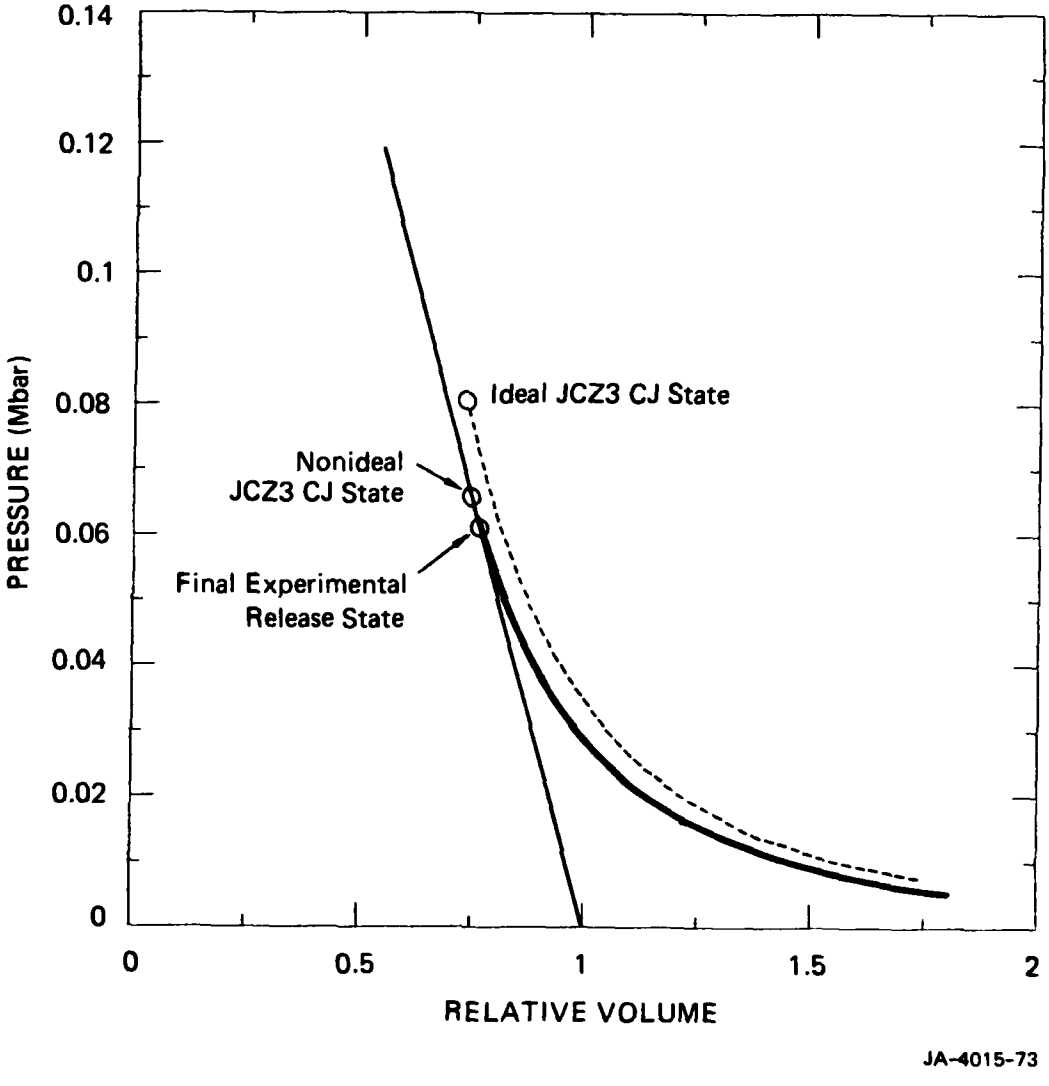

Figure 35. NPN JCZ3 pressure-relative volume CJ state and partial release adiabat, NPN nonideal.

The experimental results (light solid line) from Figure 29 and the ideal JCZ3 results (dashed line) from Figure 33 are included for comparison. See text for discussion of nonideal reaction process.

Table 4. NPN JWL coefficients.

Initial State	CJ State				Equation-of-State Parameters					
ρ_0 (Mg/m^3)	p (Mbar)	D (cm/μs)	E_0 (Mbar)	Γ	A (Mbar)	B (Mbar)	C (Mbar)	R_1	R_2	ω
1.01	0.0648	0.508	0.3187	3.023	6.783	0.1824	0.007212	7.628	2.305	0.345

The fitted (JWL) and basis (JCZ3) CJ isentropes are shown in the p-V plane in Figure 36. The JWL and JCZ3 adiabatic expansion coefficients γ, where $\gamma = (d \ln p / d \ln V)_S$, for these paths are shown in the γ-V plane in Figure 37. No adjustments are made in our fitting method to affect the agreement between the curves in Figure 37.

4.6 DISCUSSION

The NPN JWL parameters in Table 4 are the major result of the effort described in this section. They incorporate both experimental observations of compression and release behavior in the reaction zone as well as compatible thermodynamic calculations based on JCZ3, a state-of-the-art gaseous products equation of state. These JWL parameters are judged appropriate for use in initial hydrocode calculations to evaluate NPN behavior in simulators for DNA applications.

Most of the specific results of the NPN characterization subtasks were discussed as the results were presented. Here we briefly consider some general implications of this work.

The pretest effort to develop procedures for obtaining uniform NPN at densities around 1 Mg/m^3 indicated the difficulty in keeping NPN uniform at these low densities. We conclude that delicate NPN handling procedures would be necessary to get uniform performance in simulators from low density NPN. However, in DNA applications, as in the mining applications for which NPN was developed, it is likely that NPN would be used at higher densities to enhance output. In such cases, tamping the

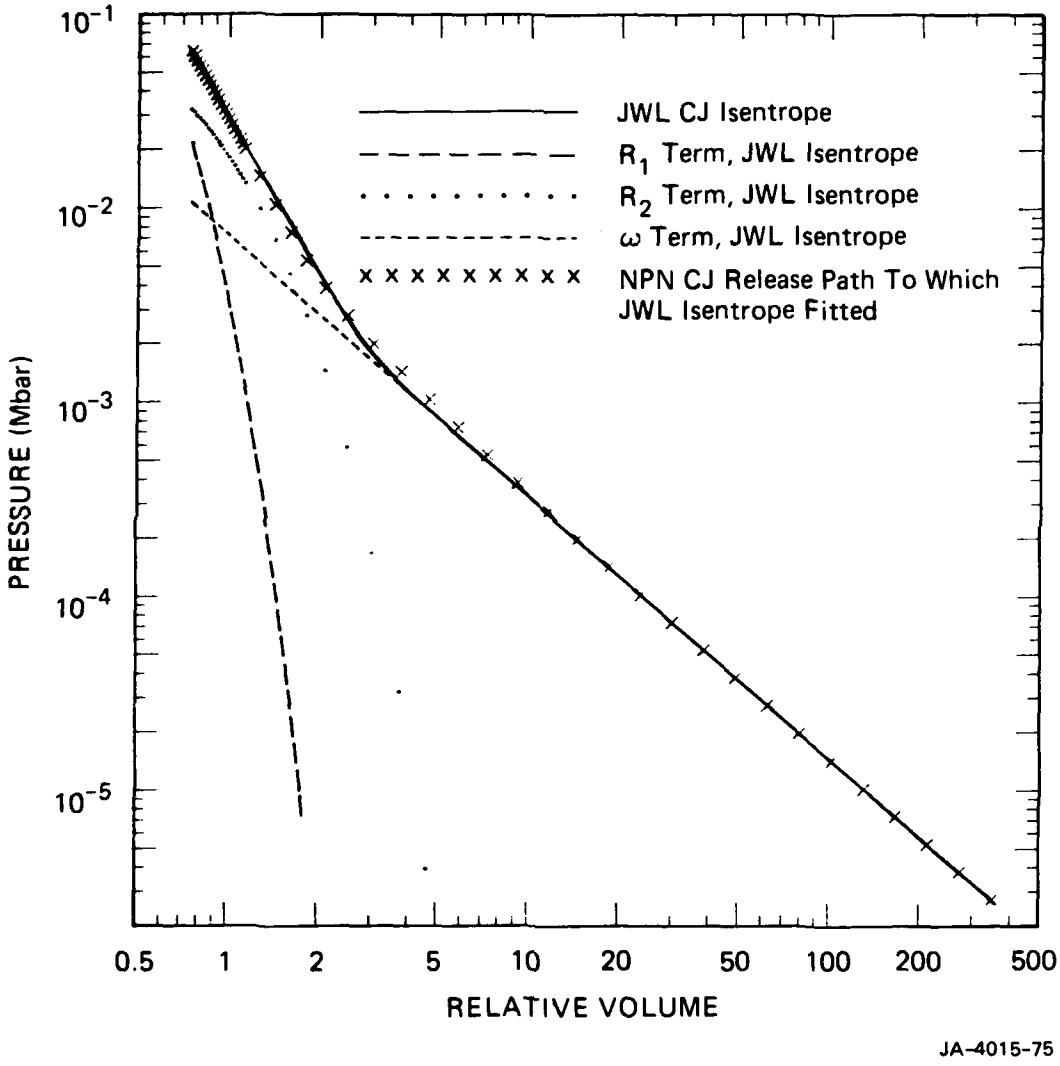

Figure 36. JWL CJ release isentrope for NPN.

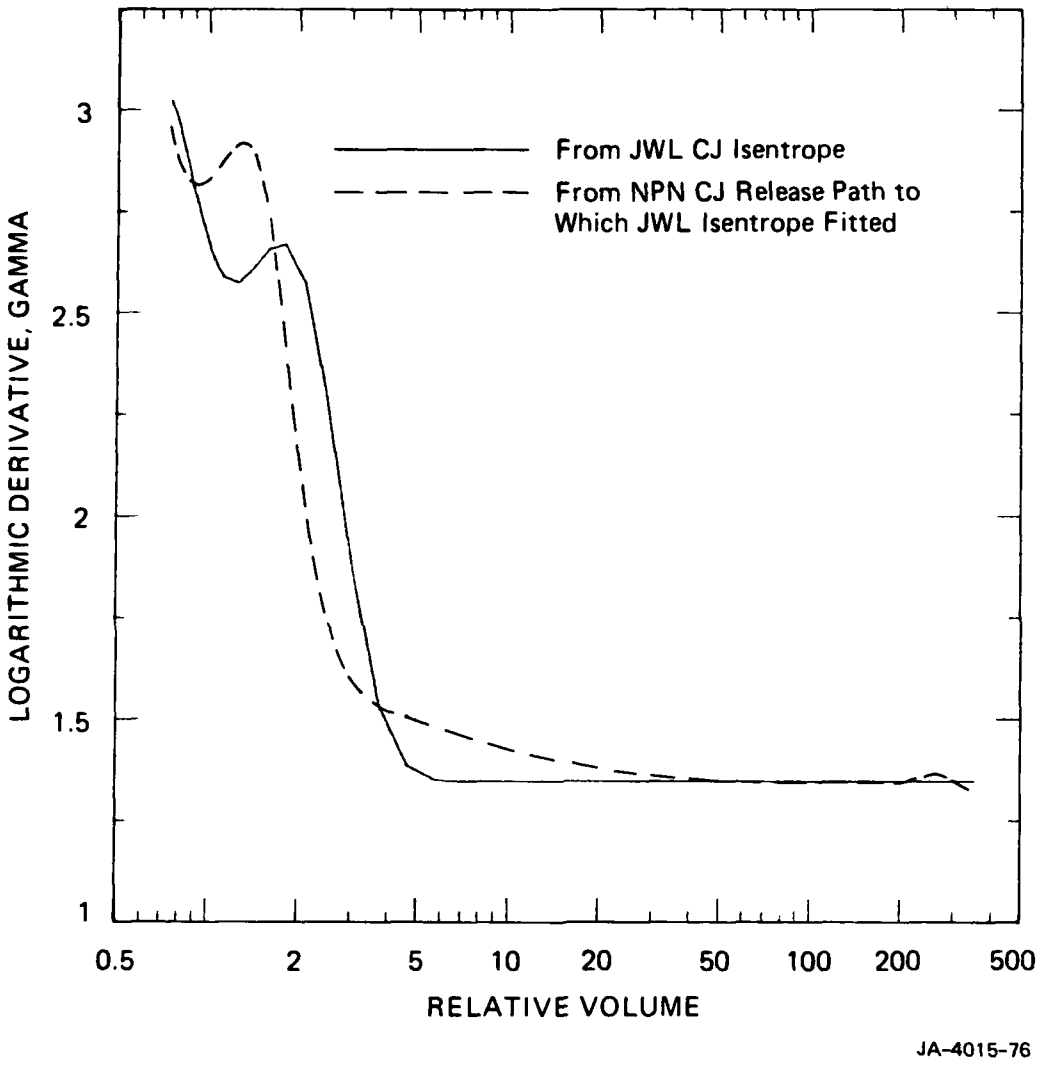

Figure 37. Gamma versus relative volume for NPN JWL CJ release isentrope and NPN CJ release path being fitted.

The two gammas are not equal at the CJ relative volume because the NPN CJ release path is not tangent to the Rayleigh line at this point.

charge during loading to achieve maximum irreversible compaction everywhere may result in a uniform as well as a high output material. The tendency of NPN to compact irreversibly should be borne in mind when considering it for a specific application.

Our experiments showed that NPN supported a steady detonation with a propagation velocity of 5.08 km/s in confined 0.3-m-diameter charges. From ANFO results, we inferred that this value is a good approximation to the infinite diameter velocity. This inference is also compatible with the experimental results of Franzen and Wisotski, for a 100-pound NPN charge[20] if the propagation velocities they report (between 2.8 and 4.1 km/s) are interpreted as being from the buildup region. There is an implication in the introduction to Reference 20 that these values represent steady detonation; however, from reviewing the data and consulting with the authors, we determined that this implication was unintentional.

The inference that our Lagrange gage experiment approximates infinite diameter behavior is also qualitatively compatible with Mallory's greater value of 5.206 km/s for NPN of higher density (1.298 Mg/m^3), in 1-inch-diameter heavily confined columns. However, because the difference in detonation velocities is rather small considering the significant density difference between Mallory's material and ours, it is possible that one or both of the velocities do not represent infinite diameter behavior. Nevertheless, in view of the large diameter of our charges and the supporting ANFO information, we believe that 5.08 km/s is a good approximation to the infinite diameter detonation velocity in NPN of 1.01 Mg/m^3 initial density.

The Lagrange particle velocity histories indicated two unusual hydrodynamic properties of the detonation process in NPN. First, the flow was steady throughout the estimated 1-D test time at each gage (at least 5-10 μs after shock arrival). Second, the decay rates of the Lagrange particle velocity and inferred pressure histories became very slow or zero about two microseconds after shock arrival. We have not observed either of these detonation properties in other HEs we have

studied with this technique. Assuming the results to be reproducible and not an artifact of the technique, we conclude that the reaction phenomenology in NPN is significantly different from that in the other HEs we have studied.

We found significant differences in the implications of thermodynamic TIGER calculations modeling the experiments with the BKW and with the JCZ3 equations of state. The TIGER/BKW calculations of detonation velocity suggested that the detonation is definitely nonideal, but the TIGER/JCZ3 calculations implied that it is only borderline nonideal. The TIGER/JCZ3 calculations indicated that most (85.5 wt%) of the AN reacts to support the detonation, whereas the TIGER/BKW calculations implied that only half the AN reacted to support the detonation. The estimated nonideal CJ state occurred during the gage recording times, at a pressure of 6.48 GPa, according to the JCZ3 calculations, but after the gage recording times, at 5.44 GPa, in the BKW calculations.

Because of the differences in the BKW and JCZ3 nonideal CJ calculations, we postulated different secondary reaction processes in the two cases: a nearly constant volume reaction occurring in the region of the CJ pressure for the JCZ3 calculations and a steady deflagration spread over a wide range of pressures and volumes for the BKW calculations. Both are artifacts to permit the completion of the calculations and provide a reasonable estimate for the locus of p-V states along the NPN CJ adiabat for constraining the JWL fit. Since each is known to have certain unrealistic features, neither is represented to be the actual process occurring in NPN; unfortunately, the present work cannot indicate which is preferable. We conclude that NPN (and probably its close relative ANFO) has a complex unknown AN decomposition phenomenology that should be studied further.

The NPN JWL parameters developed here were based on the JCZ3 calculations because the BKW calculations terminated before providing the low pressure limiting data required for our JWL fitting method. We note that most of the present JWL parameters are within the normal ranges for such coefficients developed from cylinder tests, with the possible

exception of the nonlinear coefficients R_1 and R_2. The present values for these coefficients have a ratio typical of cylinder test coefficients, but are somewhat larger than published coefficients. Larger nonlinear coefficients have the effect of bringing on the constant gamma (adiabatic exponent) behavior along the CJ isentrope at somewhat smaller relative volumes. For comparison, we list the cylinder test ANFO JWL parameters[30] and our values in Table 5 and plot the ANFO and NPN JWL CJ isentropes in Figure 38.

Table 5. Comparison of NPN and ANFO JWL coefficients.

Initial State	CJ State				Equation-of-State Parameters					
ρ_0 (Mg/m^3)	p (Mbar)	D (cm/μs)	E_0 (Mbar)	Γ	A (Mbar)	B (Mbar)	C (Mbar)	R_1	R_2	ω
1.01	0.0648	0.508	0.03187	3.023	6.783	0.1824	0.007212	7.628	2.305	0.345
ANFO[a]										
0.850	0.060	0.465	0.0325	2.063	0.4760	0.00524	0.00720	3.5	0.9	0.31

We conclude this subsection with a digression concerning the available detonation energy of NPN. The report by McMullan[25] contains a useful compilation of properties for several HEs of interest to DNA including NPN. However, it cites a value for the available energy of NPN, namely, 1180 cal/g, that is unusually high compared with the values for similar HEs. The available energy value widely quoted for ANFO, for example, and given in reference 25, is 920 cal/g. We believe that the NPN value in Reference 25 is calculated on a different basis than the values for the other HEs and could therefore lead to erroneous conclusions regarding the performance of NPN relative to these materials in DNA applications.

There is no universally accepted definition for the term available energy. In practice, computed values for available chemical energy of a detonating HE are often either (1) maximum heats of detonation

[a]From Reference 30

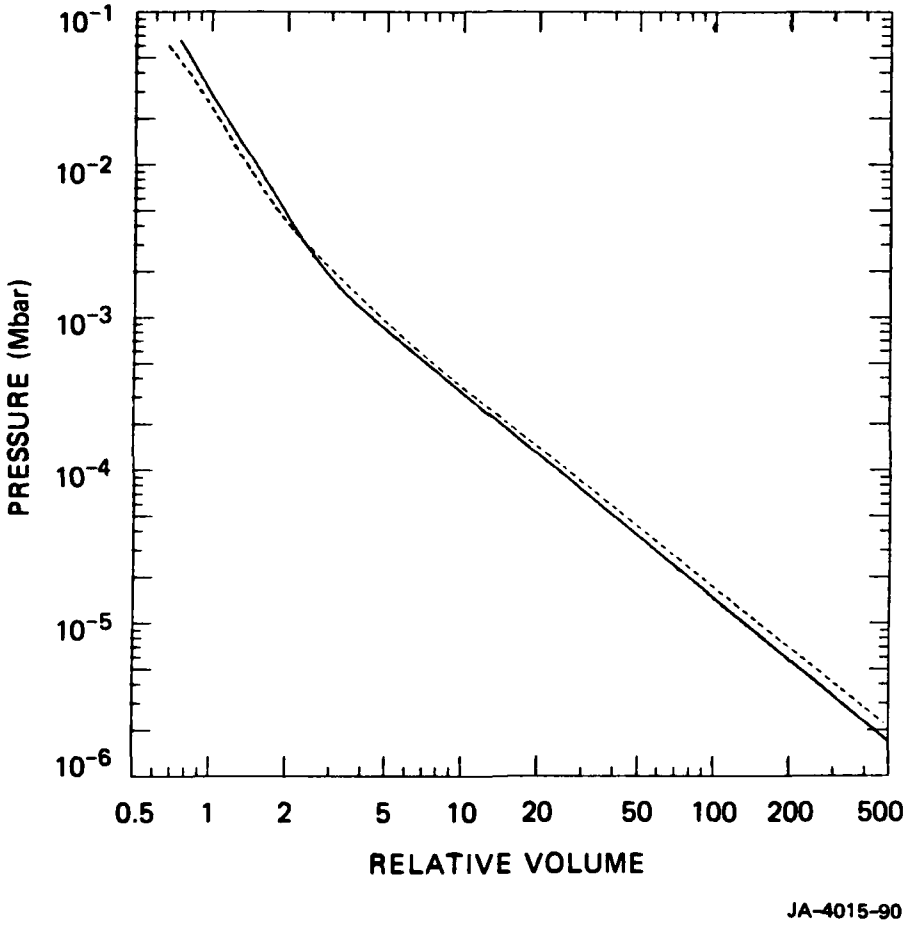

Figure 38. NPN (solid) and ANFO JWL CJ isentropes.

calculated by assuming that the initial and final states are 298 K and 101 kPa and that the detonation products are the most stable ordered set H_2O, CO_2, C(s), and N_2, or (2) smaller heats of detonation calculated assuming the same initial and final states but a more realistic detonation product composition estimated from a thermodynamic equilibrium code such as TIGER, usually for a relative expansion volume around 10 where product composition freezeout is estimated to occur. In either case, it is necessary to specify whether the H_2O is in liquid or gaseous form, with the latter assumption being usual.

We performed both types of calculations for NPN. For the baseline NPN composition, we calculate a maximum heat of detonation of 907 cal/g with respect to $H_2O(g)$. This is the value that we believe should be compared with the other available energy values in Reference 25. (For our composition, and using the second definition, we calculated a heat of detonation of 877 cal/g using the product concentrations on the non-ideal TIGER/JCZ3 CJ adiabat at a relative volume of about 9. This value is larger than the NPN E_0 value from Tables 4 and 5.)

We consider it likely that the high available energy value for NPN in reference 25 is calculated with respect to $H_2O(\ell)$, whereas the values for other HEs in reference 25 are with respect to $H_2O(g)$. When the values are calculted on a consistent basis, NPN and ANFO appear to be very similar in available energy, with ANFO being slightly more energetic per gram of HE.

SECTION 5

RECOMMENDATIONS

Results of the present NA/NP and NPN characterization efforts lead us to make five recommendations to DNA in the areas of HE use and characterization. Recommendations 1, 3, and 5 are recommended strongly.

Recommendation 1: We strongly recommend that baseline NA/NP be considered for use in applications calling for low cost liquid explosives similar in performance to nitromethane.

NA/NP is a very promising family of liquid explosives. It is a uniform, high quality HE with performance very similar to nitromethane, but the material costs are much less. Major concerns are likely to be logistics and safety problems arising from the nitric acid component. The specific blend studied in this work was rather easy to handle because of the intermediate concentration of the Baume 42 nitric acid. Because this blend seems to offer a superior combination of cost, performance, sensitivity, and handling characteristics, we endorse it for consideration by DNA as the baseline material in the NA/NP family.

Recommendation 2: We recommend that NPN be evaluated for use in applications calling for an HE similar to ANFO but with the ability to do somewhat more work at higher pressures and with more rapid kinetics.

NPN is a good blasting agent with a combination of properties that may offer net advantages over ANFO in some applications. NPN is similar in many respects to ANFO, but has a higher detonation pressure and velocity, no doubt because of its greater initial density. It also probably has a shorter steady-state reaction zone and a more rapid shock-to-detonation (SDT) transition than ANFO. However, NPN costs more than ANFO, contains a fairly volatile solvent (NP), and is difficult to keep in a uniform density state because it compacts irreversibly in response to local pressures. The irreversible compaction can be used to advantage by compressing the NPN to higher (presumably uniform) densities than studied here, where its differences from, and potential advantages over, ANFO are greatest.

NPN may be useful to DNA not only in NWE simulators, but also as an ANFO model in studies to define the nonideal AN reaction phenomenology. Because NPN displays many of the qualitative detonation behavior properties of ANFO but on a shorter time scale, it permits smaller, more cost effective experiments.

Recommendation 3: We strongly recommend Lagrange gage studies to characterize SDT in NA/NP.

Rather slow nonreproducible shock initiation of detonation was observed in one Lagrange SDT experiment in NA/NP. In addition, the detonation experiments indicated a surprisingly long steady-state reaction zone in NA/NP. Both phenomena can affect the design and performance of some NWE simulators and can be well defined through a series of Lagrange gage SDT experiments. Such experiments are the most direct means we know to characterize the reaction zone as it builds to the steady-state and to obtain engineering curves of detonation buildup useful in simulator design and modeling.

Recommendation 4: We recommend standard rate stick studies in NPN to determine the threshold diameter for size-independent (infinite diameter) detonation.

The present NPN results are believed to be a good representation of infinite diameter detonation properties, but direct confirmation is desirable. The most cost-effective way to obtain this information is through rate stick experiments varying charge diameter. The detonation buildup information needed to evaluate or use NPN for specific simulator applications can also be generated in these experiments. Later, for specific applications, buildup distances can be determined in dedicated experiments simulating the actual initiation conditions, and/or Lagrange gage SDT experiments can be performed if more extensive understanding of the buildup process is required.

Recommendation 5: We strongly recommend enlarged Lagrange gage steady detonation experiments, and computational development as needed, on NPN (or ANFO) to characterize AN reaction phenomenology in these HEs.

One of the most important findings of this study is that AN-rich HEs such as NPN and ANFO, even in large charges, have a complex unknown

AN reaction phenomenology that differs markedly from that of conventional HEs and current detonation models. Since ANFO will probably be used in future large NWE simulators, our current inability to closely model its behavior may be of major significance to DNA. Therefore, we recommend that DNA initiate experiments to unambiguously determine the AN reaction process in this very useful class of HE.

Three types of experiments available for this purpose are cylinder tests, aquarium tests, and Lagrange gage experiments. Although cylinder or aquarium tests provide expansion data to large relative volumes and are therefore useful, a greatly enlarged Lagrange gage experiment offers two major advantages in characterizing the detonation processes in these HEs. First, the Lagrange gage experiment does not involve interaction of the HE with a container, so the unperturbed peak and final reaction zone states characteristic of the explosive itself, rather than of its response to the containment system, can be determined. Second, the embedded instrumentation resolves rather than integrates flow features and provides the information necessary to identify the termination of the reaction and quantify its rate. Therefore, such experiments, possibly with NPN targets as suggested in Recommendation 2, are recommended to generate a data base characterizing the AN reaction phenomenology in these HEs.

After the detonation process in these AN-rich HEs is understood, it may be necessary to develop appropriate computational techniques to model it. Current DNA hydrocode calculations often use the JWL equation-of-state to represent the behavior of HE detonation products in simulator applications. This EOS was originally developed to model the behavior of military explosives, with negligible reaction zones, in metal pushing applications where the most significant energy exchanges occur near the CJ isentrope at relative volumes less than about 10. If the JWL EOS is used to calculate the performance of ANFO in NWE simulators, it may be applied to much different conditions: long reaction zones, two-stage reactions, low pressures, and states far from the CJ isentrope.

The effects of these extensions of present computational techniques on the accuracy of the calculations are unknown. Therefore, it is important to determine the sensitivity of specific simulator design and performance calculations to these effects by parmeter variation calculations and, if necessary, to incorporate more detailed reactive hydrodynamics or a modified EOS in the hydrocode calculations.

REFERENCES

1. M. Cowperthwaite and J. T. Rosenberg, "A Multiple Lagrange Gage Study of the Shock Initiation Process in Cast TNT," in Sixth Symposium (International) on Detonation, ACR-221, David J. Edwards, Ed. (Office of Naval Research, Department of the Navy, Arlington, VA 1976), pp. 786-793.

2. J. T. Rosenberg and M. Cowperthwaite, "Explosive Characterization by the Lagrange Gage and Analysis Technique," in 1982 Conference on Instrumentation for Nuclear Weapons Effects (Proceedings), DNA-TR-82-17-V1, M. Frankel, Ed. (Defense Nuclear Angecy, Washington, DC 1982), pp. 287-299.

3. V. M. Zaitsev, P. F. Pokhil, and K. K. Shvedov, "The Electromagnetic Method for the Measurement of Velocities of Detonation Products," Doklady Akad. Sci. USSR, 132 (6), 1339 (1960).

4. S. J. Jacobs and David J. Edwards, "Experimental Study of the Electromagnetic Velocity Gage Technique," Proceedings of the Fifth Symposium (International) on Detonation, ACR-184 (Office of Naval Research, Department of the Navy, Arlington, VA, 1970), pp. 413-426.

5. Allan B. Anderson, M. J. Ginsberg, W. L. Seitz, and Jerry Wackerle, "Shock Initiation of Porous TATB," in Seventh Symposium (International) on Detonation, NSWC MP 82-334, James M. Short, Ed. (Naval Surface Weapons Center, White Oak, MD, 1982), pp. 385-393.

6. H. C. Vantine, W. D. Curtis, L. M. Erickson, and R. S. Lee, "A Comparison of Stress and Velocity Measurements in PBX-9404 Explosive," in Proceedings of the Eighteenth Symposium (International) on Combustion (The Combustion Institute, 1981).

7. L. Seaman, "Lagrangian Analysis for Multiple Stress or Velocity Gages in Attenuating Waves," J. Appl. Phys. 42, 456-462 (1971).

8. M. Cowperthwaite and W. H. Zwisler, "TIGER Computer Program Documentation," SRI Publication No. Z106, Menlo Park, CA (January 1973).

9. Wildon Fickett and William C. Davis, Detonation, ISBN 0-520-03587-9, Library of Congress Catalog Number 77-085760 (University of California Press, Berkeley, Los Angeles, 1979).

10. M. Finger, E. Lee, F. H. Helm, B. Hayes, H. Hornig, R. McGuire, and M. Kahara, "The Effect of Elemental Composition on the Detonation Behavior of Explosives," in Proceedings of the Sixth Symposium (International) on Detonation, ACR-221, David J. Edwards, Ed. (Office of Naval Research, Department of the Navy, Arlington, VA, 1976), pp. 721-722.

11. E. L. Lee, H. C. Hornig, and J. W. Kury, "Adiabatic Expansion of High Explosive Detonation Products," UCRL-50422, Lawrence Livermore National Laboratory, Livermore, CA (May 2, 1969).

12. "LLNL Explosives Handbook--Properties of Chemical Explosives and Explosive Simulants," B. M. Dobratz, Ed., UCRL-52997, Lawrence Livermore National Laboratory, Livermore, CA (March 16, 1981).

13. H. Dean Mallory, "The Explosive Properties of Nitric Acid-Nitropropane Solutions," Increment Memo Report (Proprietary) to Joseph L. Trocino & Associates, Sherman Oaks, CA, Department of the Navy, Naval Weapons Center, China Lake, Ca (April 1981).

14. H. Dean Mallory, "Second Report Concerning the Explosive Properties of Nitric Acid Nitropropane Solutions," Memo Report (Proprietary) to Joseph L. Trocino & Associates, Sherman Oaks, CA, Department of the Navy, Naval Weapons Center, China Lake, CA (March 1982).

15. Joseph L. Trocino, "Military and Commercial Applications of Nitropropane-Weak Nitric Acid Explosive Systems," private communication from Joseph L. Trocino & Associates, Sherman Oaks, CA (May 1982).

16. M. J. Kamlet and S. J. Jacobs, J. Chem. Phys. 48, 23-35 (1968).

17. "Nitric Acid, Storage and Handling," Du Pont E-44269 9/81, E. I. du Pont de Nemours & Co., Inc., Wilmington, DE 19898.

18. "The Nitroparaffins," Technical Data Sheet, NP Series TDS No. 1, IMC Chemical Group, Inc., NP Division, 4415 W. Harrison St., Hillside, IL 60162.

19. "The Storage and Handling of Nitropropane Solvents," Technical Data Sheet, NP Series TDS No. 20, International Minerals and Chemical Corporation, 666 Garland Place, Des Plaines, IL 60016.

20. Roland Franzen and John Wistoski, "A Performance Test of the Blasting Agent NPN," Report to the Defense Nuclear Agency, Ford Laboratories, Inc., Pleasanton, CA (August 1983).

21. John R. Post, "Blasting Composition Containing an Alkanol," U. S. Patent No. 3,930,910 (1976).

22. John R. Post, "Ammonium Nitrate Blasting Agents Fueled with Nitropropane," Proceedings of Third Conference on Explosives and Blasting Techniques (Society of Explosive Engineers, Pittsburg, PA, February 1977).

23. H. Dean Mallory, "Detonation Rate of an Ammonium Nitrate-Nitropropane-Methanol Mixture," Test Report, Naval Weapons Center, China Lake, CA (December 1977).

24. Roland Franzen, "Review of Documents Concerning the Blasting Agents NPN," Topical Report to the Defense Nuclear Agency, Physics Applications, Inc., San Jose, CA (undated).

25. Frank W. McMullan, "Analysis Plan for 1985 Large-Scale Tests," DNA-TR-82-60, Kaman Tempo, Albuquerque, NM (January 1982).

26. John R. Post, General Energy Co., Littleton, CO (private communication, June 27, 1983).

27. M. Cowperthwaite and J. T. Rosenberg, "Lagrange Gage Studies of Composition B and H-6," SRI Final Report, Naval Surface Weapons Center, Contract N60821-80-C-0100 (May 1982).

28. M. Cowperthwaite and J. T. Rosenberg, "Lagrange Gage Studies of Nonideal Explosives Containing NH_4NO_3," SRI Final Report, U.S. Army Research Office, Contract DAAG29-80-0076 (June 1983).

29. M. Cowperthwaite and J. T. Rosenberg, "Lagrange Gage Characterization of Intermolecular Explosives," work in progress for U.S. Air Force AFATL/DLDE, Contract F08635-82-K-0447.

30. M. Finger, F. Helm, E. Lee, R. Boat, H. Cheung, J. Walton, B. Hayes, and L. Penn, "Characterization of Commercial Composite Explosives," in Sixth Symposium (International) on Detonation, ACR-221, David J. Edwards, Ed. (Office of Naval Research, Department of the Navy, Arlington, VA, 1976), pp. 729-739.

31. J. N. Johnson, C. L. Mader, and S. Goldstein, "Performance Properties of Commercial Explosives," Propellants, Explosives, Pyrotechnics 8, 8-18 (1983).

32. Charles L. Mader, Numerical Modeling of Detonations, ISBN 0-520-03655-7, Library of Congress Catalog Number 77-93463 (University of California Press, Berkeley, Los Angeles, London, 1979).

DISTRIBUTION LIST

DEPARTMENT OF DEFENSE

Asst to the Secretary of Defense
ATTN: Executive Asst

Defense Intelligence Agency
ATTN: DB-4C
ATTN: DT-1C
ATTN: DT-2
ATTN: RTS-2B

Defense Nuclear Agency
ATTN: SPTD
2 cy ATTN: SPSS
4 cy ATTN: STTI-CA

Defense Technical Information Center
12 cy ATTN: DD

Department of Defense Explo Safety Board
ATTN: Chairman

Field Command, DNA, Det 2
Lawrence Livermore National Lab
ATTN: FC-1

Field Command, Defense Nuclear Agency
ATTN: FCPR
ATTN: FCT
ATTN: FCTT
ATTN: FCTT, W. Summa
ATTN: FCTXE

Field Command Test Directorate
ATTN: FCTC

Joint Strat Tgt Planning Staff
ATTN: JLAA
ATTN: JPST

Under Secy of Def for Rsch & Engrg
ATTN: Strat & Space Sys (OS)

DEPARTMENT OF THE ARMY

Harry Diamond Laboratories
ATTN: DELHD-NW-P
ATTN: Commander/Tech Dir/Div Dir

US Army Ballistic Research Lab
ATTN: AMXBR-TBD, W. Taylor
ATTN: DRDAR-BLA-S, Tech Lib
ATTN: DRDAR-BLT, J. Keefer

US Army Concepts Analysis Agency
ATTN: CSSA-ADL, Tech Lib

US Army Corp of Engineers
ATTN: DAEN-ECE-T
ATTN: DAEN-RDL

US Army Engr Waterways Exper Station
ATTN: B. Welch
ATTN: Library
ATTN: WESSD, J. Jackson

DEPARTMENT OF THE ARMY (Continued)

US Army Material & Mechanics Rsch Ctr
ATTN: Tech Lib

US Army Material Command
ATTN: DRXAM-TL, Tech Lib

US Army Mobility Equip R&D Cmd
ATTN: DRDME-WC, Tech Lib

US Army Nuclear & Chemical Agency
ATTN: Library
ATTN: MONA-OPS, J. Kelley

USA Missile Command
ATTN: Documents Section

DEPARTMENT OF THE NAVY

David Taylor Naval Ship R & D Center
ATTN: Code 17
ATTN: Code 1770
ATTN: Code 1844
ATTN: Tech Info Ctr, Code 522.1
2 cy ATTN: Code 1740.5, B. Whang

Naval Facilities Engineering Command
ATTN: Code 04B

Naval Research Laboratory
ATTN: Code 2627, Tech Lib

Naval Sea Systems Command
ATTN: SEA-0351
ATTN: SEA-08
ATTN: SEA-09G53, Lib

Naval Surface Weapons Center
ATTN: Code F31
ATTN: Code R14
ATTN: Code R15
ATTN: Code R40, I. Blatstein

Naval Surface Weapons Center
ATTN: Tech Library & Info Svcs Br

Ofc of the Deputy Chief of Naval Ops
ATTN: NOP 03EG
ATTN: NOP 981

Office of Naval Research
ATTN: Code 474, N. Perrone

Space & Naval Warfare Systems Cmd
ATTN: PME 117-21

Strategic Systems Programs
ATTN: NSP-272
ATTN: NSP-43, Tech Lib

DEPARTMENT OF THE AIR FORCE

AF/INT
ATTN: INT

DEPARTMENT OF THE AIR FORCE (Continued)

Air Force Geophysics Laboratory
ATTN: LWH, H. Ossing

Air Force Institute of Technology
ATTN: Library

Air Force Systems Command
ATTN: DLW

Air Force Weapons Laboratory
ATTN: NTE, M. Plamondon
ATTN: NTED, E. Seusy
ATTN: NTEO
ATTN: NTES
ATTN: SUL

Air University Library
ATTN: AUL-LSE

Ballistic Missile Office
ATTN: ENBF, D. Gage
ATTN: PP
2 cy ATTN: ENSN

Deputy Chief of Staff
ATTN: AF/RDQI

Strategic Air Command
ATTN: DOTP
ATTN: NRI/STINFO

DEPARTMENT OF ENERGY

Department of Energy
Albuquerque Operations Office
ATTN: CTID
ATTN: D. Richmond

Department of Energy
Office of Military Application
ATTN: OMA/RD&T

Department of Energy
Nevada Operations Office
ATTN: Doc Con for Tech Lib

OTHER GOVERNMENT AGENCY

Central Intelligence Agency
ATTN: OSWR/NED

NATO

NATO School, SHAPE
ATTN: US Documents Officer

DEPARTMENT OF ENERGY CONTRACTORS

University of California
Lawrence Livermore National Lab
ATTN: Tech Info Dept Lib

Los Alamos National Laboratory
ATTN: MS P364, Reports Lib

Sandia National Laboratories
ATTN: Library & Security Classification Div

Sandia National Laboratories
ATTN: Tech Lib 3141

DEPARTMENT OF DEFENSE CONTRACTORS

Aerospace Corp
ATTN: Lib Acquisition M1/199

Applied Research Associates, Inc
ATTN: N. Higgins

Applied Research Associates, Inc
ATTN: J. Shinn

Applied Research Associates, Inc
ATTN: D. Piepenberg

Applied Research Associates, Inc
ATTN: R. Frank

BDM Corp
ATTN: Corporate Lib
ATTN: T. Neighbors

Boeing Co
ATTN: Aerospace Lib

California Research & Technology, Inc
ATTN: K. Kreyenhagen
ATTN: M. Rosenblatt

California Research & Technology, Inc
ATTN: F. Sauer

Cushing Associates
ATTN: V. Cushing

EG&G Wash Analytical Svcs Ctr, Inc
ATTN: Library

Electro-Mech Systems, Inc
ATTN: R. Shunk

Geo Centers, Inc
ATTN: E. Marram

H-TECH Labs, Inc
ATTN: B. Hartenbaum

IIT Research Institute
ATTN: Documents Lib

Institute for Defense Analyses
ATTN: Classified Library

Kaman Sciences Corp
ATTN: Library

Kaman Sciences Corp
ATTN: E. Conrad

Kaman Tempo
ATTN: DASIAC

Kaman Tempo
ATTN: DASIAC

Lockheed Missiles & Space Co, Inc
ATTN: J. Bonin
ATTN: Tech Lib

Lockheed Missiles & Space Co, Inc
ATTN: S. Taimuty
ATTN: Tech Info Ctr

DEPARTMENT OF DEFENSE CONTRACTORS (Continued)

Mitre Corp
ATTN: MS E190

National Technical Systems
ATTN: P. Libberman

University of New Mexico
ATTN: G. Leigh
ATTN: N. Baum
2 cy ATTN: D. Calhoun

Pacific-Sierra Research Corp
ATTN: H. Brode, Chairman SAGE

Pacifica Technology
ATTN: G. Kent

Physics Applications, Inc
ATTN: F. Ford

Physics International Co
ATTN: E. Moore

R & D Associates
ATTN: C. Lee
ATTN: C. Knowles
ATTN: D. Simons
ATTN: J. Lewis
ATTN: Technical Info Center

R & D Associates
ATTN: G. Ganong

Rand Corp
ATTN: P. Davis

Rand Corp
ATTN: B. Bennett

S-CUBED
ATTN: D. Grine
ATTN: Library

DEPARTMENT OF DEFENSE CONTRACTORS (Continued)

Science Applications Intl Corp
ATTN: Tech Lib

Science Applications Intl Corp
ATTN: J. Cockayne
ATTN: M. Knasel
ATTN: W. Layson

Southwest Research Institute
ATTN: A. Wenzel
ATTN: W. Baker

SRI International
ATTN: G. Abrahamson
ATTN: J. Colton
2 cy ATTN: J. Rosenberg
2 cy ATTN: D. Erlich
2 cy ATTN: D. Keough

Structural Mechanics Associates, Inc
ATTN: R. Kennedy

Teledyne Brown Engineering
ATTN: D. Ormond
ATTN: F. Leopard

TRW Electronics & Defense Sector
ATTN: D. Baer
ATTN: Tech Info Center
2 cy ATTN: N. Lipner

TRW Electronics & Defense Sector
ATTN: E. Wong
ATTN: P. Dai

Weidlinger Assoc, Consulting Engrg
ATTN: M. Baron

Weidlinger Assoc, Consulting Engrg
ATTN: J. Isenberg

Weidlinger Assoc, Consulting Engrg
ATTN: A. Misovec

END

DTIC

5-86